NORTHWESTERN UNIVERSITY

Polysaccharide-based Materials for Air and Water Decontamination

A DISSERTATION

SUBMITTED TO THE GRADUATE SCHOOL IN PARTIAL FULFILLMENT OF THE REQUIEREMENTS

for the degree

DOCTOR OF PHILOSOPHY

Field of Chemistry

By

Diego Mauricio Alzate-Sánchez

EVANSTON, ILLINOIS

September 2019

Polysaccharide-based Materials for Air and Water Decontamination

Abstract

Use of bio-renewable polysaccharides to produce materials with a high technological impact has gained a lot of attention recently. Efforts have been made, for example to produce triboelectric generators from cotton, as well as, nanostructures of chitosan gels for drug delivery. Another well-known example is the use of β-Cyclodextrin (β -CD) derivatives to remove organic contaminants from water that are present at very low concentrations. In this thesis, we study approaches ranging from adsorption to hydrolysis for the removal of contaminants from the environment. In chapter 1, we review the different methodologies employed to abate contaminants from water and air, focusing on those that make use of bio-renewable resources. In Chapter 2, we demonstrate a facile strategy to produce granular adsorbents by depositing β-CD polymers onto cellulose microcrystals. Moreover, the developed adsorbent can remove micropollutants (MPs) in a flow setup, without losing its properties after several cycles of adsorption/desorption. In Chapter 3, we expand the functionalization of the cellulose with the β-CD polymer towards cotton fabrics. The modified fabric preserves the mechanical characteristic of a standard cotton fabric, yet it is able to sequester volatile organic compounds (VOCs) from the air. Following the work with fabrics, Chapter 4 presents a rapid and facile strategy to deposit a Metal Organic Framework (MOF) onto cotton fabrics without the use of solvent or specialized equipment. The MOF deposited on the fabric can hydrolyze a nerve agent simulant, demonstrating the applicability of the composite material. In chapter 5, we explore a strategy to produce a completely bio-based crosslinked polymer. Here, we

install aldehyde groups in the β-CD that can be condensed with the amino groups in chitosan to form a cross-linked network based on imine linkages. The network forms a dynamic hydrogel that is coupled with polyacrylamide to form a double network hydrogel. The double network hydrogel is more flexible and tougher than the individual components, proving the synergistic effect of the combination of the individual hydrogels.

Acknowledgments

My academic, professional and personal life have been fulfilled with outstanding people that have contributed scientifically and emotionally to this dissertation. I would like to start thanking professor William Dichtel for being the caring advisor he is. He decided to bring me with his research group to continue growing as a scientist to Northwestern University, and this is something that I am going to be always thankful for. I also want to thank professor Juan Hinestroza for being the first person in an US institution to believe in my potential as a scientist, and for encourage me to follow professor Dichtel.

I have special thanks to friends and colleagues that I met during my time at Cornell and Northwestern. Dr. Marion Shelling and Simge Uzun from the Fiber Science and Apparel Design Department, which were the first friends and colleagues that I met when I arrived, I truly enjoyed the time spent with both during classes and doing research. Dr. Javier Jaimes and Dr. Daniel Rojas from the Colombian community at Cornell University, that were important to keep me connected with our latino culture. I want to thank all the members of the Dichtel research group from Cornell and Northwestern, all of them have impacted my way of thinking and have directly or indirectly helped me to be a better scientist and person. I would like to extend my thanks to group members that were fundamental in this process. To Professor Brian Smith and Dr. Alaeeddin Alsbaiee for being my first mentors at the Dichtel research group, they were fundamental to have a smooth transition from Engineering to Chemistry. I also want to thank Dr. Michio Matsumoto, his

academic knowledge and vision of what makes a good investigator shaped the scientist I am nowadays. Another special thank goes to Dr. Edon Vitaku for being an outstanding scientist with incredible ideas and a terrific human being, I will always remember all the time we spent together inside and outside of the lab. Also, from the Dichtel group I like to thank the first members of the "cyclodextrin" subgroup Max Klemes and Leilei Xiao, as well as, the new members of the team Luke Skala, Brittany Trang, and Anna Yang, being part of this subgroup was an enriching experience mostly due to the discussion, suggestions and collaborations with them. I also want to thank Debbie Turetsky for being a spectacular mentee, she demonstrated commitment, critical thinking, and willingness to learn; and helped me to increase my skills as a mentor.

I also want to thank all the collaborators that impacted positively with their work this dissertation. This include Yuhan Ling, Chenjun Li and Professor Damian Helbling from the Civil and Environmental Engineering Department at Cornell University. Benjamin Frank and Professor Howard Fairbrother from the Chemistry Department at John Hopkins University. Dr. Timur Islamoglu, Megan Watson and Professor Omar Farha from the Chemistry Department, and Dr, Reiner Bleher from the Biocryo Facility at Northwestern University.

Moreover, my research could not be done without the financial support of several agencies. This research was supported by the National Science Foundation (NSF) through the Center for Sustainable Polymers (CHE-1413862). This research made use of the Cornell Center for Materials Research User Facilities, which are supported by the NSF (DMR-1120296). This work also made use of the IMSERC, and NUANCE facilities at Northwestern University, which have received support from the Soft and Hybrid Nanotechnology Experimental (SHyNE) Resource (NSF ECCS-1542205); the State of Illinois and International Institute for Nanotechnology (IIN). Additionally,

this work was supported by the National Science Foundation under the Center for Sustainable Nanotechnology (CSN), CHE-1503408. Finally, I would like to thank two institution that supported me financially during the first years of my studies. The Organization of the American States (OAS) for supporting me through the program of post-grade academic studies, and COLCIENCIAS for their support through the abroad doctorate students support program.

Finally, I want to give my sincere thanks to my family and friends here in United States and Colombia, first for believing in me, and second for advising and encouraging me during the challenging periods I had to face. Special thanks to my spouse Viviana Obando, she has played an enormous role in the consecution of my goals, always supporting me and encouraging me to continue. My parents Ruby Sanchez and Oswaldo Alzate, who always believed in my potential, my siblings, specially my brother Camilo Alzate and all the other members of my family. Friends have also played an important role during these years. In Colombia, I would like to thank Keler Quintana, Ginna Ossa, Claudia Gonzales, and professor Cesar Sierra for all the conversations, advices, and good times they gave me. Here in the US, I want to thank Matthew Moschitto, Andrea Carlini, Majed Fataftah, Chris Forman, Joaquin Alzola, Jenna Logsdon, and Shelly Rao for all the good moments I had with them. This has been a hard yet gratifying experience, and it was possible due to the support of all the persons involved in the process.

List of Abbreviations and Symbols

1-NA	1-naphthyl amine
2,4-DCP	2,4-dichlorophenol
2-NO	2-naphthol
AC	Activated carbon
Al_2O_3	Aluminum oxide
BA	Benzoic acid
BDC-NH_2	2-aminoterephthalic acid
BMP	Biomethane potential
BPA	Bisphenol A
BPS	Bisphenol S
Brita AC	Activated Carbon from Britta® filters
C_0	Initial concentration
C8	Tetrachloroethylene/water/anionic surfactant/calcium hypochlorite solution
CDs	Cyclodextrins
CD-TFN	β-cyclodextrin polymer
CD-TFN@CMC	β-cyclodextrin polymer deposited on Cellulose Microcrystals

CD-TFP	β-cyclodextrin polymer
CD-TFP@cotton	β-cyclodextrin polymer deposited on cotton fabrics
C_e	Concentration at equilibrium
$Ce_8[Nb_6O_{19}]$	Cesium polyoxiniobate
CH_4	Methane
CMC	Cellulose Microcrystals
CO_2	Carbon dioxide
Cotton-COOH	Carboxylated cotton
CS	Chitosan
CTAB	Cetyltrimethylammonium Bromide
CWAs	Chemical warfare agents
D_2O	Deuterium oxide
DCl	Deuterium chloride
DFP	Diisopropyl flurophosphate
DFP	Diisopropyl fluorophosphate
DFT	Density functional theory
DMAP	4-dimethylaminopyridine
DMF	N,N-dimethylformamide
DMNP	Dimethyl-4-nitrophenyl phosphate
DMSO	Dimethyl sulfoxide
DN	Double network

DS2	Diethyltriamine/ethylene glycol monomethyl ether/sodiumhydroxide
EDS	Energy dispersive spectroscopy
EPI-CDP	Epichlorohydrin β-CD Polymer
Eq	Equation
Equiv	Equivalents
F	Fluorine
FTIR	Fourier-transform infrared spectroscopy
G’	Storage modulus
G’’	Loss modulus
GA	Tabun
GAC	Granular Activated Carbon
GB	Sarin
GD	Soman
GF	Cyclosarin
H_2O	Water
H_2O_2	Hydrogen peroxide
H_2O_2/Fe^{2+}	Fenton’s reagent
HCl	Hydrochloric acid
HP	Heat-press
HPLC	High performance liquid chromatography

HPβCD	Hydroxypropyl-β-CD
HPγCD	Hydroxypropyl-γ-CD
ICP-OES	Inductively coupled plasma optical emission spectroscopy
K_2CO_3	Potassium carbonate
$K_8[Nb_6O_{19}]$	Potassium polyoxiniobate
k_c	Equilibrium constant
K_D	Affinity constant
K_F	Unit capacity coefficient
LC	Liquid chromatography
$Li_8[Nb_6O_{19}]$	Lithium polyoxiniobate
MALDI-TOF	Matrix-assisted laser desorption/ionization-time of flight mass spectrometry
MeOH	Methanol
MOF	Metal organic framework
MPs	Micropollutants
MS	Mass spectrometry
N	Nitrogen
N_2	Nitrogen gas
NA	Nerve agent
NAC	Norit Activated Carbon

$NaHCO_3$	Sodium bicarbonate
NaOD	Sodium deuteroxide
n_F	Freundlich constant
NMR	Nuclear magnetic resonance
NOx	Nitrogen oxides
NP-CDP	Non-porous β-CD Polymer
O_3	Ozone
OH•	Hydroxyl radicals
OSHA	The United States Occupational Safety and Health Administration
P	Phosphorous
PAAm	Polyacrylamide
P-CDP	Porous β-CD Polymer
PEG	Polyethylenglycol
PON1	Mammalian serum paraoxonase
PP	Polypropylene
PS	1,8-bis(dimethylamino)naphthalene
PXRD	Powder x-ray diffraction
q_e	Capacity at equilibrium
q_{max}	Maximum capacity at equilibrium
rpm	Revolutions per minute

S	Sulphur
SEM	Scanning electron microscopy
SOx	Sulphur oxides
STEM	Scanning transmission electron microscopy
TCCA	Trychloroisocyanuric acid
TEMED	N,N,N′,N′-tetramethylethane-1,2-diamine
TEMPO	2,2,6,6-tetramethylpiperidin-1-yl)oxy
TFN	Tetrafluoroterephthalonitrile
TGA	Thermogravimetric analysis
THF	Tetrahydrofuran
TiO_2	Titanium oxide
τ^*	Relaxation time
t_a	Adsorption time
UiO-66	Bencendicarboxylate zirconium mof
UiO-66-NH_2	Amino-bencendicarboxylate zirconium mof
UiO66-NH_2@cotton	Amino-Bencendicarboxylate Zirconium MOF deposited on Cotton
UiO-66-NH_2@cotton-COOH	Amino-Bencendicarboxylate Zirconium MOF deposited on Carboxylated Cotton
US	United States
UV	Ultraviolet

UV-vis	Ultraviolet-visible
VOCs	Volatile organic compounds
XE-555	Activated carbon/cation-exchange/anion-exchange resin adsorbent
XPS	X-ray photoelectron spectroscopy
ZnO	Zinc oxide
Zr_6-node	Dodecanuclear zirconium benzoate cluster
α-CD	α-cyclodextrin
β-CD	β-cyclodextrin
β-CD/CS/PAAm	Chitosan/cyclodextrin/polyacrylamide double network hydrogel
β-CD-CHO	Per(5-formyl-5-dehydroxymethyl)-β-cyclodextrin
β-CD-CHO/CS	Chitosan/cyclodextrin hydrogel
γ-CD	γ-cyclodextrin

This dissertation is dedicated to my wife Viviana Obando for her constant support.

Table of Content

List of Figures

Appendix figures

Chapter 2

Chapter 5

List of Schemes

List of Tables

1. STRATEGIES USED FOR THE REMOVAL OF HARMFUL CHEMICALS FROM THE ENVIORONMENT.

1.1 Preface

In this chapter, I will give insights to the reader about previous and current technologies to mitigate the contamination of the environment. Initially, I will discuss novel strategies used for the removal of contaminants from water. Pollutant adsorption will be emphasized and further expanded upon in chapter 2. Next, I will discuss different approaches for the removal of harmful gases from air. The use of adsorbents for the elimination of gases from the air will be covered chapter 3. In the last part of the chapter, I will discuss the abatement of nerve agents. This topic is closely connected to the removal of contaminants from water and air for two main reasons: the hazardousness of these chemicals and the strategies employed for their elimination. In this section, I will survey the historic background and initial approaches to combating poisoning via these substances. Furthermore, I will discuss the use of catalysis for the deactivation of these compounds, as well as the novel formulations that incorporate those catalysts in more realistic situations.

1.2 Abstract

Over the past 100 years, the human footprint on the earth has increased dramatically, sending tons of contaminants to our water resources, to the atmosphere, and in some cases liberating high amounts of hazardous chemicals in specific locations around the globe. The implementation of strategies to mitigate our impact in the environment are mandatory to ensure the survival of humanity, thus significant efforts have been made by governments, scientists and the public. Waste water treatment plants and decontamination stations have helped in the reduction of contaminants

released to the environment. However, we are facing new challenges derived from the poor removal of contaminants at low concentrations that possess high affinity to water and/or air. In this chapter, I discuss many approaches to mitigate the impact of human activities on the environment. First, we explore novel methodologies to remove micropollutants from water. Then, we focus on the sequestration of volatile organic compounds that are in the vapor phase. Finally, we cover the capture and hydrolysis of nerve agents by different systems. Additionally, throughout the chapter we highlight examples that propose the use of bio-renewable resources in the development of materials that remediate environmental pollution.

1.3 Introduction

The ecological impact of industrialization can be found everywhere. One major problem is the contamination of our water resources by heavy metals,[1] pharmaceuticals[2] and pesticides.[3] Additionally, human activities significantly contribute to air pollution by producing and sending enormous amounts of greenhouse gases,[4] volatile organic compounds[5] and particulate matter[6] into the atmosphere. Other sources of contamination that are acutely hazardous over a much shorter period of time, are the use of chemical weapons on the battle field.[7] The use of these chemicals has been proven to be a threat, not just to human life, but to any living organism that comes into contact with them. Therefore, different strategies to get rid of these contaminants have been explored by the scientific community.

Water contamination comes from different sources, which are summarized in Figure 1.1. One of the highest contributors to water contamination is agricultural runoff that sends pesticides to the rivers.[8] A recent study by Posthuma and Zwart demonstrated that the presence of toxic mixtures

in some Ohio rivers come from agricultural activities, and they negatively affected the population of several species of fish.[9] Additionally, in some developing countries that do not have strict policies about contamination, rivers are polluted with harmful metals like mercury or anions like cyanide which are commonly used in the extraction of gold.[10,11] For example, Malm studied the amount of mercury in sediment, soil, air, fish and humans in three Amazonian rivers. He found high levels of mercury focused in areas with a history of gold mining. Moreover, he discovered significant levels of mercury in some areas away from the gold mines.[12] In general, the purpose of waste water treatment plants is to remediate contaminated water, and depending on the location, the process has slight variations.[13] Despite various differences, all the different setups contain flocculation, precipitation, filtration and bleaching steps.[14] Still, these decontamination steps do not remove all the pollutants dissolved in water, specially contaminants, that tend to be in very low concentrations.[15] Therefore, novel procedures like advanced oxidation,[16] reverse osmosis[17] and adsorption[18] are envisioned to improve the water quality that is released to the environment.

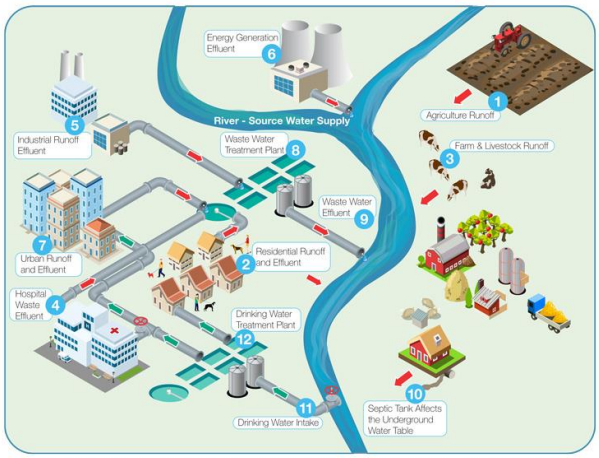

Figure 1.1 Source points of emerging contaminants. Image taken with permission from www.thermofisher.com.

In addition to water contamination, human activities also have an enormous effect on the quality of air. Use of fossil fuels in our homes, transportation and industries sends 40 billion tons of CO_2 to the atmosphere per year, according to a 2014 study.[19] Moreover, the burning of the fossil fuels also liberates other molecules like SOx and NOx to the atmosphere on a lower scale (tens of million tons).[20] Consequently, Bernard et al. demonstrated that more than 5 million people in the US have been exposed to harmful gases to levels above the National Ambient Air Quality Standard.[21] Another class of air contaminants produced by human activities, are small organic molecules that have high vapor pressures, known as volatile organic compounds (VOCs).[22] These compounds are generally discharged to the atmosphere in manufacturing and treatment plants.[23] Dahlgren et al. assessed the exposure of residents living near a wood treatment plant to a different gas contaminants. They found high levels of polycyclic aromatic hydrocarbons and combustion products in the soil, the homes and the blood of the residents. Moreover, the air level of the VOCs benzo(a)pyrene and tetrachlorodibenzodionin in this neighborhood exceed the recommended levels for these compounds.[24] Plants that generate or use VOCs mitigate their release to the atmosphere using activated carbon, solvents, cooling columns, and other less common methods.[25] However, some of these processes are inefficient, and the active material also gets exhausted in short periods of time, producing a runoff of the VOC.

Chemical weapons are not generally classified as contaminants. However, the impact they have over the ecosystems in the short term is similar to the impact that pesticides have over the long term. Consequently, effective and quick methodologies are needed to remove this kind of contaminant from water and air. Among all the chemical weapons, nerve agents (NAs) have been highly used, being involved in recent attacks to people around the world.[26,27] NAs are highly

reactive molecules that disrupt the nervous system by inhibiting the function of the enzyme acetylcholinesterase, producing a loss of control of bodily functions and even death.[28] Different ways to prevent poisoning with NAs have been proposed, including the use of the antidote atropine[29] and hydrolysis by mildly basic solutions of sodium carbonate.[30] However, these methods are slow, and do not remove completely the NAs. Recently, several groups have explored the catalytic properties of metal organic frameworks (MOFs) in the hydrolysis of NAs.[31] The Farha group demonstrated that the MOF UiO-66-NH_2 is able to hydrolyze 50% of methyl-paraoxon (a NA simulant) in just 1 min,[32] which has led to the application of MOF-type materials in organophosphorus nerve agent poisoning prevention.

1.4 Removal of Micropollutants from Water

Emerging contaminants are chemicals and microbial agents that were not traditionally considered pollutants. However, their increase in environmental concentration and their persistence in the environment have recently attracted attention. The rise in occurrence of these contaminants can be associated with industrial, agricultural and municipal activities.[33,34] Therefore, approaches to decrease the concentration of these chemicals in wastewater treatment plants and water potabilization stations are necessary. I will cover three of the most promising methodologies to remove a class of emerging contaminants known as organic micropollutants.

1.4.1 Advanced Oxidation of Micropollutants

Advanced oxidation is a process that relies on the reaction of organic micropollutants with hydroxyl radicals (OH•) that are produced *in situ*.[35] These radicals can be formed from ozone (O_3),

hydrogen peroxide (H_2O_2) and transition metals that are activated by auxiliary energy sources such as UV radiation, an electronic current, or ultrasound, among others.[36] Research has been focused on finding the appropriate combination of reagents that completely mineralize organic micropollutants dissolved in water. In a recent report, Oturan et al. explored the use of electrochemical oxidation to generate Fenton's reagent (H_2O_2/Fe^{2+}) *in situ*. In their study, platinum and boron-doped diamond anodes were used for the mineralization of 55 micropollutants dissolved in a landfill leachate. By studying the concentration of the contaminants after advanced oxidation, the authors claimed that their process removed 49 compounds with an efficiency higher than 99%.[37]

1.4.2 Reverse Osmosis and Nanofiltration

Reverse osmosis and nanofiltration both use semipermeable membranes to remove pollutants from water. The membranes for both of these techniques should allow water molecules to pass freely but should not allow large molecules, ions or organic molecules to pass through.[38] The removal mechanism in reverse osmosis is based on size exclusion and diffusion of the molecules. Therefore, the process efficiency depends on pressure, flow rate and pore size.[39] Several materials have been proposed as membranes for the removal of organic molecules.[40] Some of these membranes have a judicious design of their pore size and functionalities that prevent fouling, however it reduces the selectivity and the efficiency of the membranes.[41,42] Recent work by the Elimelech group overcame this challenge, where the authors obtained a highly selective membrane from a sustainable polymer that resists fouling. In their report, the authors used 1,3,5-tris(1H-benzo[d]-imidazol-2-yl)benzene to template linoleic acid through hydrogen bonding. The

supramolecular structure self-assembled to form vertically aligned pillars. Then, they crosslinked the double bonds in the linoleic acid and removed the template, resulting in a membrane with a defined pore size (Figure 1.2). The authors tested the rejection ability of the membrane with molecules that have different charges and sizes. They found that molecules with a diameter between 1.2-1.4 nm and a positive charge are adsorbed by the membrane, while molecules with a diameter greater than 1.5 nm and/or with a negative charge are rejected by the membrane.[43]

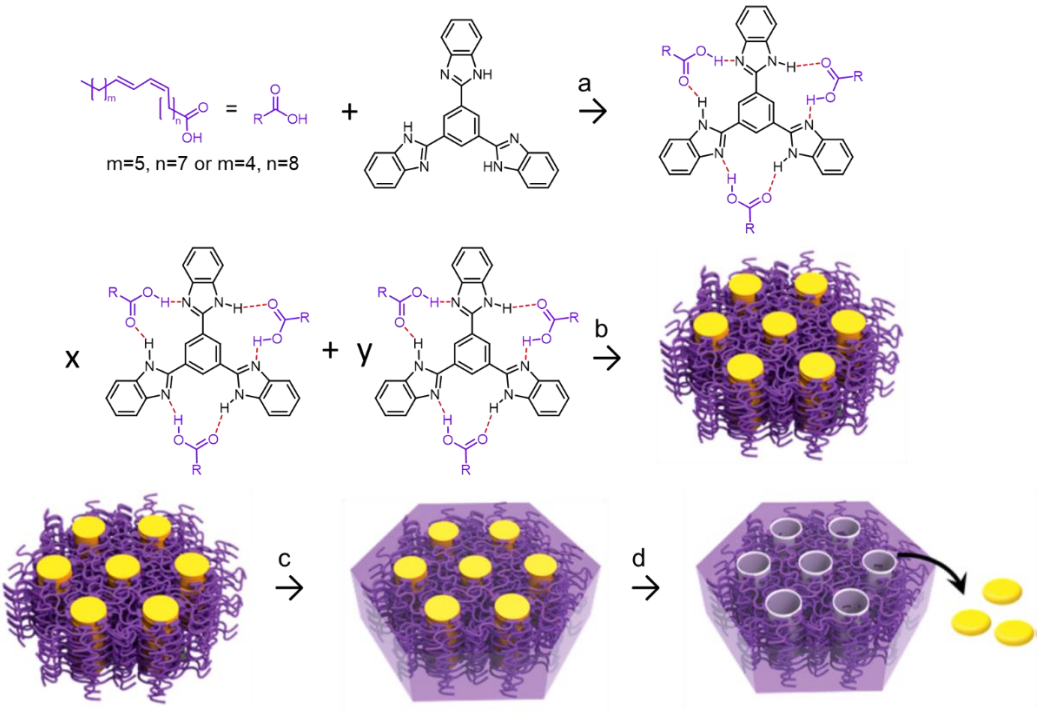

Figure 1.2 Fabrication of the ordered membranes from natural fatty acids. a. Templation of the fatty acids. b. Self-assembly of the templated fatty acids to form pillars. c. crosslinking of the double bonds. d. Removal of the template to generate the pores. Image adapted with permission from *ACS Nano* **2017**, 11 (4), 3911-3921. https://pubs.acs.org/doi/10.1021/acsnano.7b00304. Further permissions related to the material excerpted should be directed to the ACS.

1.4.3 Adsorption of Micropollutants from Water

Adsorption in liquid solutions can be defined as the accumulation of a substance at the liquid/solid interface by means of physical and chemical processes.[44] Adsorption is the most widely used technology for the removal of emerging contaminants, and numerous adsorbents have been proposed to remove pollutants, ranging from heavy metals to pathogens.[45,46] A good adsorbent should be reusable, have high capacity, fast uptake, ability to remove contaminants at low concentrations (high affinity), and should not be fouled by spectator molecules.[47] However, there are other important properties that are not always considered to classify adsorbents; like facility of regeneration, use of bio renewable resources, low energy consumption for manufacturing, and compatibility (stability) with the medium.

Activated carbon is the most common adsorbent to remove a broad spectrum of contaminants.[48] It is a highly porous material that provides a large surface area to which contaminants might adsorb. Therefore it has high capacity and fast uptake of different pollutants at high and low concentrations.[49,50] However, activated carbon is easily fouled by natural organic matter, decreasing its effectiveness to remove contaminants at low concentration.[51] Moreover, activated carbon production and regeneration requires enormous amounts of energy, rendering reusability inconvenient and impractical.[52] Alternative adsorbents to activated carbon such as clay minerals, zeolites, metal oxides, agricultural wastes and polymeric materials have been successfully used in the removal of contaminants from water.[53] But, high production energies, low renewability, and high toxicity have hampered the implementation of some of those adsorbents. Although traditional adsorbents suffer from these drawbacks, several studies have demonstrated that adsorbents based

on cyclodextrins are promising candidates to outperform the adsorption properties of activated carbon.[54]

Cyclodextrins (CDs) are cyclic oligosaccharides composed from α-D-glucopyranose units linked by 1,4-glycosidic bonds. CDs are produced by an enzymatic degradation of starch and can be obtained in different sizes. The most abundant and commercially available CDs are α-CD, β-CD and γ-CD (Figure 1.3). CDs have toroidal shape, in which the primary and secondary hydroxyl groups are located in the small and large openings of the toroid, respectively, rendering their exteriors hydrophilic. In contrast, the interior of CDs bear a tetrahydropyran moiety that is considerably less hydrophilic than the exterior of CDs. Due to their exterior hydrophilic character, CDs are soluble in water. Additionally, their interior hydrophobic cavity, allows CDs to form host-guest complexes with thousands of organic compounds.[55]

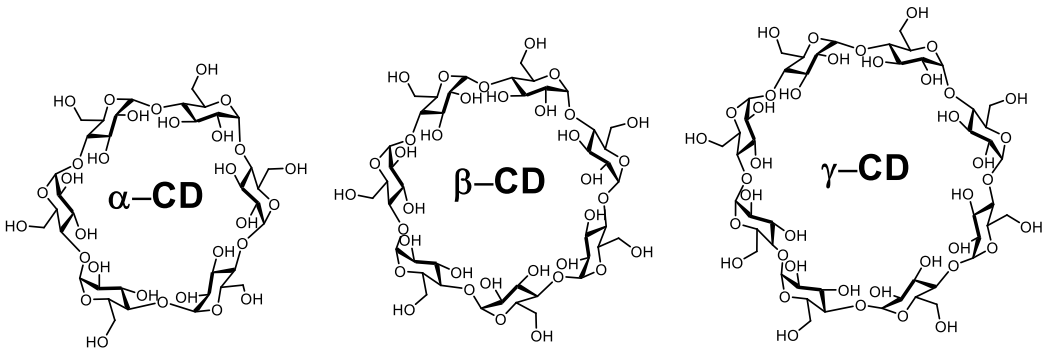

Figure 1.3 Structure of α-CD, β-CD and γ-CD. 6, 7 and 8 α-D-glucopyranose units respectively.

CDs are soluble in water; therefore, they cannot be used directly to remove contaminants from water. Consequently, different crosslinkers like epichlorohydrin, di-isocyanates and polycarboxylic acids have been used to produce water insoluble CD polymers, which are

envisioned to remove contaminants from water.[56,57] However, most of these polymers lack important characteristics of a good adsorbent, such as fast uptake and high capacity. Recently, we solved these problems by synthesizing the first highly porous β-CD polymer, by employing a novel crosslinker (tetrafluorophtalonitrile). The new β-CD polymer can remove bisphenol A (a model pollutant) from water in just seconds, outperforming other β-CD polymers and high-class activated carbons (Figure 1.4a). Additionally, the β-CD polymer can uptake a variety of pollutants at environmentally relevant concentrations, demonstrating not just fast uptake, but also high affinity (Figure 1.4b).[58] We also have demonstrated that by tuning the crosslinker and/or changing its functional groups, we can target specific contaminants like polyfluoroalkyl substances.[59]

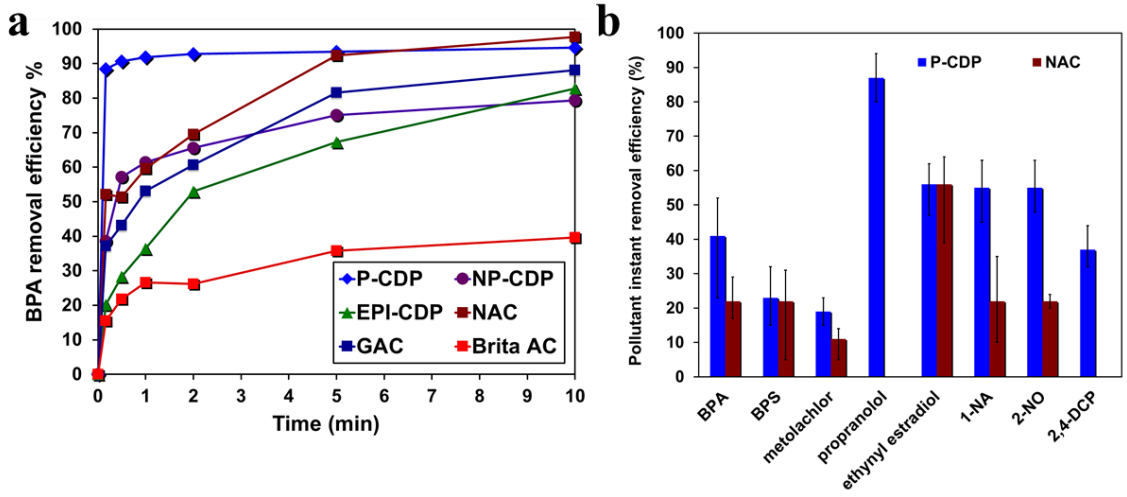

Figure 1.4 a. Time-dependent adsorption of aqueous bisphenol A (0.1 mM) by each adsorbent (1 mg mL−1) P-CDP: Porous β-CD polymer, EPI-CDP: Epichlorohydrin β-CD polymer, GAC: Granular activated carbon, NP-CDP: Non-porous β-CD polymer, NAC: Norit activated carbon, Brita AC: Activated carbon from Britta® filters. b. Percentage removal efficiency of a pollutant mixture obtained by rapidly flowing the adsorbate solution (8 ml) through a thin layer (0.3 mg) of

P-CDP (blue) or NAC (red). Individual pollutant concentrations (in units of μg L^{-1}) in the mixture were: 100 (BPA); 2.5 (BPS); 5 (metolachlor); 100 (propranolol); 50 (ethinyl oestradiol); 5 (1-NA); 25 (2-NO); and 2.5 (2,4-DCP). Image adapted with permission from *Nature* **2016**, 529, 190-194. https://www.nature.com/articles/nature16185.

CD polymers are not the only bio renewable adsorbents. Several groups have demonstrated the utility of modified cellulose and chitosan in water remediation.[60] For example, incorporation of negative charges on the surface of cellulose particles enhances the adsorption of cationic molecules. He et al. explored this approach by synthesizing carboxylated cellulose nanocrystals via hydrolysis of microcrystalline cellulose with ammonium persulfate. Adsorption studies performed with methylene blue (a cationic dye) showed a maximum capacity of 127 mg of dye per gram of cellulose, the authors also demonstrated the adsorbent can be reactivated by an acetonitrile washing.[61]

1.5 Sequestration of Volatile Organic Compound from Air

Volatile organic compounds (VOCs) are organic molecules with low boiling points due to their high vapor pressure. Therefore, VOCs evaporate or sublimate easily and enter the surrounding air. VOCs are emitted into the atmosphere from both anthropogenic and biogenic sources. [62,63] On a worldwide basis, VOCs coming from biogenic sources are more abundant than the ones coming from anthropogenic sources. However, in specific locations like highly populated cities, the VOCs produced by anthropogenic sources dominate.[64]

VOCs generated by anthropogenic sources are considered contaminants, because they have a negative impact in the environment and in our health.[65] Typical anthropogenic emissions results from vehicles, landfills, refineries, solvent usage and industrial facilities.[66] Different approaches have been implemented for the removal of VOCs, and those methodologies depend on the application. For instance, the technology used to remove VOCs from an industrial facility is different from the technology used in a respirator mask. The most common techniques employed for the removal of VOCs are oxidation, absorption and adsorption.[25]

1.5.1 Oxidation of VOCs

Oxidation of VOCs encompasses thermal, catalytic and digestive strategies. Thermal oxidation occurs in fume incinerators held between 700 to 1000 ºC, that eliminate 95-99% of all the VOCs produced in the facility. However, this method requires high amounts of energy. [67] Catalytic oxidation is an alternative to reduce the high energy inputs needed for thermal oxidation, because the use of catalysts like noble metals or oxides dramatically reduces the temperatures required to degrade the VOCs, while maintaining the same efficiency.[68] Nevertheless, catalytic oxidation also suffers from drawbacks, such as catalyst poisoning, partial oxidation of the VOCs, and high cost of the catalysts. The last oxidation method is the digestion of the VOCs by microbes. Herein, microorganisms convert VOCs to water, carbon dioxide and biomass.[69,70] This technology does not require high amounts of energy and is environmentally friendly. However, it is not as versatile and robust as the previous oxidation techniques because it does not work on hydrophobic VOCs, due to the low bioavailability and slow biological oxidation of these compounds.[71] In general, removal of VOCs by oxidation is widely used in industrial facilities and vehicles. However,

complete mineralization of the VOCs to CO_2 and water is challenging, producing even more harmful chemicals in some cases.[72] Therefore, techniques that remove VOCs by sequestration are an exciting alternative.

1.5.2 Absorption of VOCs

Absorption removes the VOCs from a gas stream by dissolving them in a liquid solvent. Typically, VOCs will be absorbed depending on their solubility in the solvent used. An increase in the absorption can be accomplished by using reagents that strongly interact with the VOC that needs to be removed.[73] For example, removal of acidic VOCs is more effective if a basic solvent is used. Different liquids and liquid mixtures have been employed to remove VOCs by absorption, one of which being ionic liquids. Recently, in a report by Quijano et al. the authors used two of the most common imidazolium ionic liquids to absorb dimethyl sulfide, dimethyl disulfide and toluene. The authors showed that the partition coefficients, a value used to evaluate the effectiveness of absorption, were comparable to typical liquid absorbents.[74] Though absorption is a very effective method to remove VOCs, it is a process more suitable for industry. In this application, it is possible to design absorption towers that provide the liquid and vapor more contact area and time to facilitate mass transfer.[75] Thus, new methodologies to remove VOCs that can be used outside of industrial facilities are required.

1.5.3 Adsorption of VOCs

Gas adsorption is a surface phenomenon. In this process, the atoms, ions or molecules from a gas are adhered to the surface of the adsorbent. The adsorption of gaseous molecules has the same

characteristics of the adsorption of contaminants dissolved in water (section 1.4.3). In industry, activated carbon is also the most common adsorbent used to remediate VOC emissions. Activated carbon has a high capacity towards VOCs due to its high surface area and can be packed into towers that facilitate interaction with the gas stream.[76,77] However, activated carbon regeneration requires heating up the adsorbent to remove the VOCs, which will send the trapped VOCs to the atmosphere again. Also, the efficiency towards certain VOCs is highly affected by the presence of water in the gas stream, due to a competition of the water molecules with the VOCs for active sites of the adsorbent.[78]

Adsorption has also been used outside of industry. It has been used to remove VOCs in gas masks respirators,[79] functional garments[80] and some gas filters.[81] For instance, Ramos et al. designed a carbon cloth derived from cellulose for VOC adsorption. In their report, the authors impregnated cellulose strips with phosphoric acid, and then heated the strips up to 864 °C and 963 ºC. The authors found that the cellulose treated at 963 ºC has higher surface area than the one treated at 864 ºC. Afterwards, the authors evaluated the capacity of the cloths to adsorb *n*-hexane, benzene and toluene in the gas phase at 25 ºC. The results indicate that the cloth with the higher surface area has higher capacity towards the three VOCs, with benzene being adsorbed the most effectively (7.45 mmol benzene/g of fabric).[82]

Cyclodextrins have also been used in the removal of VOCs, due to the high affinity that they possess toward organic molecules. Contrary to the adsorption of organic molecules in water, adsorption in the gas phase can be done with native CDs. However, due to their low porosity, the gas transport of VOCs is tortuous, and the adsorption process is inefficient. Nevertheless,

adsorption of VOCs using CDs as the active materials has been reported.[83] Recently, Celebioglu et al. increased the surface area of hydroxypropyl-β-CD (HPβCD) and hydroxypropyl-γ-CD (HPγCD) by forming nanofibers via electrospinning. The nanofibers' high surface area is hypothesized to enhance the efficiency of the interaction between the CDs and the VOCs. The authors tested the ability of both powdered CDs and their nanofibers to remove benzene and aniline in the gas phase, and they found that the CD nanofibers possess a higher capacity than the CD powders. Additionally, HPβCD has a higher capacity than HPγCD due to the high binding constant of HPβCD with aniline and benzene.[84]

Crosslinked polymers of CDs have also been employed for the removal of VOCs.[85] But more interestingly, the crosslinkers are also being used to graft CDs to different substrates. Cellulosic materials like cotton fabrics are an interesting support because they can be directly used as protective gear. In line with this approach, Dehabadi et al. fixed β-CD on cotton fabrics using polyaminocarboxylic acid as the crosslinker, which forms amide linkages between the glucose units of the cellulose and the β-CD (Figure 1.5). The authors studied the influence of various parameters on the grafting efficiency of β-CD onto the cotton fabrics. Then, they tested the ability of the modified cotton fabrics to sequester cyclohexane, chlorobenzene, cyclohexen-1-one and toluene in the gas phase.[86]

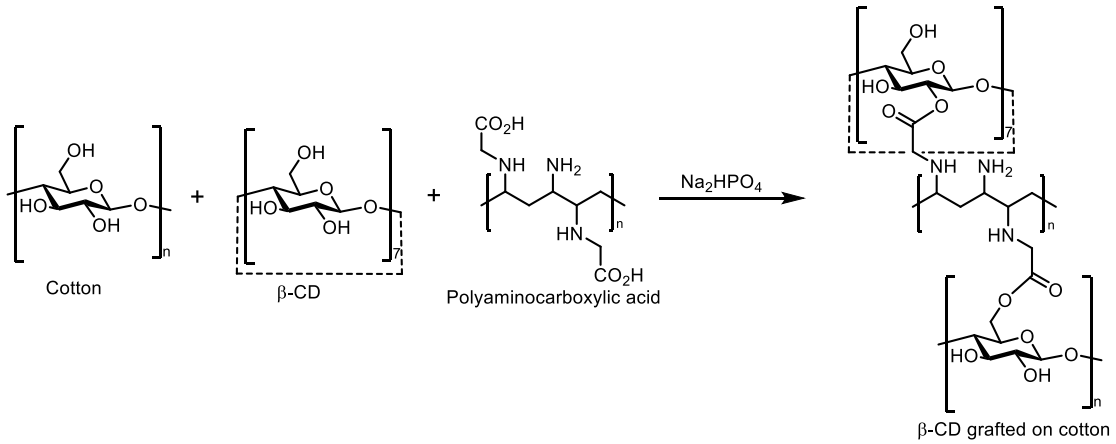

Figure 1.5 Reaction scheme of the functionalization of cotton fabrics with β-CD, using a polyaminocarboxylic acid as the crosslinker.

1.6 Hydrolysis of Organophosphorus Nerve Agents

Organophosphorus compounds are highly lethal molecules discovered during the development of pesticides in the 1930s by the chemist Gerhard Schrader when he was working for the German chemical company IG Farben. He was subsequently recruited by the Nazi government, and during this time he discovered four more NAs, that were denominated as the G-series (Figure 1.6a).[87] Later, in the 1950s Imperial Chemical Industries discovered additional organophosphorus compounds when they were developing new pesticides. Due to their high toxicity, the British Armed Forces continued their study, and labeled them the V-series (Figure 1.6b).[88] G-series compounds are non-persistent and react rapidly with water in the environment. In contrast, V-series compounds are persistent chemicals that degrade slowly, are difficult to wash away, and can remain on clothes or other surfaces for long periods of time.[89]

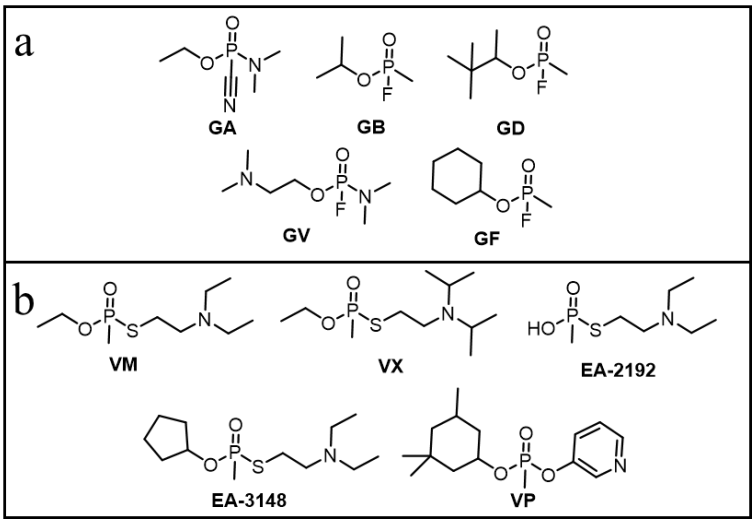

Figure 1.6 a. Structures of selected G-series organophosphorus compounds. b. Structures of selected V-series organophosphorus compounds.

The deactivation of these NAs is accomplished by the hydrolysis of the highly reactive P-X bond in alkaline water, where X can be F, N, S, etc.[90] However, more efficient ways of decontamination are necessary, specifically in places like battlefields, laboratories, pilot plants, storage and destruction areas, where there is a high probability of a NA leak. Different methodologies for the deactivation of NAs have been proposed, and some of them are currently in use on the battlefield.[91] In this section I will cover different strategies to eliminate NAs.

1.6.1 Liquid Media Hydrolysis

Decontamination of NAs can be done using nonaqueous and aqueous solutions. Nonaqueous solutions like DS2 (diethyltriamine/ethylene glycol monomethyl ether/sodiumhydroxide, 70/28/2) offer good solubility of the NAs, but large amounts of organic waste are generated. Moreover, the solution can damage materials such as plastic and leather. Additionally, it is corrosive to the skin.[92]

Water is a good medium to deactivate NAs, but the solubility of these compounds is low in aqueous solutions, requiring additional reagents to improve decomposition of the NA.[30] Consequently, a combination of solubility and reactivity are necessary for liquid media hydrolysis. Therefore, a mixture of aqueous and non-aqueous solutions is envisioned to be more effective in the deactivation of NAs. This strategy is exemplified by an emulsion of tetrachloroethylene/water/anionic surfactant/calcium hypochlorite (15/76/1/8) known as C8. This emulsion is non-corrosive and can penetrate into paint and react with adsorbed NAs without damaging it.[92] However, this emulsion suffers from being high-weight and unstable. Thus, strategies to remove NAs that are easier to be carried out are necessary.

1.6.2 Solid sorbents for Nerve Agents Capture

Solid sorbents are an alternative to liquid solutions because they have high capacity and reduced weight, which facilitates their transport, especially for soldiers on the battlefield. Additionally, they are less toxic than liquid solutions of organic solvents. Solid sorbents can be embedded into fiber pads for ease of use, and in general the active material is a combination of sorbents. For example, a sorptive cloth trademarked as XE-555 consist of an adsorbent (activated carbon), a cation-exchange resin, and an anion-exchange resin.[93] Ideally, the sorptive resin will trap the NAs. Then, the physisorbed NAs are hydrolyzed by the exchange resins. However, several studies have demonstrated that while the adsorption process is efficient, the hydrolysis of the NAs by the exchange resins is very slow or null[92] Hence, more efficient solid sorbents to hydrolyze the NAs will contribute to the development of better decontamination systems.

1.6.3 Catalytic Deactivation

The methods discussed in the previous sections were the first approaches for the deactivation of NAs. However, current state-of-the-art decontaminants rely on the use of catalysts that degrade the NAs in short times and with high efficiency.[94] The first catalytic systems proposed for the hydrolysis of NAs were metal ions and enzymes in aqueous solutions.[95] More recently, different approaches to generate better catalysts have been addressed.[96,97]

Recently, Kinnan et al. reported the use of polyoxiniobates, a class of polyoxometalates, for the degradation of NAs. The authors suggested that these polyatomic ions can be dissolved in aqueous and nonaqueous solvents, are stable when exposed to environmental factors like UV light, and can be easily attached to supports like fabrics. The researchers synthesized three polyoxiniobates ($Li_8[Nb_6O_{19}]$, $K_8[Nb_6O_{19}]$ and $Ce_8[Nb_6O_{19}]$). Then, they studied the kinetics of the hydrolysis of two NAs (GB and GD) and the simulant diisopropyl fluorophosphate (DFP). Hydrolysis of the simulant by the lithium polyoxiniobate is faster compared to the other two catalysts when they are used in solution. However, the rate of hydrolysis is lower for the three polyoxiniobates when they are used in a heterogeneous system *i.e.* the half-life increased from 3.2 h in solution to 10.38 h in suspension for $Li_8[Nb_6O_{19}]$. Hydrolysis of the NAs was done using the suspension, and the authors found a much faster hydrolysis of the NAs compared to the simulant (DFP $t_{1/2}$=10.38 h, GD $t_{1/2}$=0.27 h and GB $t_{1/2}$=0.03 h for $Li_8[Nb_6O_{19}]$), which encourages the incorporation of polyoxiniobates to a support for heterogeneous NAs hydrolysis.[98]

In an interesting report, Gupta et al. explored the catalytic hydrolysis of organophosphorus compounds by directed evolution of hydrolases enzymes. First, the authors identified that the

enzymes used as antidotes for NAs poisoning were not effective in degrading the more toxic S_p isomer of the G-series compounds.[99] The authors selected the mammalian serum paraoxonase (PON1) as a starting point for directed evolution for three reasons: it only shows promiscuous hydrolysis of organophosphate compounds, has low catalytic efficiency, and it reacts primarily with the less toxic R_p NAs isomer. The authors applied random and targeted mutagenesis of PON1 to select enzymes with major potential to degrade the toxic S_p isomer of a cyclosarin (GF) simulant. Then, to increase selectivity for the actual nerve agent, the authors developed a method to generate GF *in situ* and used it to select the enzymes that most effectively hydrolyze it. This strategy allowed the authors to go from a S_p-cyclosarin hydrolysis rate of 0.13 μM/min for the wild type enzyme to 17.5 μM/min for the most evolved enzyme, which is an increase in the hydrolysis efficiency of 135 times. Moreover, the authors tested the *in vivo* prophylactic activity of their evolved enzyme in mice. They found that mice injected with 2.2 mg/kg of the enzyme increases the survival rate from 0 to 75% when 290 μg/kg of the cyclosarin simulant was administrated, while the wild type enzyme shows no increase in the survival rate under the same conditions.[100] This report demonstrates an approach to make catalysts more efficient towards the selective hydrolysis of NAs, and extrapolation of the catalyst used in a more realistic scenario.

Catalysts for the hydrolysis of organophosphorus compounds that combine the stability and applicability of polyoxometalates, with the efficiency and selectivity of enzymes are a promising area of ongoing research. Recently, due to the advances of metal organic frameworks (MOFs) stability against water hydrolysis, research groups around the world have started to consider this type of materials for the catalytic degradation of NAs.[101] MOFs are compounds consisting of metal ions or clusters of ions coordinated by organic linkers that form three dimensional structures.[102] In

general, MOFs are porous crystalline materials that have been used for gas storage, separation and catalysis.[103–105] Different groups have demonstrated that the metal ions present in MOFs can catalytically hydrolyze compounds with a phosphoester functionality.[106] For example, the Farha group demonstrated that a twelve-coordinate Zr_6-based MOF (UiO-66) can hydrolyze a nerve agent simulant (4-nitrophenyl phosphate, DMNP) in aqueous solution.[107] Further studies demonstrated that the hydrolysis mechanism of UiO-66 is similar to the mechanism of phosphotriesterase enzymes.[108] Many groups have focused on the increase of the hydrolysis efficiency of NAs in water by different MOFs, reaching half-life values as low as 30 seconds.[109] However, approaches related to the incorporation of such MOFs into fabrics or filters, while preserving the integrity and activity of the catalyst are scarce.[110,111] An interesting approach for the incorporation of the MOF UiO-66-NH_2 into a textile was proposed by Lee et al. In their report, the authors coated a non-woven polypropylene (PP) fabric with three different metal oxides (Al_2O_3, TiO_2 and ZnO) via atomic layer deposition. Next, they prepared a suspension of a pre-synthesized UiO-66-NH_2 with β-CD and cetyltrimethylammonium bromide (CTAB). Then, they immersed the coated fabrics in this suspension to deposit the MOF. The use of β-CD and CTAB promotes the surface attachment of the MOF and prevents the solution-phase agglomeration of the MOF crystals. The authors demonstrated that UiO-66-NH_2 on the fabric preserves its crystallographic and sorptive properties. Moreover, the polypropylene fabric coated with zinc oxide has the highest amount of MOF attached (30.7%). Finally, the authors studied the catalytic degradation of DMNP in aqueous solution by both UiO-66-NH_2 powder and UiO-66-NH_2 attached to fabric. Under their reported conditions, UiO-66-NH_2 does not lose efficacy in hydrolyzing DMNP when it is attached to the polypropylene fabric. They found a half-life of 6.5 min for the hydrolysis of DMNP by the

fabric and the powder when the same amount of MOF is used. This is in contrast with, the initial fabric and the ZnO-coated fabric which show no significant hydrolysis of DMNP (Figure 1.7). Additionally, the authors demonstrated that shorter lifetimes (2.8 min) can be reached by increasing the amount of MOF-fabric used for the hydrolysis.[112] MOFs are very interesting materials for the deactivation of NAs, because they combine the high catalytic activity seen in enzymes, with the facility to incorporate metal-organic materials in different supports.

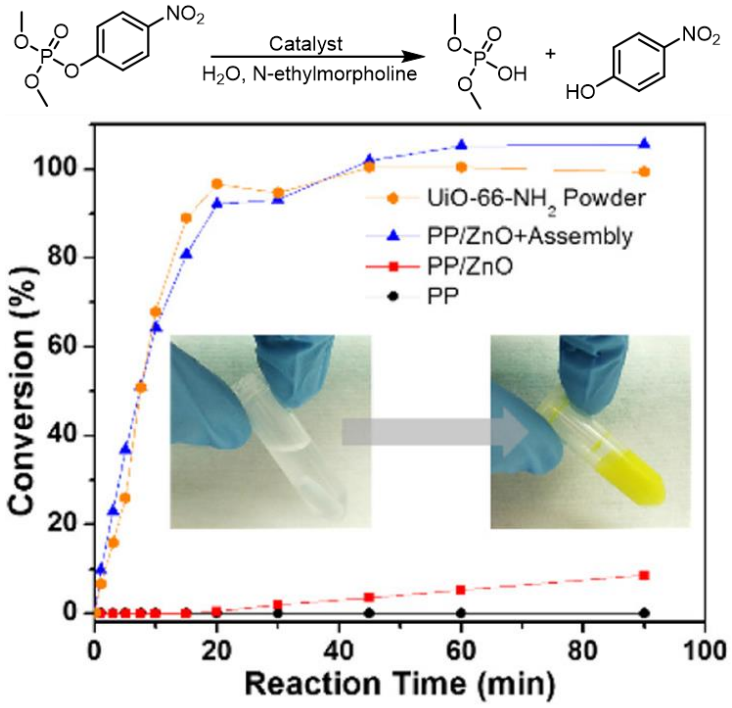

Figure 1.7 Conversion profiles for the hydrolysis of DMNP in the presence of PP, PP/ZnO, PP/ZnO + Assembly, and UiO-66-NH2 powder at room temperature as a function of time. Image adapted from *Chem. Mater.* **2017**, *29* (11), 4894–4903. https://pubs.acs.org/doi/abs/10.1021/acs.chemmater.7b00949 Further permissions related to the material excerpted should be directed to the ACS.

1.7 Future Directions

Developing novel strategies to mitigate the effects of contaminants is a current research priority of scientists around the globe. Important advances in the potabilization of water have been demonstrated, but there is still room for improvement. In terms of micropollutant removal, technologies like advanced oxidation, ultrafiltration and adsorption have drawbacks that can be addressed if techniques are combined. For example, adsorption of MPs from water removes the contaminants from the solution. However, they are incorporated into the adsorbent, and there is no consensus on the best way to manage the contaminated adsorbent. Therefore, strategies that not only adsorb but eliminate the contaminants are desired. On this front, research that combines adsorption with advanced oxidation will be promising to remove and mineralize the MPs. Another front in the area of water purification is the prevention of fouling. Fouling is a serious problem that faces ultrafiltration and adsorption techniques. Prevention of fouling during adsorption is key to avoiding loss in efficacy of the adsorbent, and this can be addressed by synthesizing an adsorbent with more specific binding sites. Therefore, it is important to incorporate supramolecular hosts in the development of adsorbents to target specific families of contaminants. Finally, combination of adsorbents with selectivity towards groups of compounds, instead of generating a general adsorbent, will be the way to develop an outstanding material that can be used to remove a larger scope of pollutants.

Removal of VOCs from air is important, especially for communities living near industrialized areas that tend to have higher levels of contamination. However, current efforts to develop adsorbents applicable to gas removal are powder-like materials, which are not suitable in real-life

situations. Therefore, the focus in upcoming years should be in the incorporation of adsorbents onto supports. Finding the best way to deposit and adhere an adsorbent onto fabrics is an urgent priority. Additionally, approaches to avoid deterioration of the adsorptive properties of materials when they are incorporated into the support are envisioned as a hot topic in the near future. Finally, incorporation of detection systems that alert the user when the adsorbent is saturated are important. Some work has been done in this area, but there is still room for improvement, particularly in finding sensors that do not react immediately with the contaminant, but instead when the adsorbent is saturated.

The field of catalyst development for the hydrolysis of nerve agents is constantly evolving, and reports improving our understanding of the mechanism and its implications to produce better catalysts are continuously being published. However, most of the catalysts are still being tested in non-realistic situations. The field needs to move away from hydrolysis in aqueous solutions and implement ways to test their catalysts when the NA, or the simulant is in the air. Another important factor that was discussed in the previous paragraph, but that also applies for the development of NAs catalysts, is their incorporation into supports. Once again, fabrics are ideal substrates, because their transition from the laboratory to real-life is faster. The scientific community should start evaluating and improving the catalytic activity when the NA is in the air, and when the catalysis is deposited on a support.

Finally, fulfillment of green initiatives has to be addressed in developing new adsorbents or catalysts. Use of greener reagents and solvents as well as bio renewable resources, are encouraged in the development of new technologies for the decontamination of the environment.

1.8 Conclusions

Contamination of the environment by human activities ranging from food production to war is a serious threat that is affecting all the living organisms in our planet. We humans are responsible for this contamination, and we need to find efficient ways to control it. In this chapter, I summarized strategies for the control of specific contaminants, placing emphasis on the use of green alternatives to remove them.

Removal of micropollutants from water is gaining a lot of attention due to the negative effect of these contaminants, even at low concentrations. Herein, I showed different methodologies like advanced oxidation, ultrafiltration and adsorption to remove them. Additionally, I demonstrated that adsorption is an easy and scalable strategy for the removal of these contaminants from water. Moreover, I discussed novel adsorbents based on β-cyclodextrin that could potentially replace the classic activated carbon.

Other kinds of contaminants that spread out easily are volatile organic compounds. Although this name includes many types of compounds, I focused on those that are manmade and come from manufacturing processes, oil burning and byproducts release. The removal of these types of compounds is highly related to the point of source, and different strategies are used depending on if the VOC is generated in an industry or in the use of a household product. However, adsorption is a very effective way to capture these compounds independently of their point of source. Activated carbon is the main material used for capture of hazardous gases, but I showed that cyclodextrins and their derivates are starting to gain attention due to the advantages that these materials have over activated carbon.

Finally, I classified nerve agents as a special class of contaminants due to their hazardousness. Although they are not generally considered contaminants, I demonstrated that strategies used in the removal of MPs from water and VOCs from air have been used for the removal of nerve agents. Furthermore, I discussed the early strategies used in the battlefield to neutralize these compounds, as well as the drawbacks of such methodologies. Finally, I jumped to new materials that can catalytically hydrolyze nerve agents in short periods of time in different scenarios. I placed particular emphasis on the use of hydrolytically stable MOFs as novel catalytic systems, because they combine adsorption and catalysis in a single material, which enhances their efficiency to deactivate organophosphorus compounds.

2. β-CYCLODEXTRIN POLYMERS ON MICROCRYSTALLINE CELLULOSE AS A GRANULAR MEDIA FOR ORGANIC MICROPOLLUTANT REMOVAL FROM WATER.

2.1 Preface

In this chapter, I show our efforts in the synthesis of an adsorbent based on β-cyclodextrin that can be used to remove micropollutants in a continuous manner. We hypothesized that deposition of the polymer on a support with a fixed particle size and morphology would facilitate the water permeability, and therefore the adsorption of contaminants in a flow setup. The formation of the β-cyclodextrin polymer on the surface of the support is demonstrated by combination of different techniques. Moreover, the characterizations done allow a better understanding of the system and give insights of its performance in removing micropollutants from water. Additionally, we tested our hypothesis that a morphological control of the adsorbent would expand its use to continuous water cleaning. Also, we challenged the system by testing its ability in removing pollutants from water at environmentally relevant concentrations. Herein, we present our approach to produce an alternative adsorbent for continuous water remediation, on the basis of our previous polymerization knowledge, as well as the incorporation of strategies used in other areas.

This work was performed in collaboration with Yuhan Ling, Chenjun Li, Prof. Damian Helbling from the School of Civil and Environmental Engineering at Cornell University. Benjamin P Frank, Prof. Howard Fairbrother from the Department of Chemistry at Johns Hopkins University. And Dr. Reiner Bleher from the Department of Materials Science and Engineering at Northwestern University. This work was first published in *ACS Appl. Mater. Interfaces* **2019**, 11 (8), 8089-8096.

2.2 Abstract

Organic contaminants at low concentrations, known as micropollutants, are a growing threat to water resources. Implementing novel adsorbents capable of removing micropollutants during packed-bed adsorption is desirable for rapid water purification and other efficient separations. We previously developed porous polymers based on cyclodextrins that demonstrated rapid uptake and high affinity for dozens of micropollutants (MPs) in batch experiments. However, these polymers are typically produced as powders with irregular particle size distributions in the range of tens of microns. In this powdered form, cyclodextrin polymers cannot be implemented in packed-bed adsorption processes because the variable particle sizes yield insufficient packing and consequently generate high back-pressure. Here we demonstrate a facile approach to remove micropollutants from water in a continuous manner by polymerizing cyclodextrin polymer networks onto cellulose microcrystals to provide a core/shell structure. Batch adsorption experiments demonstrate rapid pollutant uptake and high accessibility of the cyclodextrins on the adsorbent. Similarly, column experiments demonstrate rapid uptake of a model pollutant with minimal back-pressure, demonstrating potential for use in packed-bed adsorption processes. Furthermore, the pollutant-saturated columns were regenerated using methanol and reused three times with no change in performance. Column experiments conducted with a mixture of 15 micropollutants at environmentally relevant concentrations demonstrated that removal was determined by the affinity of each micropollutant for cyclodextrin polymers. The cyclodextrin

polymer grafted onto cellulose microcrystals is more resistant to both anaerobic and aerobic biodegradation as compared to cyclodextrins and unmodified cellulose crystals, presumably due to the aromatic crosslinkers, demonstrating durability. Collectively, the findings from this study demonstrate a general strategy to incorporate novel cyclodextrin adsorbents onto cellulose substrates to enable rapid and efficient removal of micropollutants during packed-bed adsorption, as well as their promising long-term stability and regeneration capabilities.

2.3 Introduction

Humans introduce thousands of organic compounds, known as micropollutants (MPs) when present at trace concentrations, into ground and surface waters.[113] These MPs are substances used in agriculture, manufacturing, medicine, and other human activities.[114] Several studies have demonstrated that exposure to MPs may negatively influence both human health and aquatic ecosystems.[115,116] For example, the presence of bisphenol A (BPA), a suspected endocrine disruptor used to make plastics and epoxy resins, has raised concerns in human health because it can produce adverse effects in mammary glands and the immune system at concentrations below its acute toxicity levels.[117]

Some polar and semi-polar MPs are stable and persistent in the environment, while others undergo biotic or abiotic transformation to form products that are persistent in water at trace concentrations, because they are only partially removed in conventional water treatment processes.[15] Therefore, enhanced treatments such as advanced oxidation, ultrafiltration, and adsorption are expected to play a role in MP removal, especially as the health and ecological effects of MPs are better understood.[38,118–120] Adsorption is a widely applicable technique because it can remove

contaminants without introducing degradation byproducts,[121] and thus the scientific community has explored numerous materials for adsorption of contaminants in water.[60,122] The performance of such adsorbents have been evaluated in batch and/or packed-bed adsorption configurations.[123,124] Remediation of ground and drinking water relies in the use of granular adsorbents in packed-bed columns.[125] Therefore, the development of adsorbents to decontaminate water in a continuous setup is needed. Granular adsorbents have been employed to remove heavy metals and organic dyes from water in packed-bed columns.[126,127]However, the implementation of granular adsorbents capable of MP removal in packed-beds has not been addressed yet.

Adsorption capacity and fast mass transport are important characteristics for adsorbents developed for packed-bed adsorption processes.[128] However, the rate of adsorption and the mass transfer may become slow due to poor accessibility to the binding functional groups. To solve this problem development of core-shell adsorbents has been explored.[129,130] Furthermore, control of the adsorbent size and shape contributes to a rapid flow of water in packed-bed columns, which is desirable for continuous water remediation. Among the different materials explored as supports for sorbent deposition, cellulose possess the desired characteristics. Its hydroxyl groups allow reactions with different functional groups, producing covalent bonds between the adsorbent and the support.[131] Additionally, cellulose can be obtained in sizes ranging from tens of nanometers to hundreds of microns, and in different morphologies.[132] Finally, it is cheap, non-toxic and a green material. Consequently, cellulose is an outstanding material to support an adsorbent capable of removing MPs.

β-cyclodextrin (β-CD) is an inexpensive and renewable carbohydrate produced from corn starch that forms host-guest complexes with thousands of organic compounds, including many

micropollutants.[55,133] This property has led to the development of numerous β-CD-based adsorbents.[134,135] Moreover, cellulosic materials functionalized with β-CD have been proposed previously for the removal of pharmaceuticals from water. However, the particle size of the proposed adsorbent is not suitable for packed-bed adsorption, and only relatively untunable monomeric β-CDs were employed.[136] We recently reported the first permanently porous β-CD polymer network, which was obtained by crosslinking β-CD with tetrafluoroterephthalonitrile (TFN) via a nucleophilic aromatic substitution.[58] The β-CD polymer removes pollutants more quickly and effectively than coconut shell activated carbon, is easily regenerated, and is not fouled by humic acids, a major constituent of natural organic matter.[137] However, when packed into columns, its particle size and morphology limit the water flux, preventing the evaluation of its performance in column experiments that simulate packed-bed adsorption processes. Here we polymerize a β-CD polymer onto the surface of 100 µm long rod-like cellulose microcrystals, using knowledge about the use nucleophilic aromatic substitution gained in our previous reports.[138,139] Batch adsorption of Bisphenol A (BPA) demonstrates that the polymer retains its binding characteristics in this form. Moreover, the modified microcrystals were packed into columns that generated comparable back pressure to the unmodified microcrystals, and exhibit even faster MP adsorption compared to the unsupported polymer. We also demonstrate the in-situ regeneration and reusability of the new material, and its performance in removing a mixture of fifteen micropollutants at environmentally relevant concentrations in column experiments. Finally, the biodegradability of the polymer is tested under anaerobic and aerobic conditions. These combined observations demonstrate the utility and durability of the β-CD polymer for MP removal from water.

2.4 Results and Discussion

2.4.1 Synthesis and Characterization

Polymerization of the β-CD polymer onto cellulose microcrystals (CMCs) was performed by combining β-CD, TFN, CMCs, and K_2CO_3 in a solvent mixture of DMSO:H_2O (7:3 *v*/*v*) at 85 °C for 24 h (Figure 2.1). These conditions were adapted from a recent mechanistic study of the polymerization[138] and those used to graft the β-CD polymer onto cotton.[139]

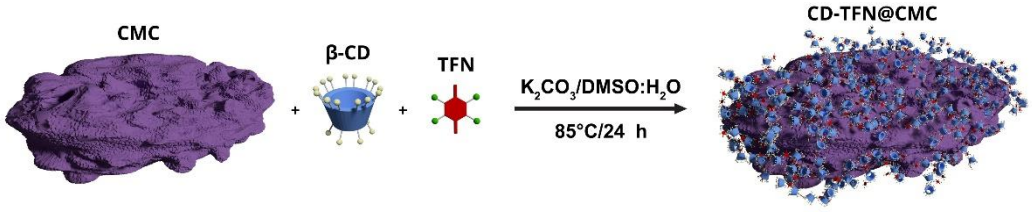

Figure 2.1 Reaction scheme of the CD-TFN@CMC synthesis.

The solid recovered under these reaction conditions provided the highest yield and exhibited the highest capacity for adsorbing bisphenol A (BPA) (Figure 2.S1). However, scanning electron microscopy (SEM, Figure 2.2a) indicated that the solid was a physical mixture of small particles later assigned as the β-CD homopolymer (CD-TFN) and larger particles that were CMCs with CD-TFN grafted to their surfaces (CD-TFN@CMC). These populations were separated by sieving using a 45 μm mesh, and then characterized by SEM and powder X-ray diffraction (PXRD). The CD-TFN homopolymer is amorphous, whereas CMCs exhibit a characteristic powder pattern of crystalline cellulose. Cellulose diffraction peaks are prominent in both the as-synthesized sample (Figure 2.2A) and in the larger particles retained on the sieve (Figure 2.2B). However, these peaks

are relatively faint in the diffraction pattern obtained from the particles that passed through the sieve (Figure 2.2C), indicating that these particles contain fewer CMCs. SEM images of the larger particles after sieving confirmed that CD-TFN@CMC retained their original morphology and size, suggesting negligible crosslinking between CMC particles by the β-CD polymer (Figure 2.2B), while the CD-TFN sample consisted of particles with smaller size and rounded morphology (Figure 2.2C).The separated CD-TFN@CMC and CD-TFN samples were each evaluated for their micropollutant removal performance and compatibility with column designs.

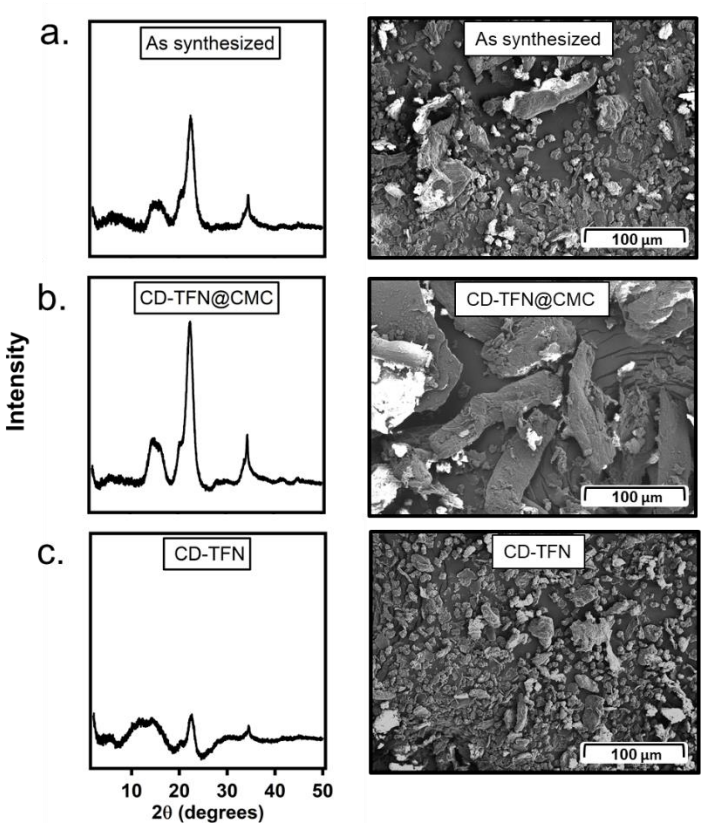

Figure 2.2 PXRD data (left) and SEM images (right) of a. the crude solid isolated from the precipitation, b. the solid retained by the sieve (predominantly CD-TFN@CMC), and c. solid passed by the sieve (CD-TFN).

Fourier-transform infrared spectroscopy (FTIR) and surface composition analysis of the sieved CD-TFN and CD-TFN@CMC samples were consistent with the expected structures. Notably, the FTIR spectra of the two materials are similar because both β-CD and cellulose are comprised of 1,4-linked glucose units, and no significant differences in the position of the FTIR absorption bands were observed after sieving (Figure 2.S2). The spectra exhibit typical bands for carbohydrates (O-H stretching and C-O stretching at 3400 and 1025 cm^{-1}, respectively) and the C≡N stretches and C=C stretches of the TFN groups at 2240 and 1475 cm^{-1}, respectively.[58,140] X-ray photoelectron spectroscopy (XPS) of CD-TFN and CD-TFN@CMC indicated the presence of both nitrogen and fluorine, confirming the incorporation of the crosslinker, whereas spectra of unmodified CMCs show no N or F signals (Figure 2.S3). These combined observations indicate that the β-CD polymer is present on the surface of CMCs in the CD-TFN@CMC sample.

Combustion analysis and powder X-ray diffraction (PXRD) were used to estimate the loading of the β-CD polymer in the CD-TFN@CMC sample. The amount of CMC in CD-TFN@CMC and CD-TFN was calculated from the PXRD spectra. We determined a loading of 78.6 ± 1.9 wt% of CMC in CD-TFN@CMC. In contrast, 22.2 ± 0.7 wt% residual CMC in the CD-TFN homopolymer was found, indicating that some CMC particles passed through the sieve (see the appendix for detailed calculations). The N content of each sample obtained from combustion analysis provided an estimate of 28.1 ± 0.2 and 12.4 ± 0.5 wt% TFN for CD-TFN and CD-TFN@CMC respectively. The combination of PXRD and combustion analysis were used to estimate that the β-CD content in the CD-TFN homopolymer and CD-TFN@CMC was 50.4 ± 0.7 and 11.6 ± 1.9 wt%, respectively. Based on the F content of the samples, we calculated a TFN:β-CD molar ratio of 3.2 ± 0.05 and 6.1 ± 1.0 for CD-TFN and CD-TFN@CMC and an average degree of substitution of

the TFN of 2.9 ± 0.03 and 2.7 ± 0.05, respectively (Table 2.1). These combined results indicate more TFN per β-CD in CD-TFN@CMC, although some of these crosslinkers are likely to be attached to the glucose subunits of the cellulose microcrystals. Nevertheless, the inherent reactivity of TFN is similar to the CD-TFN homopolymer, since the average degree of substitution is similar for the two samples. The overall bulk compositional analysis indicates that CD-TFN@CMC contains approximately 21.4 wt% of the β-CD polymer covalently bound to the cellulose microcrystals.

Table 1 Composition of CD-TFN@CMC and CD-TFN samples calculated from PXRD and elemental analysis results.

	CMC (wt%)	β-CD (wt%)	TFN (wt%)	TFN:β-CD molar ratio	TFN substitution
CD-TFN@CMC	78.6±1.9	11.6±1.9	12.4±0.5	6.1±1.0	2.9±0.03
CD-TFN	22.2±0.7	50.4±0.7	28.1±0.2	3.2±0.05	2.7±0.05

Elemental mapping using energy dispersive spectroscopy (EDS) demonstrates that the β-CD polymer is found on the CMC in the CD-TFN@CMC sample. In the fluorine mapping image, higher counts are homogeneously distributed around the CMC particles, corresponding to the presence of the TFN groups (Figure 2.3b). The CD-TFN homopolymer particles show a similar fluorine signal (Figure 2.S5), whereas unmodified CMC shows no fluorine (Figure 2.3e), but both particles show carbon and oxygen (Figure 2.S4). The CD-TFN on the surface of the CMCs was visualized with excellent contrast using scanning transmission electron microscopy (STEM). The CD-TFN@CMC particles were dispersed into a methacrylate resin, cured, microtomed to 200 nm-thick sections, and analyzed by STEM. The cross-sectional image (Figure 2.3c) reveals a core surrounded by a shell. Unmodified CMC subjected to the same analysis do not show a shell-like

structure (Figure 2.3f). The thickness of the β-CD polymer shell is 1.50 ± 0.39 μm (Figure 2.S6), which is smaller than the average particle size of the CD-TFN homopolymer (>10 microns, Figure 2.S7). These findings indicate the formation of the β-CD polymer as a thin coating around the cellulose in CD-TFN@CMC.

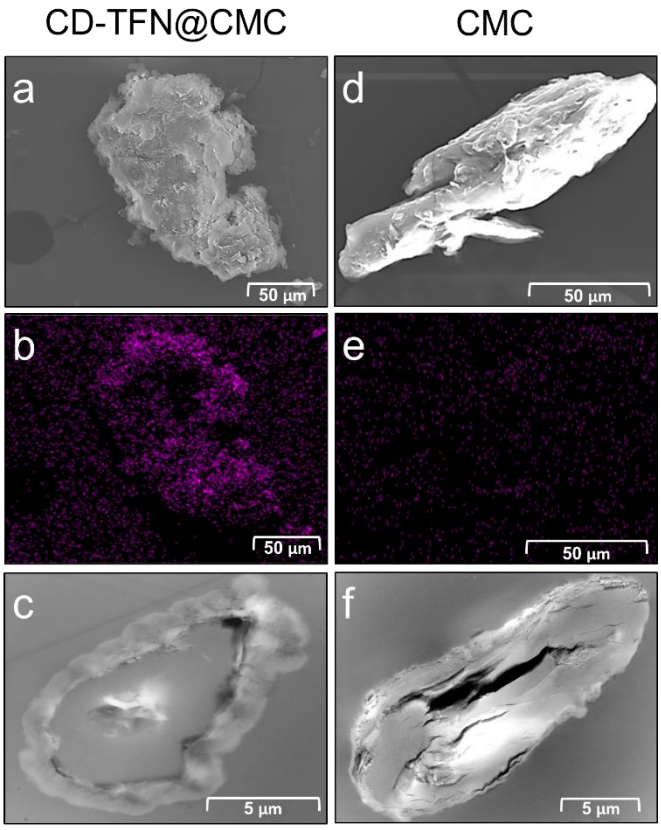

Figure 2.3 a. Scanning electron micrograph, b. fluorine mapping, and c. cross sectional STEM of CD-TFN@CMC; d. scanning electron micrograph, e. fluorine mapping, and f. cross sectional STEM of unmodified CMC. The cross-sectional images were obtained by embedding the samples in a methacrylate resin, which was cured, microtomed, and imaged.

2.4.2 Bisphenol A Uptake in Batch Experiments

We performed batch isotherm experiments with CD-TFN, CD-TFN@CMC, and CMC to determine the adsorption capacity of each material for BPA. Isotherm experiments were conducted with 1 mg adsorbent per mL of solution and with initial BPA concentrations ranging from 0.1 to 1 mM. The results are presented in Figure 2.4a and Figure 2.S8. We used the Langmuir isotherm model (Equation S2.8) to estimate the maximum adsorption capacity (q_{max}) in terms of mg BPA/g adsorbent and mg BPA/g β-CD (Figure 2.S8, 2.S9 and Table 2.S1).[141]

CMC exhibited limited BPA removal in all experiments, and no fit was possible to the Langmuir isotherm. CD-TFN and CD-TFN@CMC both exhibited significant uptake of BPA and Langmuir isotherms were developed. We found that the q_{max} for CD-TFN is 193.6 ± 7.8 mg BPA/g solid, which corresponds to a combination of specific (formation of an inclusion complex with β-CD) and nonspecific (interaction with the crosslinker and pores of the network) BPA adsorption.[58] The maximum BPA capacity for CD-TFN@CMC is 34.7 ± 1.6 mg BPA/g solid. We found that the capacity of the adsorbents per unit mass of β-CD for CD-TFN and CD-TFN@CMC are 384.2 ± 31.6 mg BPA/g β-CD and 299.1 ± 27.3 mg BPA/g β-CD respectively (Figure 2.S8, Table 2.S1), which indicates that CD-TFN and CD-TFN@CMC have similar capacity per unit mass of β-CD. Uptake values of the adsorbents demonstrate that β-CD is present in CD-TFN and CD-TFN@CMC, and it is completely available to form inclusion complexes with micropollutants like BPA, which is an important characteristic to maximize adsorbent performance.

We also measured the kinetics of BPA uptake in batch experiments conducted with 1 mg/mL polymer loading and [BPA] = 0.1 mM. The results demonstrate that CD-TFN@CMC removes

BPA more quickly than CD-TFN itself (Figure 2.4b). CD-TFN reaches its equilibrium uptake of BPA within 2 min, which is comparable to our previous reports.[58,137] CD-TFN@CMC reaches equilibrium within 20 seconds under identical conditions. The relative kinetics of adsorbents with different capacities may be compared directly by calculating a parameter known as adsorption time (t_a), with shorter times corresponding to more rapid micropollutant binding (see appendix for details of the calculation).[142] The t_r of CD-TFN and CD-TFN@CMC are 3.75 ± 0.50 s and 0.89 ± 0.03, respectively (Figure 2.S10 and Table 2.S1). We conclude that CD-TFN@CMC's rapid BPA uptake occurs because the formation of a thin outer layer of polymer in the CMCs, and the highly accessible network of β-CD polymers crosslinked with TFN,[58] such that BPA can rapidly access the β-CD binding sites. This rapid uptake suggests outstanding potential for implementing CD-TFN@CMC in packed-bed adsorption processes.

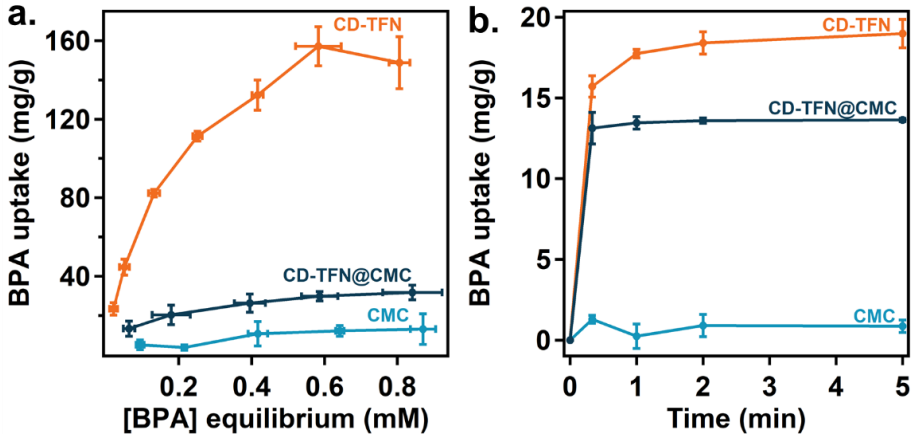

Figure 2.4 a. BPA uptake of CMC, CD-TFN and CD-TFN@CMC as a function of the equilibrium BPA concentration (1 mg of solid/mL of solution, measured at equilibrium), and b. BPA uptake by CMC, CD-TFN and CD-TFN@CMC and as a function of time (1 mg of solid/mL of solution, $[BPA]_0$=0.1mM).

2.4.3 Permeability Test

Because of CD-TFN@CMC's larger particle size, packed columns exhibit significantly lower back pressure than those prepared from the CD-TFN homopolymer. Back pressure in packed columns depends on particle size, morphology, and distribution, and thus large, homogenous particles are desirable.[143] CD-TFN has an irregular shape and a broad size distribution, while CD-TFN@CMC has a size distribution centered at 100 μm. Chromatography columns were packed with equal masses of CD-TFN@CMC, CD-TFN, or CMC and connected to a liquid chromatography (LC) pump to measure back pressure as a function of flow rate. CD-TFN@CMC had only slightly higher back pressure than unmodified CMC (Figure 2.5), and CD-TFN had much higher back pressure. This higher permeability, combined with its rapid uptake, makes CD-TFN@CMC a promising candidate for implementing CD-TFN@CMC in packed-bed adsorption processes.

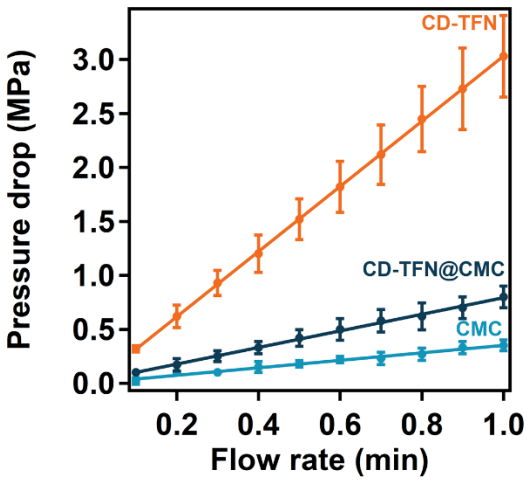

Figure 2.5 Back pressure as a function of flow rate for CMC, CD-TFN, and CD-TFN@CMC packed in liquid chromatographic columns, using water as the mobile phase, and 200 mg of adsorbent.

2.4.4 Bisphenol A Uptake in Column Experiments

A chromatography column was packed with 200 mg of CD-TFN@CMC and used to evaluate the removal of BPA from water. The column was subjected to breakthrough tests using BPA solutions of varying concentrations (0.1, 0.5 and 1.0 mM). The CD-TFN@CMC column exhibits breakthrough volumes that depended non-linearly on BPA concentration (Figure 2.6a). By contrast, columns packed with CMC showed more rapid breakthrough that was independent of BPA concentration, indicating that CMC does not remove BPA from water (Figure 2.S11). Furthermore, the amount of BPA adsorbed in each experiment is similar to the quantity measured in batch experiments (Figure 2.S12). This finding indicates that the capacity of the adsorbent is not affected when is tested in a continuous adsorption setup and demonstrates that batch adsorption can be used to predict the behavior of CD-TFN@CMC in column experiments. Finally, the CD-TFN@CMC column was saturated with a 1.0 mM BPA solution and regenerated by in situ washing with MeOH and re-equilibrating with clean H_2O. After three adsorption/regeneration cycles, the capacity and breakthrough time of the column were unchanged (Figure 2.6b). These breakthrough and regeneration experiments support the use of CD-TFN@CMC in packed-bed adsorption processes and motivate further experiments at environmentally relevant concentrations.

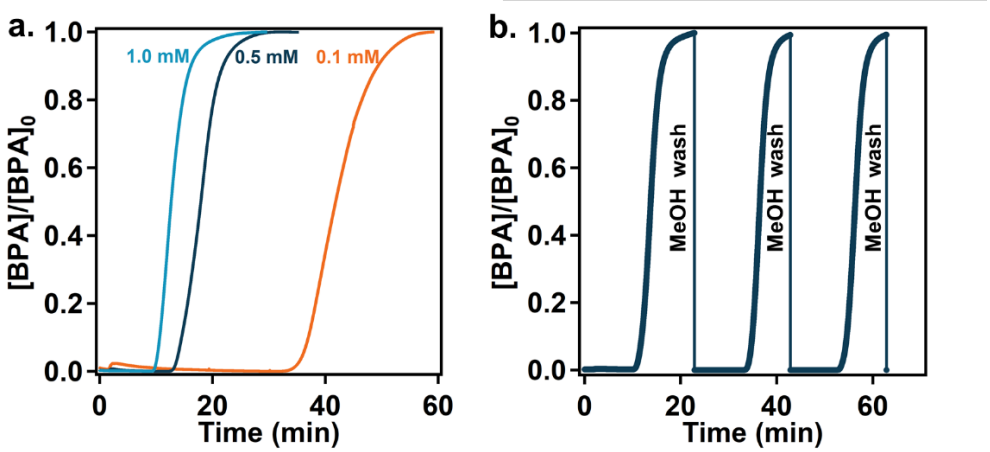

Figure 2.6 a. Packed-bed uptake of BPA at three different BPA concentrations, measured as a function of time for CD-TFN@CMC packed in a column, and b. Packed-bed regeneration of CD-TFN@CMC packed in a column. Saturation was performed with a 1.0 mM BPA solution a 1.0 mM BPA solution and methanol was used for regeneration.

A column packed with 200 mg of CD-TFN@CMC also removes MPs at environmentally relevant concentrations. We selected 15 MPs that exhibited varying affinity for CD-TFN in previous batch experiments and prepared a mixture containing 10 µg L^{-1} of each MP.[137] We designed a series of column experiments to evaluate the removal of the 15 MPs from water (see appendix for experimental details). The results of the experiments are presented in Figure 2.7. Seven MPs exhibited complete removal over the duration of the 60 minute experiment; these MPs also exhibited the greatest affinity for CD-TFN in previous batch experiments ($\log K_D > 0.3$).[137,138] The remaining MPs exhibited varying levels of removal over the duration of the experiment, and we report the total removal calculated by taking the area above the breakthrough curve as described in the appendix and summarized in Figure 2.7, Figure 2.S13 and Figure 2.S14. Two compounds (sucralose and PFOA) exhibited complete breakthrough within the 60 minute duration of the

experiment, and the remaining MPs that were partially removed exhibited varying degrees of breakthrough within 60 minutes. The K_D values of the partially removed MPs are also proportional to their removal levels in the column experiments. Based on these experiments, we conclude that CD-TFN@CMC removes MPs in column experiments to varying degrees that correlate significantly with their K_D values measured in batch reactors (t-test, $p<0.00001$). Therefore, the removal of other MPs by CD-TFN@CMC should also be predictable based on their affinity observed in batch experiments.

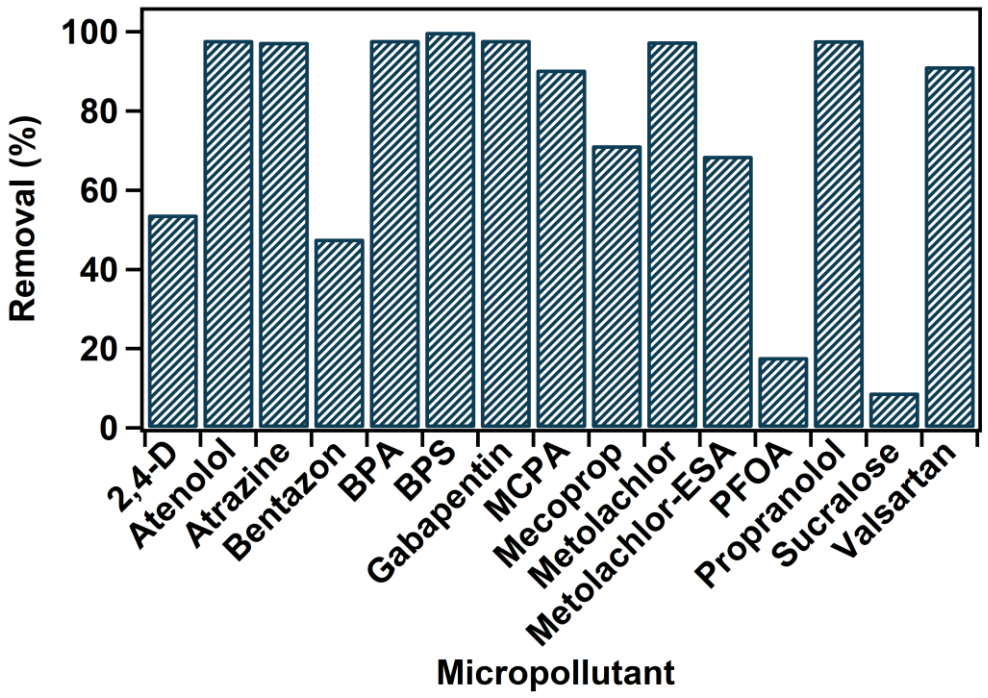

Figure 2.7 Packed-bed adsorption of 15 MPs (10 ppb each) by CD-TFN@CMC packed in a column (200 mg). Flow rate was 0.2 mL/min. Removal was calculated as the ration of the area above the breakthrough curve over the total area from 0 to 60 min.

2.4.5 Stability Towards Biodegradation

The CD-TFN homopolymer shows excellent stability to microorganisms under both anaerobic and aerobic conditions. CD-TFN@CMC is partially biodegradable, which we attribute to the β-CD polymer coating that slows down the degradation of the CMC core. The anaerobic biodegradation of the materials was characterized by monitoring their biogas production in an anaerobic bioreactor for 103 days. Unmodified CMC (Figure 2.8a) and β-CD (Figure 2.S15) are degraded by the mixed culture anaerobic bacteria as tracked by their mineralization into biogas, which plateaus at 40 days. In contrast, the biogas production for CD-TFN remained at baseline levels for the duration of the experiment, indicating that it is not biodegradable by virtue of the TFN crosslinker (Figure 2.S15). CD-TFN@CMC produced biogas above baseline levels, which ceased after 60 days. However, its biodegradation is slower and less extensive than CMC itself. We attribute these observations to the β-CD polymer coating limiting the rate and extent of CMC biodegradation.

CD-TFN also resists degradation, and CD-TFN@CMC is partially stable under aerobic conditions, which was assessed by monitoring mass decreases after 46 days of incubation in the presence of aerobic mixed culture bacteria. CMC exhibited the greatest mass loss in aerobic media and is therefore biodegradable in both environments. CD-TFN again showed no bacterial degradation, and CD-TFN@CMC showed partial degradation (Figure 2.8b). CD-TFN@CMC showed no difference in its BPA uptake capacity after blank (no bacteria) and bacterial aging (Figure 2.S16). Additionally, SEM images of the aged samples reveal no differences in the morphology or the particle size of the adsorbents (Figure 2.S17). Based on these observations, the partial biodegradability of CD-TFN@CMC likely comes from gaps on the CMC surface that were not

coated by the polymer. Based on these experiments, we anticipate that CD-TFN@CMC will show superior stability to aerobic bacterial aging during water remediation compared to cellulose-based materials without a protecting layer. The extent of this stabilization will depend on the nature of the β-CD polymer coating in an optimized application-specific form.

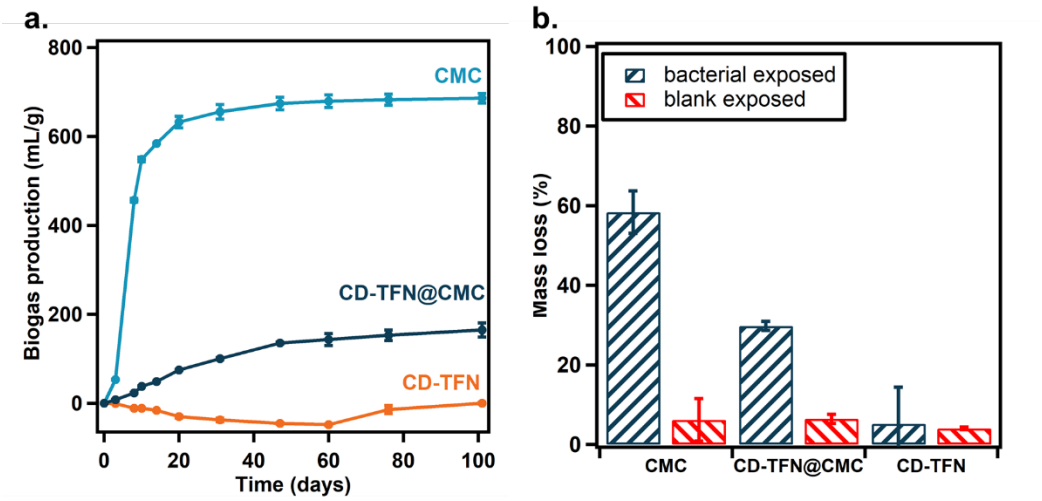

Figure 2.8 a. Biogas production per unit mass of CMC, CD-TFN@CMC and CD-TFN as a function of time in an anaerobic environment, and b. mass loss during aerobic degradation of CMC, CD-TFN@CMC, and CD-TFN.

2.5 Conclusions

Cellulose is a natural support for cross-linked cyclodextrin polymers because it is inexpensive, available in many morphologies and sizes, and its hydroxyl groups participate in polymerizations alongside those of β-CD itself. CD-TFN polymers have shown excellent affinity and superior kinetics compared to activated carbons in previous reports, but its native particle size and morphology preclude leveraging these desirable properties for water treatment during packed-bed

adsorption. Here we have used CMC as a support for CD-TFN to obtain an adsorbent with a core/shell structure, with similar adsorption efficiency as the native material, fast kinetics, and low back pressure when packed into columns. These characteristics enabled the first breakthrough experiments of CD-TFN adsorbents. The columns were amenable to regeneration with no observed performance loss. Column experiments with pollutant mixtures with varying affinity to CD-TFN at environmentally relevant concentrations, indicated complete removal of high-affinity MPs and selectivity consistent with previous batch studies. CD-TFN and CD-TFN@CMC showed significant resistance to biodegradation despite their high carbohydrate content, which we attribute to their heavy TFN cross-linking and core-shell structure of CD-TFN@CMC. Overall, this work represents a significant step forward towards leveraging the desirable characteristics of cyclodextrin adsorbents for removing micropollutants from impacted water resources. This approach represents an important step in developing high-performance and economical granular forms of β-CD polymers, as future developments will focus on methods that produce granular materials exclusively.

2.6 Acknowledgments

This work was supported by the National Science Foundation (NSF) through the Center for Sustainable Polymers (CHE-1413862). This work made use of the IMSERC, and NUANCE facilities at Northwestern University, which have received support from the Soft and Hybrid Nanotechnology Experimental (SHyNE) Resource (NSF ECCS-1542205); the State of Illinois and International Institute for Nanotechnology (IIN). This work was also supported by the National Science Foundation under the Center for Sustainable Nanotechnology (CSN), CHE-1503408. The

Center for Sustainable Polymers and the Center for Sustainable Nanotechnology are part of the NSF Centers for Chemical Innovation Program.

2.7 Chapter 2 Appendix

2.7.1 Materials and Instrumentation

Reagents: β-cyclodextrin (β-CD) (>97%), cellulose microcrystal (CMC) (50 μm average particle size), and tetrafluoroterephthalonitrile (TFN) (>99%) were purchased from Sigma Aldrich and used without further purification. Dimethyl sulfoxide (DMSO) (99.8%) and potassium carbonate (>99%) were purchased from Fisher Scientific and used without further purification. Aqueous solutions of micropollutants (MPs) were prepared using 18 MΩ deionized H_2O at neutral pH. Micropollutant compounds were obtained from Sigma-Aldrich, except for Valsartan which was obtained from USP. All were used as received. Reagents used in biodegradation studies were obtained from Sigma-Aldrich. Wastewater for biodegradation tests were obtained from Back River Waste Water Treatment Plant (Baltimore, MD).

Instrumentation: Infrared spectroscopy was performed on a Thermo Nicolet iS10 spectrometer with a diamond ATR attachment. Coating of the samples was performed in a Denton Desk III TSC sputter coater. Scanning electron microscopy (SEM) and energy dispersive spectroscopy (EDS) were performed on a Hitachi S-3400N-II spectrometer. Cross sections were obtained in an ultramicrotome Leica, Buffalo Grove, IL, USA, model UC7, using a diamond knife Diatome, Hatfield, PA, USA. Scanning transmission electron microscopy (STEM) was done in a Hitachi HD2300 STEM at 200 kV acceleration voltage. Liquid chromatography (BPA studies) was performed on a Bruker Amazon-X instrument using a C-18 column for separation and a UV-vis

photodiode as a detector. Powder X-ray diffraction was performed on a Stoe STADI-MP diffractometer using Cu Kα radiation in transmission mode. Back pressure experiments were performed on a Shimadzu LC-20AD liquid chromatograph. High-concentration breakthrough experiments were performed in a Hewlett Packard 1100 series using a UV-vis photodiode as a detector. The photoelectron spectra (XPS) were recorded with a Thermo Scientific ESCALAB 250Xi instrument using an Al Kα X-ray source (1486.6 eV) with a monochromated X-ray beam of 500 μm and 150 watts. Low-concentration breakthrough and removal experiments were performed on a Dionex UltiMate 3000 HPLC system coupled with a QExactive high resolution mass spectrometer from Thermo Fisher Scientific.

2.7.2 Experimental protocols

Synthesis of CD-TFN@CMC: Functionalization of the cellulose microcrystals (CD-TFN@CMC) was performed by varying the previously reported synthesis of the cyclodextrin porous polymer.[138] A 350 mL high-pressure vessel equipped with a magnetic stir bar was charged with TFN (7.505 g, 37.5 mmol) and DMSO (170 mL), and the solution was stirred until TFN was completely dissolve. In another flask, β-CD (6.0052 g, 5.29 mmol), K_2CO_3 (18.452 g, 133.5 mmol), and CMC (12.001 g) were suspended in deionized H_2O (73 mL). This suspension was then added dropwise into the DMSO solution, and the resulting mixture was bubbled with N_2 for 10 min. Subsequently, the N_2 inlet was removed, the flask was sealed, and the mixture was stirred at 500 rpm at 85 °C for 24 h. The dark-red suspension was then cooled to room temperature, filtered, and the solid was sequentially washed with THF (20 mL X 3), water (20 mL X 3), 1M HCl (until CO_2 evolution stopped, 20 mL), water (20 mL X 3), and methanol (20 mL X 3). The

yellow solid was subsequently washed with hot methanol using a Soxhlet extractor for 24 h and then dried under high vacuum overnight. This yellow solid was isolated in 82.1% yield (19.2759 g). The functionalized cellulose was then isolated from the non-bonded cyclodextrin polymer by using a 45 μm sieve (Verder Scientific Inc.), where the solid passing through the mesh is the β-CD homopolymer (CD-TFN, 9.426 g, 48.9%) and the solid which stays on top of the sieve is the functionalized cellulose (CD-TFN@CMC, 9.850 g 51.1%).

Synthesis of m-CD-TFN: Synthesis of the β-CD polymer was performed by employing the same methodology used for CD-TFN@CMC. A 150 mL high-pressure vessel equipped with a magnetic stir bar was charged with TFN (3.757 g, 18.8 mmol) and DMSO (72 mL), and the solution was stirred until TFN was completely dissolved. In another flask, β-CD (3.007 g, 2.65 mmol) and K_2CO_3 (9.251 g, 66.9 mmol) were dissolved in 36 mL of deionized H_2O. This solution was added dropwise into the DMSO solution, and the resulting mixture was bubbled with N_2 for 10 min. The N_2 inlet was removed, the flask was sealed, and the mixture was stirred at 500 rpm at 85 °C for 24 h. The dark-red suspension was cooled to room temperature, filtered, and the solid was sequentially washed with THF (20 mL X 3), water (20 mL X 3), 1M HCl (until CO_2 evolution stopped, 20 mL), water (20 mL X 3), and methanol (20 mL X 3). The yellow solid was subsequently washed with hot methanol using a Soxhlet extractor for 24 h and then dried under high vacuum overnight. This yellow solid (CD-TFN) was isolated in 57.2% yield (3.316 g).

Scanning electron microscopy: The following procedure was the same for all the samples. 5 mg of CD-TFN@CMC was suspended in 5 mL of water. The solution was stirred for 5 min, and then a 20 μL aliquot was taken and deposited in a holder covered with carbon tape. The water was

allowed to evaporate overnight, and the sample was coated with a 10 nm gold/palladium layer. The sample was transferred to the microscope and both SEM and EDS spectra were recorded using a working distance of 10 mm. A charge voltage of 5 kV and 25 kV were used for SEM and EDS imaging, respectively.

Scanning transmission electron microscopy: The following procedure was the same for all the samples. 50 mg of CD-TFN@CMC were suspended in 2 mL of water for 24 h, then in MeOH for 24 h, and finally in propylene oxide for 48 h. Afterwards, the solid was suspended in a mixture 3:1 propylene oxide: LR White resin (EMS, Hatfield, PA, USA, cat no. #14383-UC) for 2h, then in a mixture 1:1 for another 2h, and finally in a mixture 1:3 for another 2 h. The sample was filtered and infiltrated with the LR White resin for 48h, transferred into fresh resin in gelatin capsules, and polymerized at 60° C for 48 h. 200 nm thick sections were obtained with an ultramicrotome using a diamond knife. Sections were collected on copper slot grids with Fomvar/carbon support film (EMS, cat no G2010-Cu) and observed at 200 kV acceleration voltage.

Aqueous BPA kinetic uptake experiments: Adsorption kinetic studies were performed in 20 mL scintillation vials. All studies were conducted at ambient temperature and were stirred at 300 rpm, and the procedure was identical for all the adsorbents tested. 8 mg of CD-TFN@CMC were initially suspended in 7.2 mL of deionized water, stirred for 5 min, and then 0.8 mL of BPA (1 mM) was added to the stirring polymer suspension, producing a CD-TFN@CMC loading of 1 mg/mL and an effective BPA concentration of 0.1 mM. After a specific contact time, a 0.5 mL aliquot was taken and filtered immediately through a Whatman 0.2 μm inorganic membrane syringe filter into an LC-GC vial. The residual concentration of BPA was determined by LC-UV.

Reagent uptake was determined as the average of three independent experiments performed using different samples but each isolated from the same polymerization experiment.

Aqueous BPA thermodynamic uptake experiments: Thermodynamic adsorption studies were performed in 4 mL scintillation vials. All studies were conducted at ambient temperature and 300 rpm, and the procedure was identical for all the adsorbents tested. 2 mg of CD-TFN@CMC were suspended in 2 mL of 0.125 mM BPA solution, and the suspension was stirred for 4h. After this equilibration time, a 0.5 mL aliquot was taken and filtered immediately through a Whatman 0.2 μm inorganic membrane syringe filter into an LC-GC vial. This same procedure was repeated with the 0.25, 0.5, 0.75 and 1 mM BPA solutions. The residual concentration of BPA was determined by LC-UV. Uptake was determined as the average of three independent experiments performed using different samples but each isolated from the same polymerization experiment.

Back pressure experiments: Back pressure experiments were performed at ambient temperature and the procedure was identical for all the adsorbents tested. 200 mg of CD-TFN@CMC were packed in an empty column by adding 20 mg of adsorbent at a time and tapping the column to allow the solid to settle at the bottom of the column. The column was then connected to a LC system, and water was run through the column at 1 mL/min for 2h. After this time, the flow rate was decreased to 0.1 mL/min, and the pressure was read after stabilization (1-2 min). The flow rate was then increased to 0.2 mL/min and the pressure was read again. This procedure was repeated until the flow rate reached 1 mL/min. Back pressure was determined as the average of three independent experiments performed using different samples but each isolated from the same polymerization experiment.

Aqueous BPA breakthrough and reusability experiment: Breakthrough experiments were performed at ambient temperature and the procedure was identical for all adsorbents tested, including the flow rate which was kept at 2mL/min during the entire experiment. 200 mg of CD-TFN@CMC were packed in an empty column by adding 20 mg of adsorbent at a time and tapping the column to allow the solid to settle at the bottom of the column. The column was then connected to an LC-UV, and water was run through the column for 10 min. At this time, the solvent was switched to a BPA solution (0.1, 0.5, or 1.0 mM) and the UV-vis signal was recorded until it reached a plateau.

To test reusability, the CD-TFN@CMC sample was packed and water equilibrated (200 mg, 10 min). A 1.0 mM BPA solution was run through the column and monitored by UV-vis spectroscopy until the signal reached a plateau. Right after the saturation, the BPA solution was then switched for methanol and the column was rinsed until the UV-vis signal returned to the initial signal (approximately 5 min). Finally, methanol was switched to deionized water, which was run through the column for 10 min. This procedure was repeated three times.

Aqueous micropollutant removal experiments: 200 mg of CD-TFN@CMC were packed in an empty column by adding 20 mg of adsorbent at a time and tapping the column to allow the solid to settle at the bottom of the column. Experiments to measure micropollutant removal were performed continuously on an HPLC-MS. A mixture of the 15 MPs was prepared at 10 μg L^{-1} in a 500 mL glass bottle and connected to a high pressure gradient pump (Dionex UltiMate 3000). The MP mixture was delivered to the MS detector (quadrupole-Orbitrap, QExactive) at 0.2 mL min^{-1}. All experiments were run for approximately 60 minutes and included four scenarios: (1) MP

mixture delivered directly to MS (establishes intensity of signal at 10 μg L^{-1}) in positive and negative polarity modes; (2) HPLC-grade water delivered directly to MS (establishes background intensity of signal) in positive and negative polarity modes; (3) MP mixture delivered directly to CD-TFN@CMC-packed column and then to MS (establishes intensity of signal after adsorption) in positive and negative polarity modes; and (4) HPLC-grade water delivered directly to CD-TFN@CMC-packed column and then to MS (establishes background intensity of signal) in positive and negative polarity modes. The signal intensities collected over time were analyzed to determine the removal of each MP and to visualize breakthrough from the columns.

Biodegradation studies: Biomethane potential (BMP) tests were performed to assess the anaerobic biodegradability of β-CD, CMC, TFN, CD-TFN, and CD-TFN@CMC. Using concentrations of nutrients and minerals outlined in Angelidaki, *et al*,[144] media were prepared. The media was adjusted to a pH of 7.2 and kept anoxic throughout preparation through initial boiling at 100 °C (prior to bacterial inoculation), and continuous purging with N_2 gas. A mixed culture of microorganisms, obtained from anaerobic digester sludge produced by the Back River Wastewater Treatment Plant (Baltimore, MD), was strained through a 1.19 mm sieve to remove large solids before being added to the media at 10% v/v. Samples were prepared at 150 mg in triplicate and were digested at mesophilic temperature (35 °C) in septum sealed, nitrogen purged 150 mL bottles containing 100 mL of BMP media. Biodegradability of samples was assessed through the extent of their mineralization to anaerobic biogas. As samples were metabolized into CH_4 and CO_2, this evolved biogas produced pressure in the sealed bottles which could be sampled as gas volume by inserting a needle-capped glass syringe through each bottle's septum at distinct time points. To determine the baseline level of biogas produced independent of each sample (i.e., evolved from

the media itself), triplicate samples of media with no loaded sample were also tracked. Volumes from these blanks were subtracted from each sample to obtain the true biogas production attributable to the sample.

Aerobic biodegradability was assessed using a novel mass loss tracking method which was designed to be suitable for powdered samples. Samples were reacted in either blank aerobic media (i.e., no bacteria, just nutrients), or aerobic mixed culture bacterial media. The blank bacterial media consisted of MilliQ water combined with sodium acetate trihydrate as a carbon source (200mg/L) and a 10% v/v of salt stock containing 7.18 mM K_2HPO_4, 2.79 mM KH_2PO_4, 0.757 mM $(NH_4)_2SO_4$, 0.0406 mM $MgSO_4*7H_2O$, and trace elements necessary for bacterial growth. The aerobic bacterial media featured the same proportions of salts and acetate, but also had 10% v/v primary effluent obtained from Back River Wastewater Treatment Plant added. 50mg of each sample were added as powders to 40 mL of blank and aerobic bacterial media in a 50 mL conical vial. Each sample was centrifuged (4300 rpm, 10 min.) to form a pellet at the bottom of the vial. For samples exposed to bacteria, this centrifugation was performed prior to bacteria addition to avoid pelletization of microorganisms in the media. The purpose of this centrifugation is to pack the sample powder strongly enough in the bottom of the vial so that it can be easily recovered from the media and massed after biodegradation. Samples were exposed to both bacteria and blank media for 46 days on a shaker at 125 rpm and 28 °C before being recovered, dried and weighed. In this process, the remaining solid was separated from the media by first decanting off the supernatant. The residual solid was then washed with 70% ethanol to lyse residual bacterial cells and remove biofilm before being thoroughly rinsed with MilliQ water and dried in aluminum dishes on a hot plate to mass. Mass loss values were calculated by subtracting mass loss in the

blank media from mass loss in the bacterial media to determine mass loss due to bacterial mineralization. Mass loss in blank media was around 5-6 % for all samples, and likely due to sample lost during drying and sample transfer rather than any biodegradation process. The loss of up to 57 % of mass after exposure to bacteria in CMC underlines that bacterial mineralization is the primary contributing factor of mass loss in these experiments.

2.7.3 Synthesis and Characterization

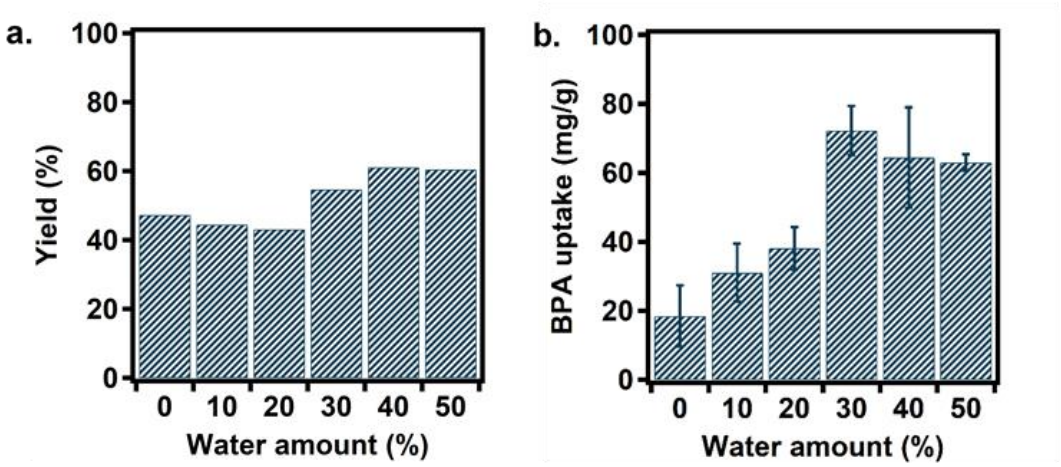

Figure 2.S1 a. Mass yield calculated from the total mass at the beginning and at the end of the reaction as a function of water amount in the solvent mixture. b. BPA thermodynamic uptake after 4h at room temperature, and 300 rpms, using 1 mg of polymer per mL of 1mM BPA solution as a function of water amount in the solvent mixture.

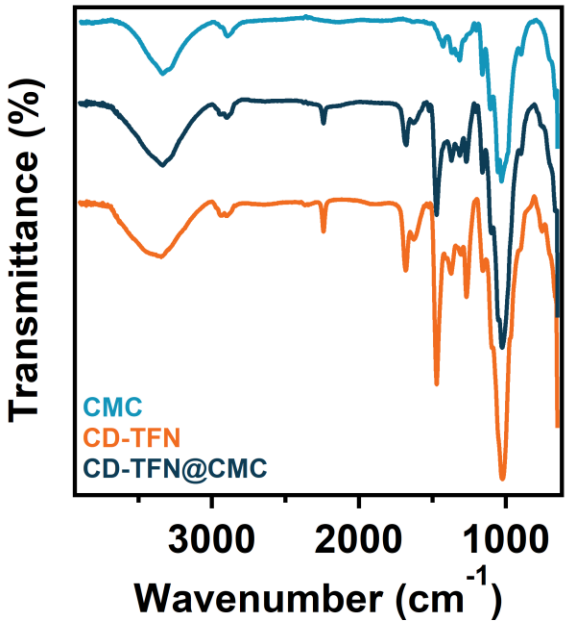

Figure 2.S2 FTIR data of CMC, CD-TFN, and CD-TFN@CMC.

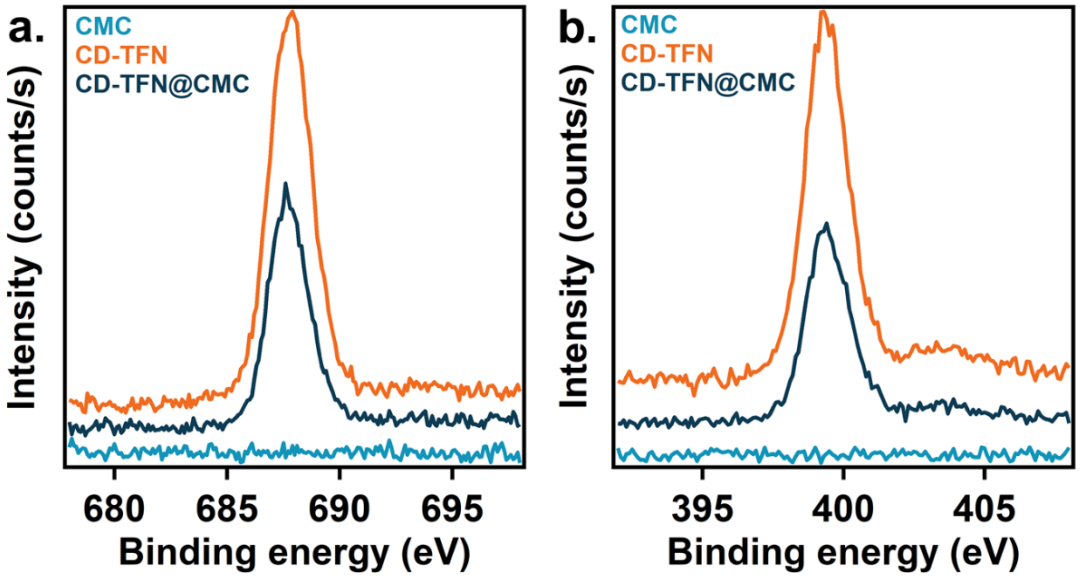

Figure 2.S3 XPS data for CMC, CD-TFN, and CD-TFN@CMC, including (a) F 1s data and (b) N 1s data.

Composition analysis

Composition of both CD-TFN and CD-TFN@CMC were determined based in combination of both PXRD and elemental analysis data.

PXRDs were recorded for CD-TFN, CD-TFN@CMC, CMC, m-CD-TFN and air. Then the percent of crystallinity application on the STOE WinXPOW software was used to calculate the amount of cellulose of the sieved samples. By using, CMC as the crystalline standard, m-CD-TFN as the amorphous standard, air as the air scatter, CD-TFN and CD-TFN@CMC as the raw data.

Elemental analysis of CD-TFN and CD-TFN@CMC was performed to obtain the amount of C, H, N and F in the samples. The N content of each sample obtained from combustion analysis provided an estimate of wt% of TFN.

$$wt\%TFN = \frac{wt\%N}{14g/mol} \times \frac{1molTFN}{2molN} \times \frac{200gTFN}{1molTFN} \text{ (eq 2.S1)}$$

Then, from the wt% TFN we calculated the amount of C of the crosslinker and subtracted it from the total C content to obtain the carbon coming from CMC and β-CD. Finally, we calculated the amount of wt% CMC + β-CD.

$$wt\%C(TFN) = \frac{wt\%N}{14g/mol} \times \frac{8molC}{2molN} \times \frac{12gC}{1molC} \text{ (eq 2.S2)}$$

$$wt\%C(CMC + \beta CD) = wt\%C - wt\%C(TFN) \text{ (eq 2.S3)}$$

$$wt\%(CMC + \beta CD) = \frac{wt\%C(MC+\beta CD)}{12g/mol} \times \frac{1molglucose}{6molC} \times \frac{162.14gglucose}{1molglucose} \text{ (eq 2.S4)}$$

The average degree of substitution (DS) of the crosslinker was determined by the mol% N to mol% F ratio of the samples.

$$DS = 4 - 2 \times \frac{\frac{wt\%F}{19g/mol}}{\frac{wt\%N}{14g/mol}} \quad \text{(eq 2.S5)}$$

Finally, the amount of β-CD in the samples was calculated by subtracting the wt% of CMC found in the PXRD from the wt% of CMC + β-CD from the elemental analysis.

$$wt\%\beta CD = wt\%(CMC + \beta CD) - wt\%CMC(PXRD) \text{ (eq 2.S6)}$$

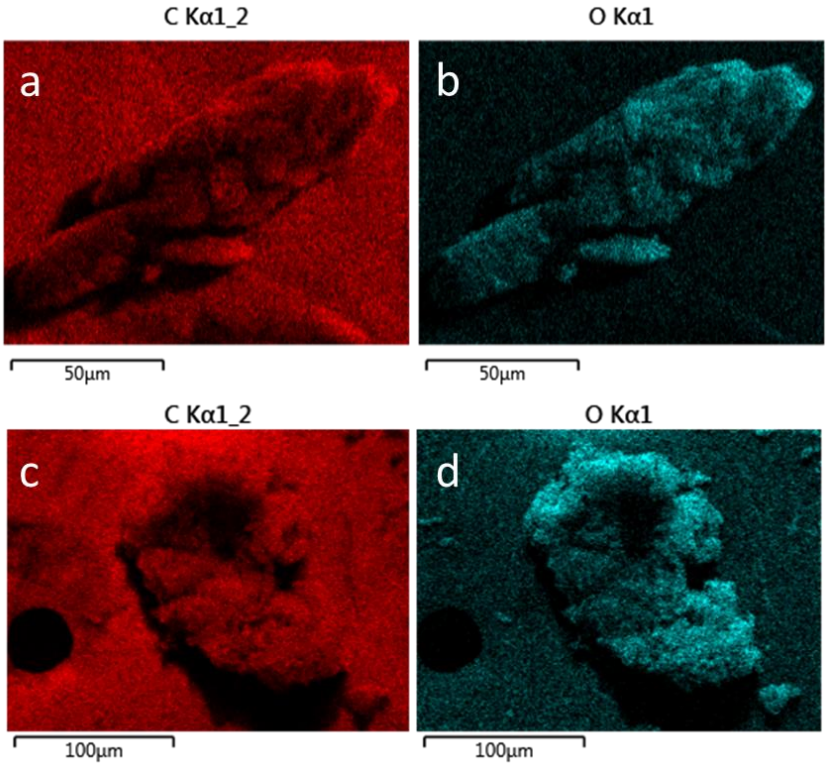

Figure 2.S4 SEM and EDS images of CMC, including (a) carbon and (b) oxygen mapping data. SEM and EDS images of CD-TFN@CMC, including (c) carbon and (d) oxygen mapping data.

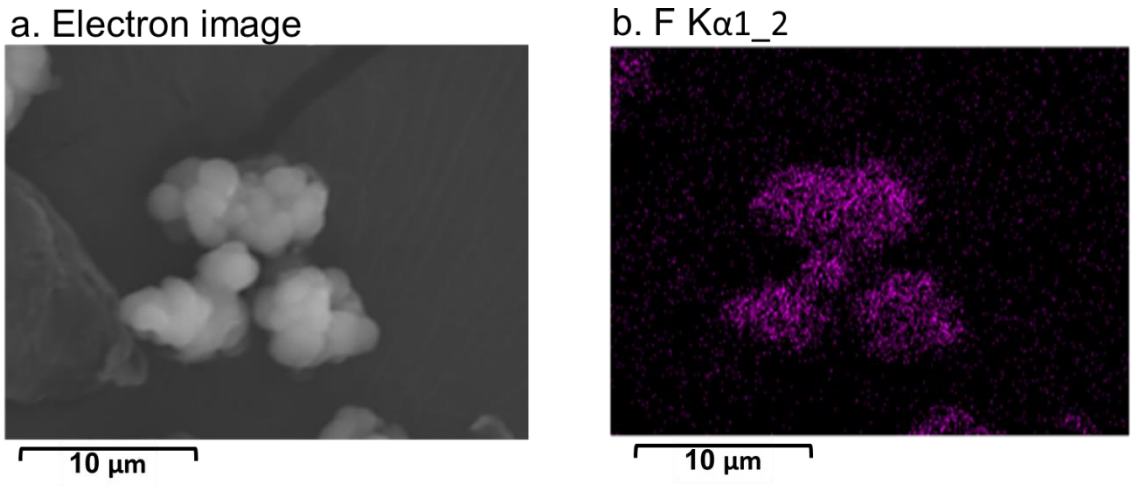

Figure 2.S5 a. Electron image, and b. fluorine mapping of CD-TFN.

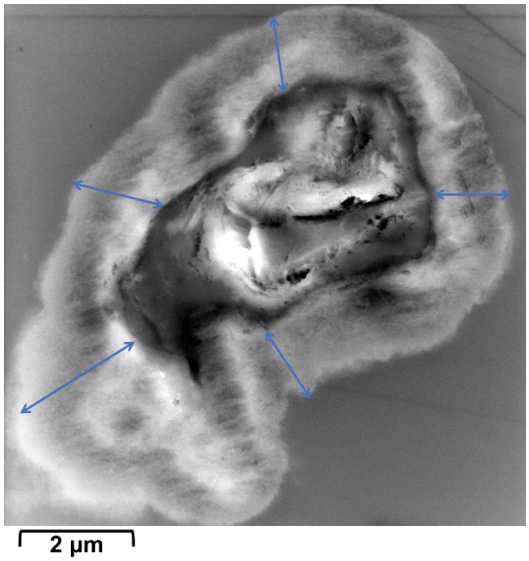

Figure 2.S6 High resolution cross sectional STEM image of CD-TFN@CMC.

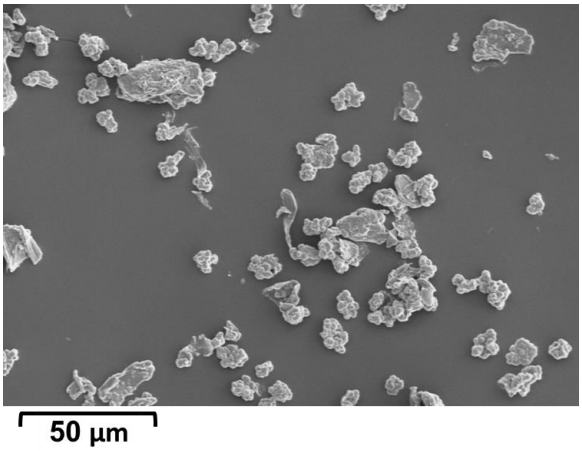

Figure 2.S7 SEM image of CD-TFN.

2.7.4 BPA adsorption in batch experiments

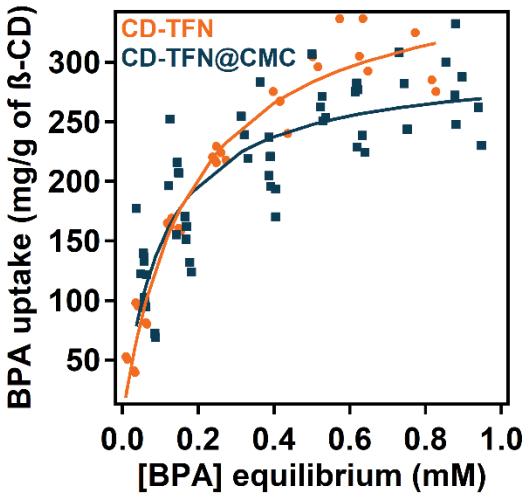

Figure 2.S8 BPA uptake, in terms of mg of BPA per g of β-CD present in CD-TFN and CD-TFN@CMC as a function of equilibrium BPA concentration (1 mg of solid/mL of solution, measured at equilibrium).

The Langmuir model that considers homogeneous adsorption surface, is given as[141]

$$q_e = q_{max} \frac{C_e K_L}{C_e K_L + 1} \quad \text{(eq 2.S8)}$$

Where q_e (mg BPA/g solid) is the amount of BPA adsorbed per gram of adsorbent at equilibrium. q_{max} (mg BPA/g solid) is the maximum adsorption capacity of adsorbent at equilibrium, K_L (L/mol) is the equilibrium constant and C_e(mM) is the concentration at equilibrium. We obtained the Langmuir parameters by fitting the thermodynamic data using the curve fitting tool of IGOR Pro 6.3.7.2.

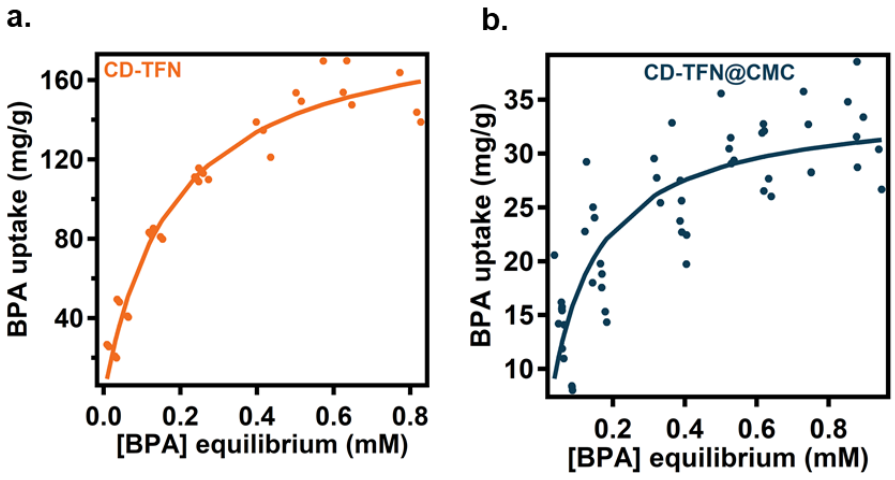

Figure 2.S9 BPA uptake of a. CD-TFN and b. CD-TFN@CMC as a function of the equilibrium BPA concentration (1 mg of solid/mL of solution, measured at equilibrium).

In the pseudo second order rate law, both the rate constant and the capacity at equilibrium are interrelated, making it complicated to make the comparison of materials with different capacities towards a specific sorbate. To solve this problem, we use the adsorption time equation given as[142]

$$q_t = q_e \frac{t}{t+t_a} \quad \text{(eq 2.S9)}$$

Where q_t (mg BPA/g solid) is the amount of BPA adsorbed per gram of adsorbent at a given time. q_e (mg BPA/g solid) is the amount of BPA adsorbed per gram of adsorbent at equilibrium at a given initial concentration, t (s) is the time, and t_a(s) is the adsorption time of the adsorption process, and it is the inverse of the rate constant. By fitting the kinetic parameters using the curve fitting tool of IGOR Pro 6.3.7.2 we obtained the kinetic parameters.

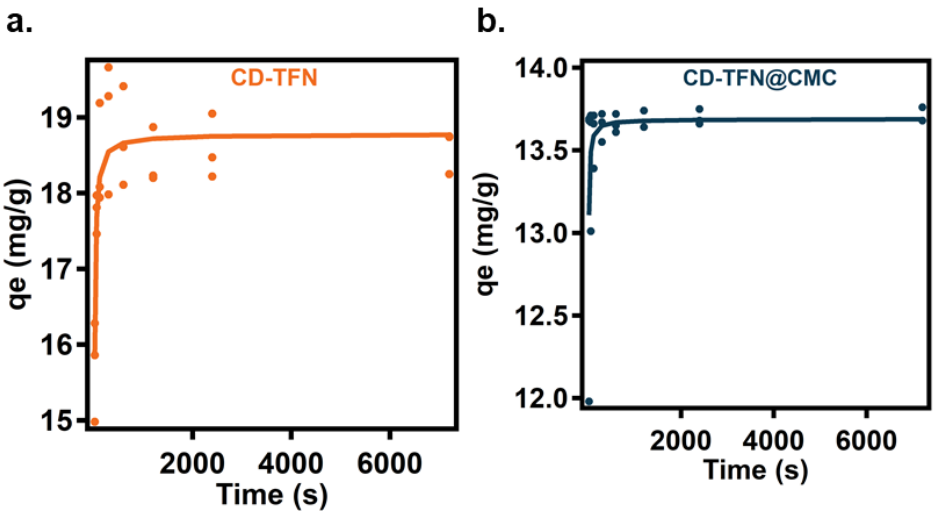

Figure 2.S10 BPA uptake of a. CD-TFN and b. CD-TFN@CMC as a function of time (1 mg of solid/mL of solution, [BPA]=0.1mM.

Table 2.S1 Thermodynamic and kinetic parameters of CD-TFN@CMC and CD-TFN obtained from Langmuir and adsorption time kinetic models, respectively.

Sample	q_{max} (mg BPA/g solid)	K_L (g solid) (L/mol) X10^3	q_{max} (mg BPA/g β-CD)	K_L (g β-CD) (L/mol) X10^3	q_e (mg BPA/g solid)	t_a (s)
CD-TFN@CMC	34.7±1.6	9.6±1.7	299.1±27.3	9.6±3.4	13.69±0.08	0.89±0.03
CD-TFN	193.6±7.8	5.6±0.6	384.2±31.6	5.6±1.3	18.78±0.13	3.75±0.50

2.7.5 Breakthrough adsorption

BPA removal

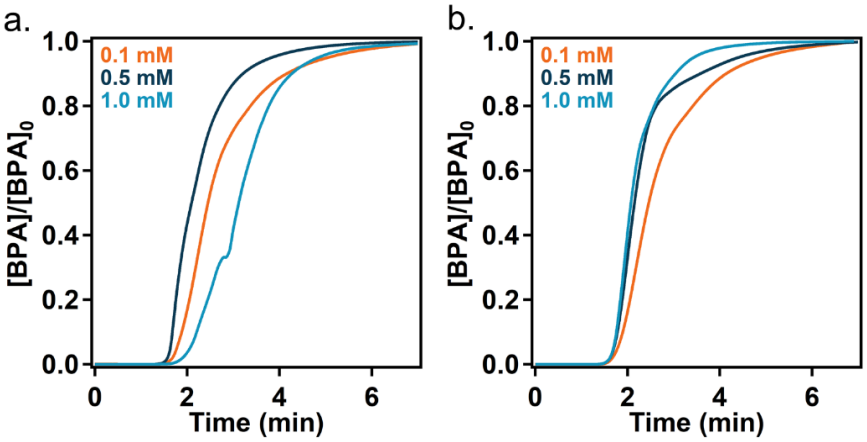

Figure 2.S11 a. In flow BPA uptake as a function of time of the empty column at three different concentrations, and b. In flow BPA uptake as a function of time of the CMC (200 mg) packed in a column at three different concentrations.

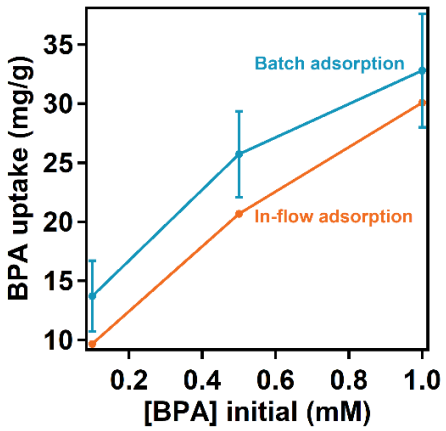

Figure 2.S12 a. In flow vs batch BPA uptake of CD-TFN@CMC as a function of initial concentration.

Micropollutant removal

The percent removal of each MP by the packed column was determined as the ratio of the area above the breakthrough curve (Figure 2.S13) to the total area of the time window (60 minutes). For example, atenolol exhibited no breakthrough after 60 minutes, thus the area above the breakthrough curve is equivalent to the total area of the time window and its calculated removal is 100%. As another example, 2,4-D exhibited consistently increasing breakthrough and nearly complete breakthrough after 60 minutes; the calculated removal is 54%

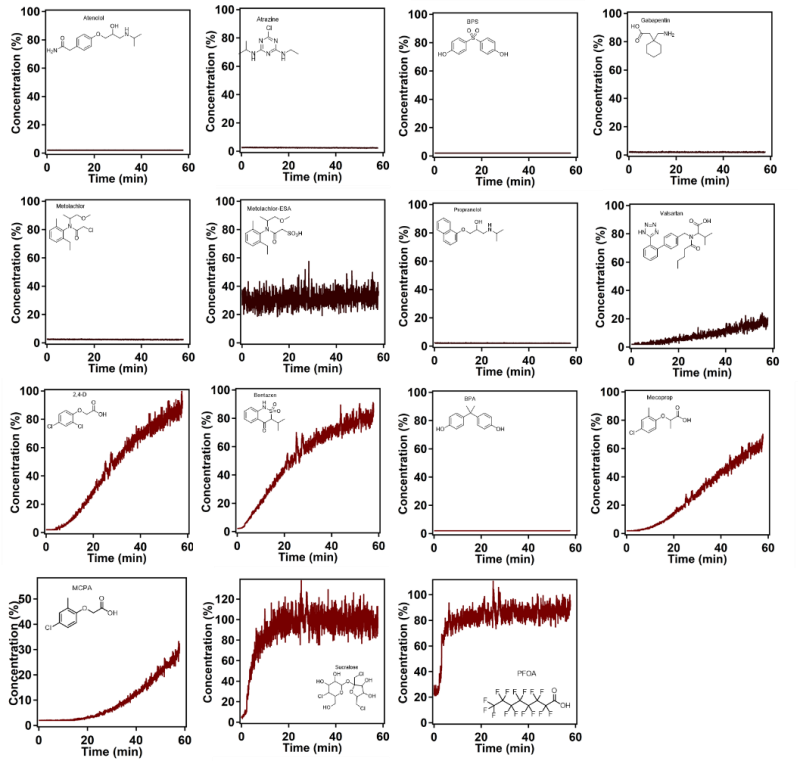

Figure 2.S13 In flow MP uptake as a function of time of CD-TFN@CMC (200 mg) packed in a column. Dark red, MPs determined in positive polarity mode. Light red, MPs determined in negative polarity mode.

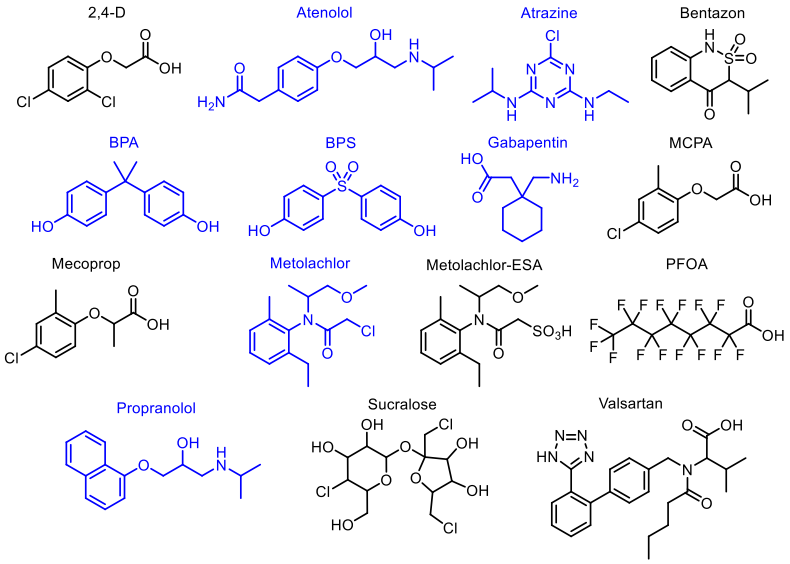

Figure 2.S14 Structures of the fifteen MPs. Labeled in blue are the MPs that are completely removed.

2.7.6 Biodegradation studies

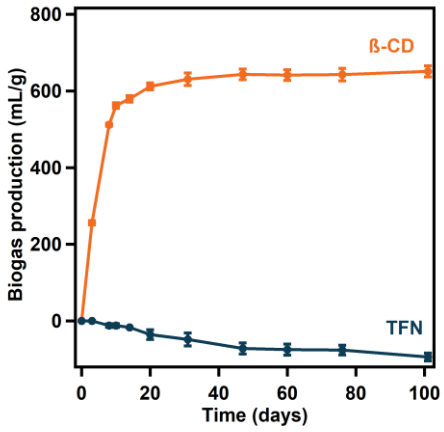

Figure 2.S15 Biogas production per unit mass of β-CD and TFN as a function of time in an anaerobic environment.

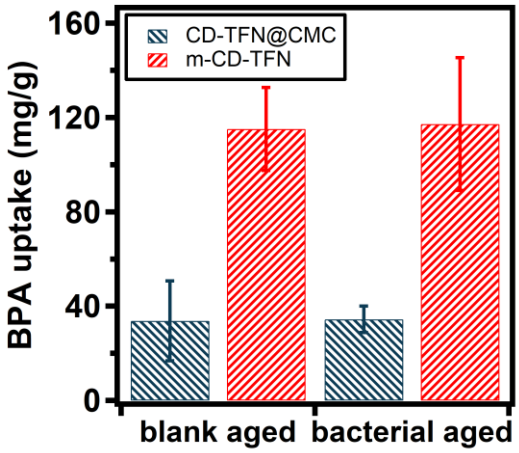

Figure 2.S16 BPA thermodynamic uptake of CD-TFN@CMC and m-CD-TFN after the biodegradation experiment (1 mg of polymer per mL of 1mM BPA solution, measured at equilibrium).

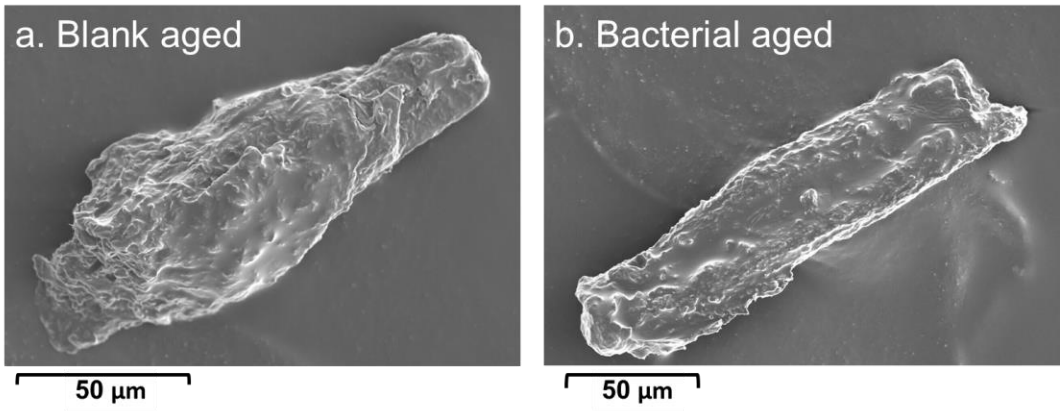

Figure 2.S17 SEM image of CD-TFN@CMC after (a) blank degradation (control) and (b) bacterial degradation.

3. COTTON FABRIC FUNCTIONALIZED WITH A β-CYCLODEXTRIN POLYMER CAPTURES ORGANIC POLLUTANTS FROM CONTAMINATED AIR AND WATER

3.1 Preface

In this chapter, I display the extrapolation of our previous work with cellulose microcrystals to cellulose fibers, more specifically cotton fabrics. Herein, we proved that our methodology to modify cellulose microcrystals can be used for the functionalization of other cellulosic substrates like cotton fabrics. Additionally, the modified fabric is envisioned to serve as an adsorbent of contaminants from water and air, with the advantage of being an easy to handle adsorbent. We started by tuning the reactions conditions to obtain a higher grafting density of the β-CD polymer onto the cotton fabric, without damaging its integrity. Then, we investigated its performance to remove pollutants from water, in principle to demonstrate the presence of the β-CD polymer. Moreover, we studied its performance to remove volatile organic compounds from air at different concentrations. Finally, we showed that our functional fabric outperforms commercial fabrics advertised for their ability to remove VOCs from air. This work is an example of the robustness of the reaction studied in the previous chapter, being useful to functionalize different cellulosic substrates under similar reaction conditions.

This work started from a collaboration between professor Juan Hinestroza and his research group from the Department of Fiber Science & Apparel Design at Cornell University, and professor William Dichtel and his research group from the Chemistry Department at Cornell University,

then at Northwestern University. This work was first published in *Chem. Mater.* **2016**, 28 (22), 8340-8346. https://pubs.acs.org/doi/10.1021/acs.chemmater.6b03624, and it is reproduced with permission. Further permissions related to the material excerpted should be directed to the ACS.

3.2 Abstract

Cotton fabric is covalently functionalized with a porous β-cyclodextrin polymer by including the fabric in the polymerization mixture. The resulting functionalized fabric (CD-TFP@cotton) sequesters organic micropollutants, such as bisphenol A, from water with outstanding speed and a ten-fold higher capacity than untreated cotton. The functionalized fabric also readily captures volatile organic compounds (VOCs) from the vapor phase more quickly and with higher capacity than untreated cotton as well as three commercially available fabric-based adsorbents. Volatile adsorbed pollutants were fully extracted from CD-TFP@cotton under reduced pressure at room temperature, enabling simple reuse. These properties make cotton functionalized with the cyclodextrin polymer of interest for water purification membranes, odor controlling fabrics, and respirators that control exposure to VOCs. This functionalization approach is scalable, likely to be amenable to other fibrous substrates, and compatible with existing fiber manufacturing techniques.

3.3 Introduction

The presence of trace organic compounds in air or water is responsible for a broad range of desirable and undesirable effects. Certain compounds at appropriate concentrations give rise to pleasant fragrances, delectable flavors, and medicinal effects, yet others cause stench, undesirable flavors, or exhibit toxicity above threshold concentrations. Volatile organic compounds (VOCs)

are atmospheric contaminants emitted from industrial processes, transportation vehicles, and commercial products such as solvents, paints, cleaners, and lubricants.[145] Acute or chronic VOC exposure causes respiratory distress, eye and throat irritation, neurological toxicity, cancer, among other effects.[146–148] VOCs are removed by high surface-area adsorbents[25] that often include activated carbon (AC).[149] However, ACs are granular or particulate solids that are better suited for packed columns rather than clothing or other household items, and their regeneration often requires harsh treatments. Alternatives to ACs, particularly those that combine superior performance, facile regeneration, and straightforward integration with consumer products and/or textiles are desirable targets.[150–152]

β-Cyclodextrin (β-CD), a macrocycle of seven glucose units, is inexpensively derived from corn starch and represents an attractive VOC capture agent because it forms host-guest complexes with thousands of organic compounds.[153,154] This behavior has led to its widespread use to formulate and stabilize pharmaceuticals, cosmetics, foods, and fragrances.[155,156] Molecular β-CD derivatives are powders, most of which are water soluble, necessitating their incorporation into polymers or grafting onto insoluble supports for effective VOC removal or water purification. Although β-CD has been crosslinked by monochlorotriazine,[157,158] epichlorohydrin,[159] and polyfunctional carboxylic acids,[86,160,161] the resultant polymers exhibit low surface areas and poor uptake kinetics. We recently reported a new β-CD containing porous polymer crosslinked by a rigid aromatic system, tetrafluoroterephthalonitrile (TFN).[58] The CD-TFP polymer network removes organic micropollutants from water more quickly than best-in-class activated carbons and other β-CD-containing polymers and is fully regenerated at room temperature. Recognizing the chemical similarity of cellulose-based fibers to β-CD, here we functionalize cotton fabrics with the CD-TFP

polymer simply by including the fabric into the CD-TFP polymerization reaction. The CD-TFP functionalized fabric removes organic micropollutants from water and captures VOCs from air. The fabric significantly outperforms, in terms of rate and capacity, untreated cotton fabric as well as three commercial fabrics designed to remove odors. Much like the parent CD-TFP polymer, the modified fabric can be fully regenerated at room temperature.

3.4 Results and Discussion

3.4.1 Synthesis and Characterization

CD-TFP@cotton fabric was prepared by reacting β-CD, TFP, and K_2CO_3 in the presence of a cotton fabric in a solvent mixture of THF:H_2O 9:1 at 85 °C (Figure 3.1). The addition of the cotton fabric to the CD-TFP polymer reaction mixture results in simultaneous CD-TFP polymer formation and grafting of the polymer onto the cotton surface. Initial experiments that employed our previously reported polymerization conditions[58] resulted in poor attachment of the polymer to the cotton fabric, as determined by the fabric's ability to bind BPA. We attributed the poor grafting efficiency to the low solubility of three of the four components in the THF solution. H_2O increases the solubility of β-CD and K_2CO_3 in the reaction medium, which provided functionalized cotton with the best performance. A solid polymer is also formed under the reaction conditions, which was identified as the CD-TFP polymer by FTIR spectroscopy (Figure 2.S3). Combustion analysis of this material indicated a β-CD:TFP molar ratio of 1:2.4, which is lower than that observed for the high performance, porous β-CD-TFP polymer reported previously.[58] We attribute this difference in composition to the modified reaction conditions, as well as the presence of additional reactive alcohol groups on the cotton fabric. The β-CD:TFP ratio of the polymer bound to cotton

is difficult to precisely measure through combustion analysis because of the similar elemental composition of cotton and β-CD. However, polymers with low β-CD:TFP ratios tended to be non-porous and had slow pollutant uptake. The mass increase of the fabric after functionalization was (30 mg/g, 3.0%), but we believe this value does not reflect the amount of polymer loaded onto the fabric because we observed loose yarns that detached from the fabric during several of the reaction and isolation processes.

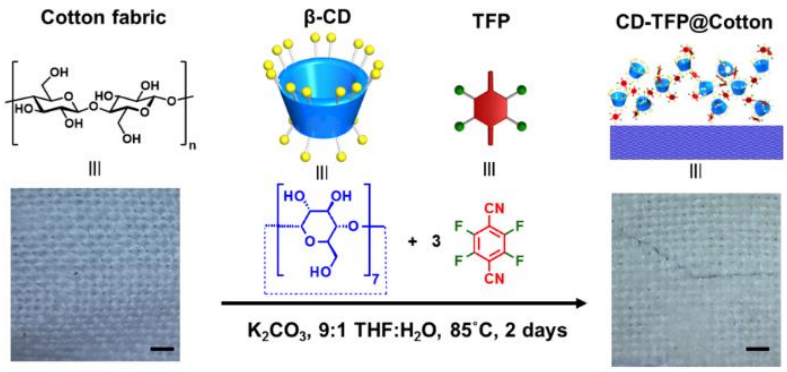

Figure 3.1 Schematic of the synthesis of the CD-TFP@cotton fabric. Bottom left: optical micrograph of untreated cotton fabric, and bottom right: optical micrograph of CD-TFP@cotton fabric. Scale bars: 1 mm.

The cotton fibers in the fabric appear unchanged after the CD-TFP polymerization reaction, as determined by scanning electron microscopy (SEM). These micrographs suggest that CD-TFP@cotton retains the physical and mechanical properties of unmodified cotton fabric, although the CD-TFP@cotton fabric's surface appears rougher (Figure 3.S1). We used the ability of β-CD to bind fluorescein to impart contrast between the cotton and CD-TFP polymer in confocal

micrographs. CD-TFP@cotton and untreated cotton fabrics were submerged in an aqueous fluorescein solution, rinsed with water, dried, and subjected to optical and fluorescent microscopy. The micrographs exhibit a clear contrast between the dim, non-selective labeling of the cotton fabric and the brighter particles on the CD-TFP@cotton, which we assign as the cyclodextrin polymer/fluorescein inclusion complex. These images illustrate that the CD-TFP polymer adopts a particulate morphology on the fabric (Figure 3.2).

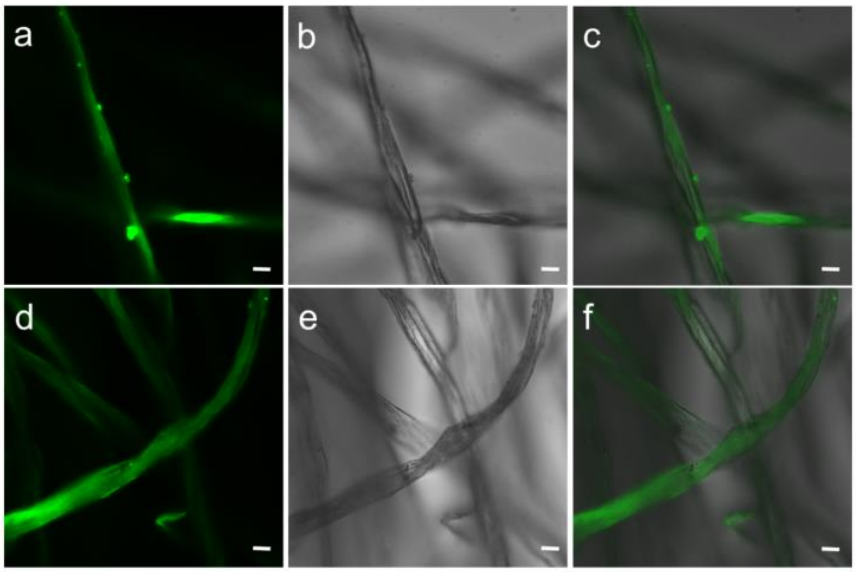

Figure 3.2 Fluorescence microscopy (left column), optical microscopy (center column) and overlaid images (right column) of CD TFP@cotton a–c and untreated cotton d–f. The traditional twisting of cotton fibers along the longitudinal axis is observed, which does not seem to be affected by the functionalization of the fibers with CD-TFP. Scale bars: 10 μm.

The compositional analysis and spectroscopic characterization of the CD-TFP@cotton confirmed the incorporation of TFN onto the cotton surface. XPS analyses indicated the presence of fluorine

and nitrogen for CD-TFP@cotton. As expected, untreated cotton shows no signals above baseline for these elements (Figure 3.3a–b and Figure 3.S2). An FTIR spectrum of the CD-TFP@cotton exhibits the typical bands for carbohydrates similar to the FTIR spectrum of the untreated cotton, in addition to absorbances at 2233 cm^{-1} and 1454 cm^{-1}, corresponding to the nitrile and C-C aromatic stretches of the TFN groups, respectively. Peaks at 1370 cm^{-1} and 1318 cm^{-1} are broadened and of different intensity in the spectrum of the CD-TFP@cotton compared to that obtained from unmodified cotton.

We attribute this change to the presence of the β-CD units on the fabric (Figures 3.3c and Figure 3.S3), although its chemical similarity to the cotton complicates making this assignment definitively. Furthermore, thermogravimetric analysis indicated no statistical difference in the decomposition temperature of the CD-TFP@cotton in comparison with the untreated cotton in a nitrogen atmosphere (Figure 3d) and air (Figure 3.S4 and Table 3.S1), and a decrease of 22.0 ±9.3 °C in decomposition temperature of both fabrics in an air atmosphere compare with a nitrogen atmosphere. Additionally, tensile testing shown a change in the mechanical properties of the fabric, a decrease in the peak strength and the modulus of fabrics subjected to the reaction conditions was seen (Table 3.S2). Collectively, these observations suggest that the CD-TFP polymer forms on the cotton fabric without major changes to its fibrous structure, which motivated us to evaluate its pollutant uptake.

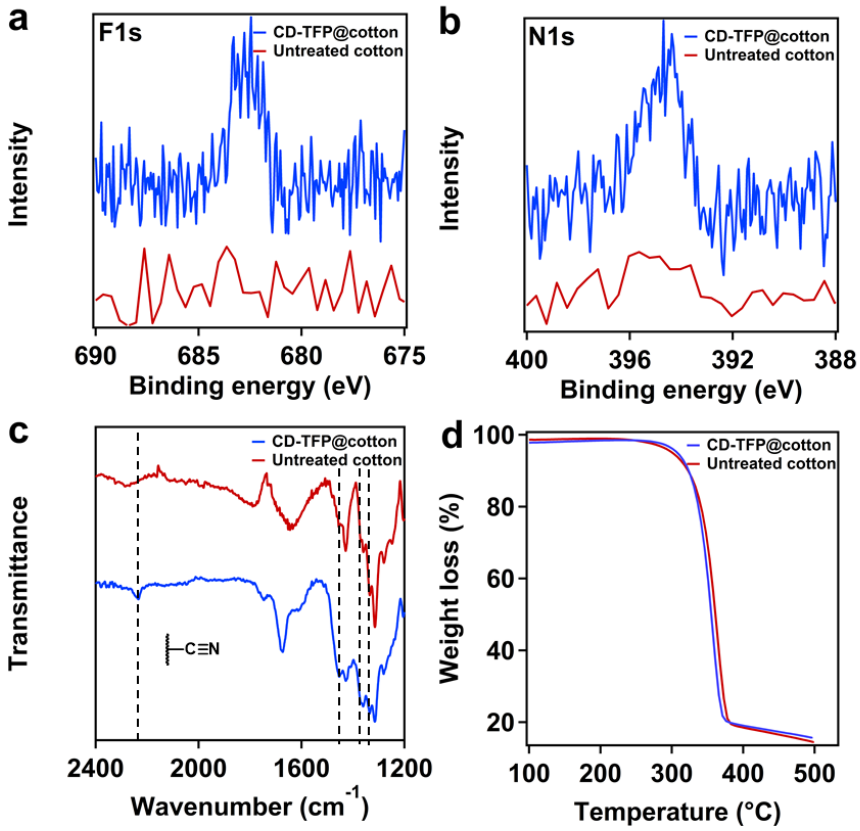

Figure 3.3 Spectroscopic characterization of the CD-TFP@cotton (blue) and untreated cotton (red) fabrics. a. F1s XPS; b. N1s XPS; c. FTIR-ATR; and d. TGA.

3.4.2 Pollutant Uptake from Solution

The presence of β-CD binding sites on the CD-TFP@cotton surface was confirmed by uptake studies in the aqueous phase. The uptake of Bisphenol A (BPA), a suspected endocrine disruptor,[162] by the CD-TFP@cotton and untreated cotton was quantified as a function of contact time with the fabric.[58] The CD-TFP@cotton showed an order of magnitude greater BPA capture versus untreated cotton (Figure 3.4a). At equilibrium CD-TFP@cotton adsorbed 3.0 mg per g of fabric (64.5% of the available BPA), and the uptake of untreated cotton was only 0.37 mg/g (7.9%

of the available BPA). Additionally, the CD-TFP@cotton can bind more BPA within the first 5 min (0.87 mg/g) compared to the BPA uptake of the untreated fabric after one day (0.37 mg/g).

Further control experiments confirmed that enhanced BPA uptake is associated with covalently attached β-CD groups. Cotton fabric subjected to identical polymerization conditions in the absence of either TFP or β-CD adsorbed similar amounts of BPA as untreated cotton (Figure 3.4b). Moreover, cotton fabric that was exposed to pre-formed CD-TFP polymer under the polymerization conditions (85 °C, 2 days, THF/H_2O) failed to show enhanced BPA uptake. These findings indicate that the pre-formed CD-TFP polymer is not efficiently grafted to the fabric under those polymerization conditions and that polymerizing the CD-TFP polymer in the presence of the fabric is necessary.

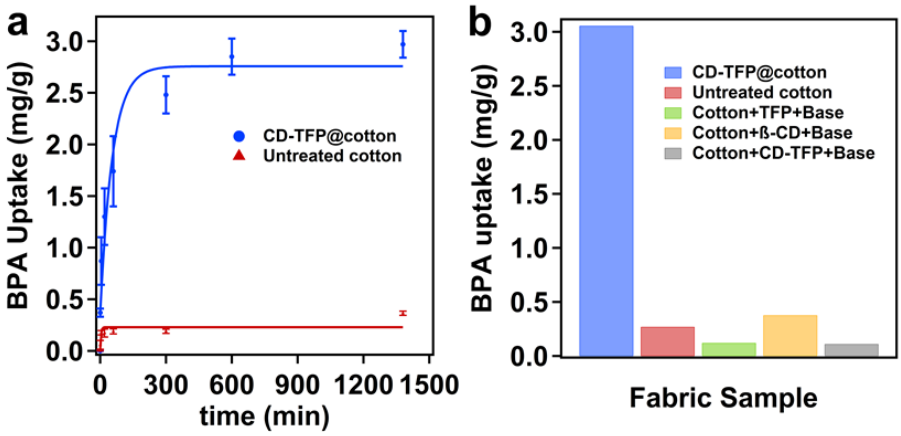

Figure 3.4 a. Time-dependent BPA (0.1 mM) uptake by the CD-TFP@cotton and untreated fabric (5 mg fabric/mL); b. BPA (0.1 mM) uptake at equilibrium by the CD-TFP@cotton fabric, the untreated cotton fabric, and three cotton fabric controls prepared by subjecting the cotton fabric to

the synthetic conditions, base and TFP (green), or base and β-CD (yellow), or base and CD-TFP (grey).

We measured thermodynamic parameters of BPA adsorption on the treated and untreated fabrics to determine if the enhanced BPA adsorption by CD-TFP@cotton originates from the formation of β-CD/BPA inclusion complexes (Figure 3.5). Langmuir and the Freundlich models were examined, as they best describe independent or interacting, poorly defined adsorption sites, respectively.[163] We immersed untreated cotton and CD-TFP@cotton into aqueous solutions with different initial BPA concentrations ($[BPA]_0$) and characterized the residual solution [BPA] at equilibrium (C_e, mM) and the adsorbed BPA (q_e, mg/g fabric) using UV-vis spectroscopy. These values were fit to Langmuir and Freundlich models, as shown in Figures S3.5, S3.6 and Table S3.3. The uptake of the untreated cotton shows a better linear fit to the Freundlich model compared to the Langmuir model (R^2 values of 0.838 and 0.691 respectively), which is consistent with the nonspecific binding of BPA. In contrast, CD-TFP@cotton fits the Langmuir model (R^2 of 0.975) reasonably well, which we attribute to specific formation of 1:1 BPA⊃β-CD inclusion complexes. Moreover, the maximum BPA adsorption capacity at equilibrium, q_e (mg BPA/g fabric), on the CD-TFP@cotton was 16.5 mg BPA/g fabric. Assuming the formation of a 1:1 complex between β-CD and BPA, this maximum loading corresponds to 82.0 mg β-CD/g fabric, or 8.2 wt% β-CD per gram of functionalized cotton. Overall, the presence of approximately 8.2 wt% of β-CD in the CD-TFP@cotton yielded at least 17 times increase in the affinity and capacity of the cotton fabric towards BPA.

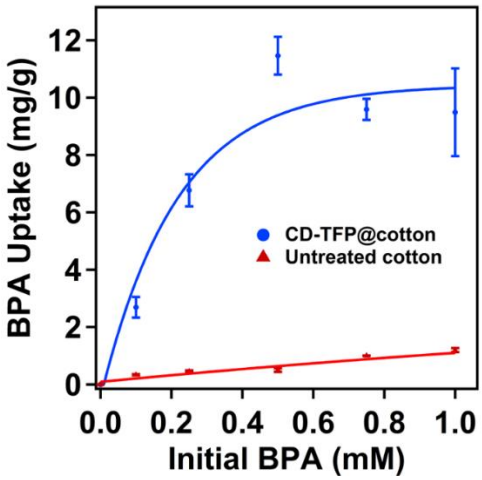

Figure 3.5 BPA uptake of the CD-TFP@cotton and untreated fabric as a function of initial BPA concentration (5 mg fabric / mL solution, measurement at equilibrium).

3.4.4 VOC Uptake

The styrene uptake of CD-TFP@cotton fabric was evaluated at low vapor pressure (Figure 3.6). We selected styrene as a model VOC because of the negative health effects associated with its exposure and its extensive industrial use in the manufacture of plastics, rubber and resins.[164] These experiments approximate environmental exposure and correspond to conditions in which materials with specific styrene binding sites are more likely to outperform nonspecific adsorption. The United States Occupational Safety and Health Administration (OSHA) has set a maximum one-time exposure limit to styrene of 600 ppm for up to 5 min.[165] The CD-TFP@cotton and untreated cotton were exposed to 830 ppm styrene vapor for 10 min (1 mg cotton/mL vapor). The amount of adsorbed styrene was quantified by UV-vis spectroscopy after extraction from the fabric using MeOH. These experiments indicated a maximum uptake of 0.22 mg styrene/g CD-TFP@cotton after 10 min of exposure, corresponding to an uptake of 26.5% of the initial styrene. Untreated

cotton removed less than 1% of the styrene vapor under these conditions (Figure 3.6). Overall, CD-TFP@cotton demonstrates rapid VOC capture at levels relevant for contaminated environments.

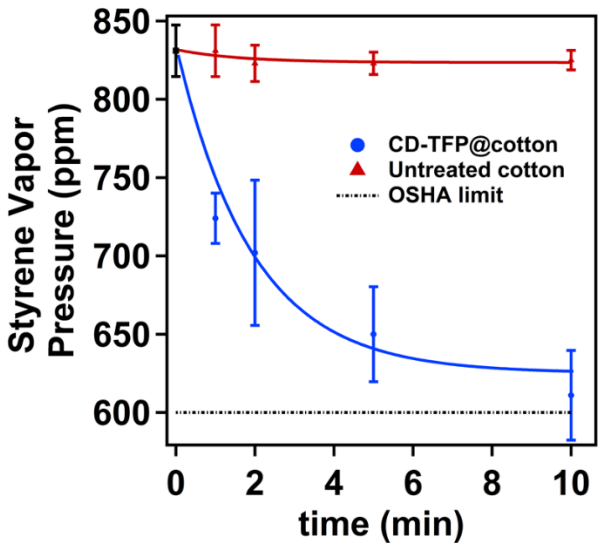

Figure 3.6 Time-dependent styrene vapor uptake at environmentally relevant concentrations, by the CD-TFP@cotton and untreated cotton fabrics (0.71 mg styrene/g fabric, 1 mg fabric/mL vapor). The line at 600 ppm illustrates the US OSHA exposure threshold (5 min exposure).

Additional uptake experiments were performed at higher styrene concentrations, which indicate that CD-TFP@cotton sequesters VOCs more effectively than untreated cotton as well as three commercial fabrics advertised for their ability to remove VOCs and malodorous compounds. Commercial fabric #1 is a polyester and commercial fabric #2 is a blend of polyester/cotton, both of which contain proprietary materials that claim to remove odors. Commercial fabric #3 is cotton with activated carbon embedded in the fabric. The CD-TFP@cotton fabric and controls were exposed to styrene-saturated air for given intervals to determine their styrene uptake rate and

capacity. The fabrics were then placed under vacuum for one hour to remove the weakly adsorbed styrene, after which the remaining styrene on the fabrics was extracted using MeOH and quantified by UV-vis spectroscopy. Under these conditions, the CD-TFP@cotton fabric has a significantly higher capacity and more rapid uptake of styrene vapor than all of the other specimens (Figure 3.7a). AC-functionalized commercial fabric #3 captures more styrene than untreated cotton and the other two commercial fabrics, but it shows four times less styrene capture than the CD-TFP@cotton fabric under comparable exposure times. Moreover, the captured styrene was easily removed from the CD-TFP@cotton fabric by washing with a small amount of MeOH at room temperature. Figure 3.7b shows four consecutive styrene adsorption/desorption cycles, and the regenerated CD-TFP@cotton exhibited similar performance compared with the as-synthesized fabric.

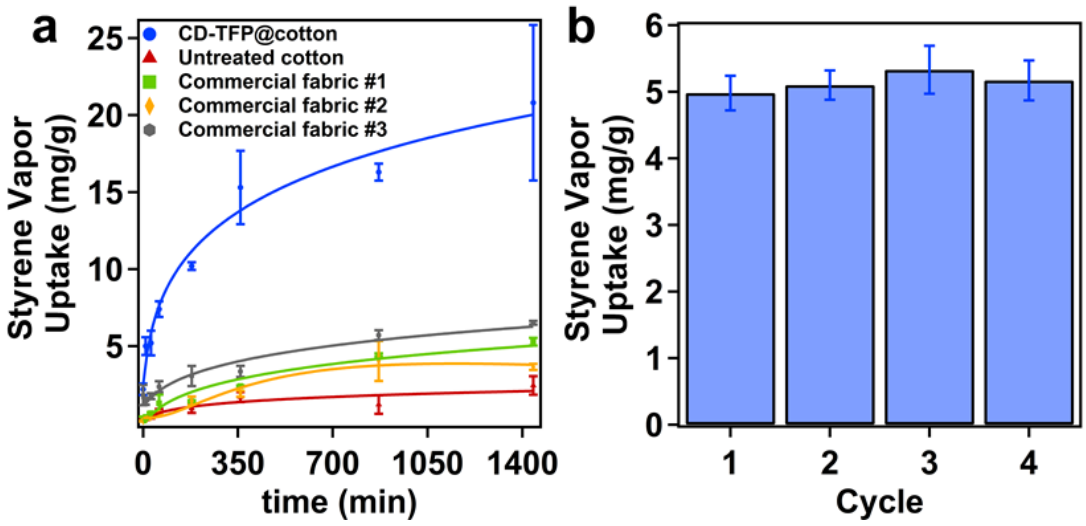

Figure 3.7 a. Time-dependent uptake of saturated styrene vapor by the CD-TFP@cotton, untreated cotton, and commercial VOC-capturing fabrics 1-3; b. Reusability test of the CD-TFP@cotton

towards saturated styrene vapor uptake after 10 minutes of exposure. Styrene desorption after each adsorption cycle was performed by soaking the fabric in 10 mL MeOH for 1 h.

The scope of CD-TFP@cotton VOC capture was explored and compared with control fabrics at short exposure times. Aniline is widely use in the production of dyes, pharmaceuticals, pesticides and rubber, and has been related with various health effects.[166] Benzaldehyde is commonly used in the food industry, pharmaceuticals and as a plastic additive, which is innocuous at low concentrations but causes irritation of the eye, skin, and respiratory system at higher concentrations.[167]

Fabrics were exposed to a saturated vapor pressure of aniline or benzaldehyde for a period of 10 min, and the captured vapors were extracted from the fabrics by MeOH and measured by UV-vis spectroscopy (Figure 3.8). For all VOCs, the CD-TFP@cotton significantly outperformed untreated cotton and the three commercial fabrics. These results indicate that the high capacity and rapid VOC capture by the CD-TFP@cotton can be generalized for a variety of VOCs that form host-guest complexes with β-CD.

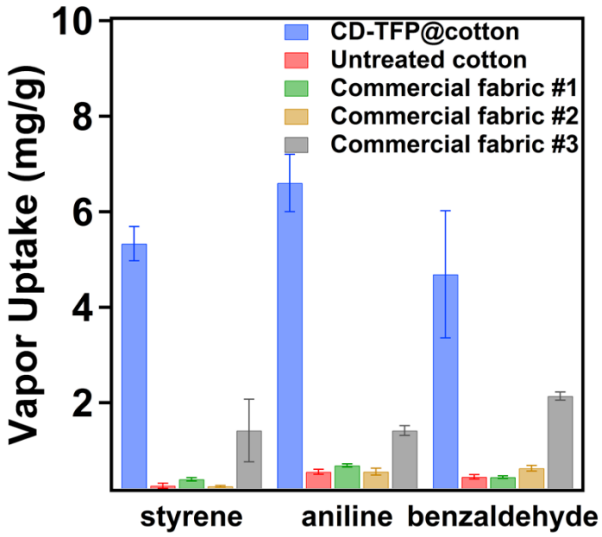

Figure 3.8 Saturated VOC uptake of styrene, aniline and benzaldehyde by the CD-TFP@cotton, untreated cotton, and the commercial fabrics #1-3 (15 mg fabric), after 10 min of exposure.

3.5 Conclusions

Cotton fabric was functionalized with a β-cyclodextrin polymer CD-TFP in one synthetic step. The resulting CD-TFP@cotton fabric removes bisphenol A, a model organic micropollutant, from water with ten-fold increased capacity compared to untreated cotton. The CD-TFP@cotton fabric also captures model VOCs at saturated and environmentally relevant vapor pressures, significantly greater and in a faster manner than untreated cotton and three commercial VOC-capturing fabrics. Furthermore, the CD-TFP@cotton can be regenerated multiple times at room temperature with no loss of performance. The CD-TFP@cotton is therefore an outstanding candidate as a membrane for water purification and VOC-capturing fabric to make cloths with de-odorant properties and fiber-based masks and filtration media that can capture toxic chemicals from air. The methodology

described in this manuscript can be expanded to other fibrous materials and it can be easily incorporated into traditional textile manufacturing processes.

3.6 Acknowledgments

We thank Simge Uzun assistance with the SEM images and tensile testing and Dr. Goeun Sim for helping with the fluorescence microscopy images. This work was supported by the National Science Foundation (NSF) through the Center for Sustainable Polymers (CHE-1413862). This work made use of the Cornell Center for Materials Research Shared Facilities which are supported through the NSF MRSEC program (DMR-1120296), and Fluorescence Microscopy was performed at the Cornell University Biotechnology Resource Center.

3.7 Chapter 3 Appendix

3.7.1 Materials and Instrumentation

Reagents: β-cyclodextrin (β-CD) (>97%) and tetrafluorotere-phthalonitrile (TFN) (>99%) were purchased from Sigma Aldrich and used without further purification. Tetrahydrofuran (THF) was purified and dried in a custom-built activated alumina solvent purification system. Cotton fabrics (cotton-400) were purchased from testfabrics. Aqueous solutions of bisphenol A (BPA) were prepared using 18 MΩ deionized H_2O at neutral pH. All model compounds were obtained from commercial sources and used as received. Commercial fabric #1 is sold under the trade name Arm and Hammer™ Curtain Fresh™ Odor Neutralizing Sheer Curtain. Commercial fabric #2 is an 85:15 polyester/cotton blend that was cut from fabric sold under the Dickies Drirelease® brand.

Commercial fabric #3 was purchased from Charcoal House under the Greenyarn Eco-fabric^{TM} brand.

Instrumentation: Ultraviolet/visible (UV-vis) spectroscopy was performed on a Cary 5000 Varian UV-vis spectrometer. UV-vis spectra were recorded at RT over the range 200–500 nm, corrected against an appropriate background spectrum, and normalized to zero absorbance at 500 nm. Infrared spectroscopy was performed on a Thermo Nicolet iS10 with a diamond ATR attachment. The photoelectron spectra (XPS) were recorded with X-probe (SSX-100) Surface Science Instrument equipped with a SSI Position Sensitive Detector, resistive anode, 40mm x 40mm. A monochromatic AlKα x rays at 1486.6 eV (8.3393 Å) was used. Photoelectrons were collected at an angle of 55-degrees from the surface normal, and the hemispherical analyzer with pass energy of 50 V. Samples were analyzed using an operating pressure < 2x10-9 Torr. Scanning electron microscopy was performed on a LEO 1550 FESEM (Keck SEM) operating at 2.00 kV and a working distance of 3–4 mm with an aperture size of 20 μm. Samples were prepared by adhesion to carbon tape on a flat aluminum platform sample holder and coated with gold at 20 mA for a period of 30 seconds. The sample was then placed directly into the instrument. Thermal gravimetric analysis (TGA) was carried out using a Mettler Toledo Tga/SDta851e. The samples were heated from 30 °C to 500 °C at a rate of 10 °C/min under a N_2 and air atmospheres at a flow rate of 50 mL/min in an aluminum pan. Bright field and confocal images were obtained using a Zeiss LSM 710 confocal microscope with a 40x objective lens in water immersion. A 488 nm laser was used as the excitation source, and a PMT was used to record light emission between 510 and 620 nm. A Zwick/Roell Z010 testing system was used to characterize the mechanical properties of the fabrics.

3.7.2 Experimental Protocols

Synthesis. Modification of the cotton fabric (CD-TFP@cotton) was performed by varying the previously reported synthesis of the cyclodextrin porous polymer.[20] In a 300 mL pressure vessel equipped with a magnetic stir bar was charged TFP (2.268 g, 11.31 mmol) and dry THF (145 mL), and the solution was stirred for 10 minutes. In another flask, β-CD (4.257 g, 3.74 mmol) and K_2CO_3 (6.369 g, 59.91 mmol) were suspended in 25 mL of deionized H_2O and sonicated for 10 min. This solution was then added dropwise into the THF solution. A sample of cotton 400 (1.429 g) was added to the reaction mixture, and the flask was bubbled with N_2 for 5 min. The N_2 inlet was removed, the flask was sealed and the mixture was placed on a hot stirring plate (85 °C) and stirred at 500 rpm for 2 d. The orange suspension was cooled and then filtered, the residual K_2CO_3 was removed by washing the fabric on the filter paper with 1 N HCl until CO_2 evolution stopped. The yellow fabric was isolated from the solid and activated by soaking in H_2O (200 mL) for 1 day, then the fabric was washed with MeOH using a Soxhlet extractor for 1 day. The fabric was filtered, and dried under high vacuum at RT for 1 day, which provided a yellow fabric sample that weighed 1.472 g.

Aqueous BPA kinetic uptake experiments: Adsorption kinetic studies were performed in 20 mL scintillation vials. All studies were conducted at ambient temperature without the use of stirring. The fabric (15 mg) was initially soaked in water for 1 min, then was transferred into a vial containing an aqueous BPA solution (3 mL, 0.1 mM). After a specific contact time, the solution was removed via syringe and filtered immediately by a Whatman 0.2 μm inorganic membrane filter into a UV-vis cuvette. The residual concentration of BPA was determined by UV-vis

spectroscopy, and finally the solution returned to the vial that contains the fabric. Uptake was determined as the average of three independent experiments performed using different fabric samples, each isolated from the same polymerization experiment.

Aqueous BPA thermodynamic uptake experiments: Thermodynamic adsorption studies were performed in 20 mL scintillation vials at ambient temperature without the use of stirring. The fabric (15 mg) was initially soaked in water for 1 min, then was transferred into a vial containing an aqueous BPA solution (3 mL, 0.1 mM) for 2 days. The solution was removed via syringe and filtered immediately by a Whatman 0.2 μm inorganic membrane filter into a UV-vis cuvette, after which the residual concentration of BPA was determined by UV-vis spectroscopy. Uptake was determined as the average of three independent experiments performed using different fabric samples, each isolated from the same polymerization experiment.

Gas-phase styrene kinetic uptake experiments performed at high styrene concentration: Kinetic adsorption studies were performed in 20 mL scintillation vials at ambient temperature. The vial was charged with styrene (200 μL), then was sealed and equilibrated for 10 min. The fabric (15 mg) was suspended in the head space of the vial (avoiding contact with the solution in the bottom of the vial). The vial was closed, and the fabric was equilibrated with the head space of the vial. After a given period of time, the fabric was removed from the vial and put under vacuum for 1 hour. Finally, the fabric was soaked in MeOH (2 mL) for 1 h. The MeOH solution was removed via syringe and filtered immediately by a Whatman 0.2 μm inorganic membrane filter and analyzed by UV–VIS spectroscopy. Uptake was determined as the average of three independent experiments performed using different fabric samples, each isolated from the same polymerization experiment.

Gas-phase styrene reusability experiments: Reusability studies were performed in 20 mL scintillation vials at ambient temperature. The vial was charged with styrene (200 μL), then was sealed and equilibrated for 10 min. The fabric (15 mg) was suspended in the head space of the vial (avoiding contact with the solution in the bottom of the vial). The vial was closed, and the fabric was equilibrated with the head space of the vial. After a given period of time, the fabric was removed from the vial and put under vacuum for 1 hour. Finally, the fabric was soaked in MeOH (2 mL) for 1 h. The MeOH solution was removed via syringe and filtered immediately by a Whatman 0.2 μm inorganic membrane filter and analyzed by UV–vis spectroscopy. The fabric was soaked in MeOH (10 mL) for 1 h, then was rinsed with additional MeOH (3 x 5 mL), excess solvent was wicked from the fabric using a paper towel, and the fabric was dried under vacuum for 1 h. The fabric sample was subjected to four reuse cycles, and the overall procedure was performed in triplicate.

Gas-phase styrene kinetic uptake experiments performed at low styrene concentration: Kinetic adsorption studies were performed in 20 mL scintillation vials at ambient temperature. The fabric (20 mg) was placed in the bottom of a scintillation vial equipped with a septum. Styrene (1 mL) was charged into a separate scintillation vial sealed with a septum under a N_2 atmosphere and equilibrated for 10 min. An aliquot of the head space of this vial (500 μL) was removed and injected into the vial containing the fabric using a gas-tight syringe, after which the fabric was equilibrated with the injected styrene vapor for a given period of time. The fabric was removed from the vial and soaked in MeOH (2 mL) for 1 h, which was filtered through a Whatman 0.2 μm inorganic membrane filter. The concentration of styrene removed from the fiber was determined

by UV–vis spectroscopy. Uptake was determined as the average of three independent experiments performed using different fabric samples, each isolated from the same polymerization experiment.

Gas-phase uptake experiments using other pollutants: Adsorption studies of benzaldehyde, aniline, and styrene were performed in 20 mL scintillation vials at ambient temperature. 200 μL of the compound was charged into a sealed scintillation vial and allowed to equilibrate for 10 min. The fabric (15 mg) was suspended in the head space of the vial (avoiding contact with the solution in the bottom of the vial). The vial was closed, and the fabric was equilibrated with the head space of the vial for 10 min. The fabric was removed from the vial and put under vacuum for 1 h. Finally, the fabric was soaked in MeOH (2 mL) for 1 h. The MeOH solution was removed via syringe and filtered immediately by a Whatman 0.2 μm inorganic membrane filter and analyzed by UV–vis spectroscopy. Uptake was determined as the average of three independent experiments performed using different fabric samples, each isolated from the same polymerization experiment.

3.7.3 Additional Characterization

SEM Images

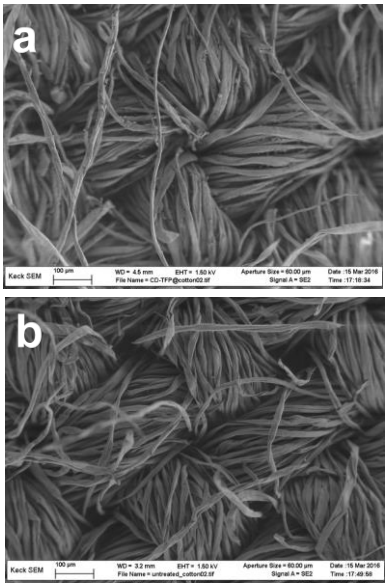

Figure 3.S1 SEM images of (a) CD-TFP@cotton; and (b) Untreated cotton

XPS survey

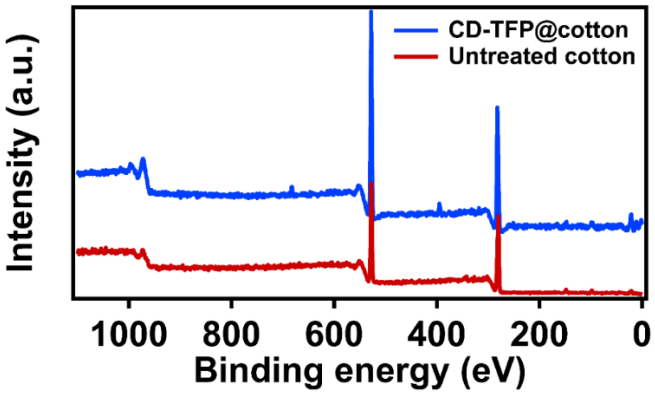

Figure 3.S2 XPS survey of the fabrics.

Additional Infrared spectra

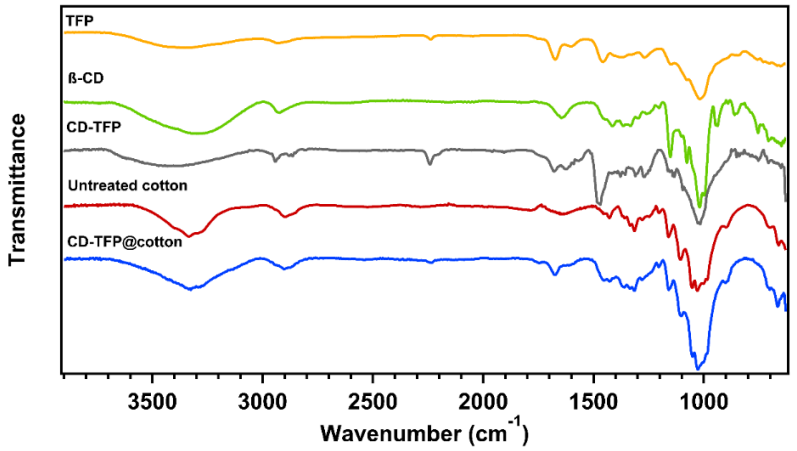

Figure 3.S3 Infrared spectra of the monomers (TFN, β-CD; yellow and green, respectively), isolated polymer (CD-TFP, green), and cotton samples (untreated, red and functionalized, blue).

Additional TGA analysis

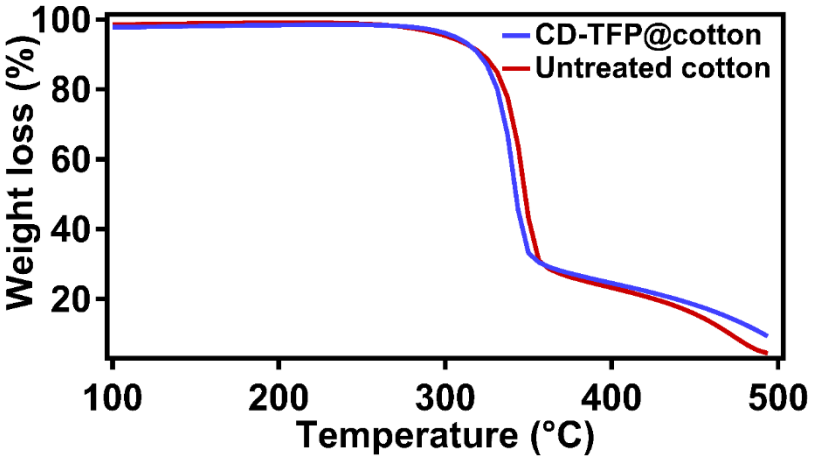

Figure 3.S4 TGA analysis in air atmosphere of the fabrics.

Table 3.S1 Decomposition temperatures of CD-TFP@cotton and Untreated cotton fabrics in nitrogen and air atmosphere.

Fabric	N_2	Air
CD-TFP@cotton	370.3±5.7	346.5±4.1
Untreated cotton	373.7±3.8	353.5±4.6

Tensile testing

Table 3.S2 Tensile testing of CD-TFP@cotton, Untreated cotton and a cotton fabric subjected to the same reaction conditions but without TFN (Reacted cotton).

Fabric	Failure strain (mm/mm)	Peak Strength (MPa)	Modulus (MPa)
CD-TFP@cotton	0.105 ± 0.009	25.2 ± 1.7	286.5 ± 4.3
Untreated cotton	0.087 ± 0.001	35.7 ± 2.1	599.4 ± 19.9
Reacted cotton	0.140 ± 0.013	35.3 ± 2.0	431.1 ± 51.3

3.7.4 Additional Calculations

Thermodynamic studies: The Langmuir and Freundlich models were selected to study the thermodynamic adsorption of BPA in the fabrics.[168]

The Langmuir model, which treats the material as having a homogeneous adsorption surface, is given in linear form as

$$\frac{1}{q_e} = \frac{1}{q_{max,e} k_c} \times \frac{1}{C_e} + \frac{1}{q_{max,e}} \quad \text{(eq 3.S1)}$$

Where q_e (mg BPA/g fabric) is the amount of BPA adsorbed per gram of fabric at equilibrium. $q_{max,e}$ (mg BPA/g fabric) is the maximum adsorption capacity of adsorbent at equilibrium, k_c (mol^{-1}) is the equilibrium constant and C_e(mM) is the concentration at equilibrium.

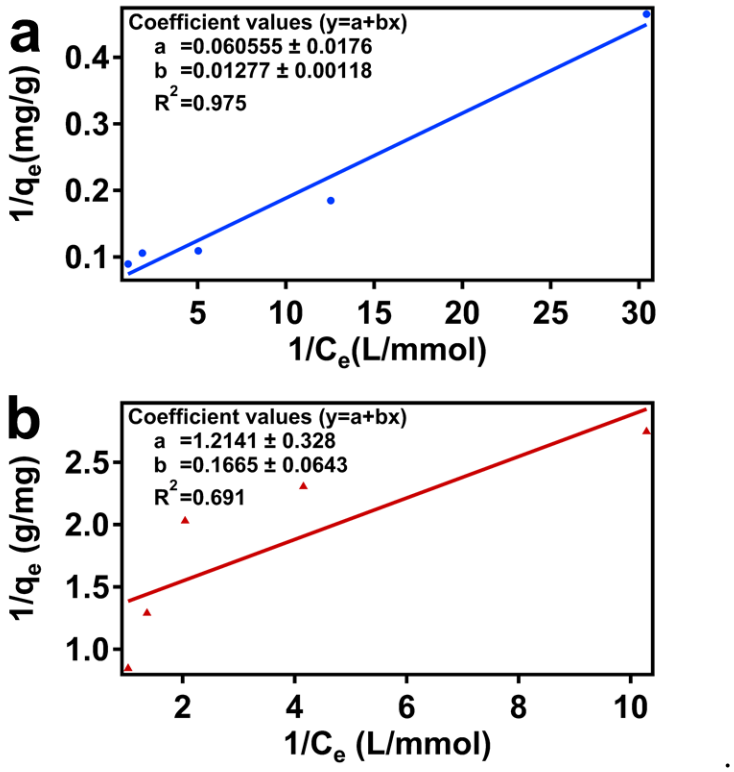

Figure 3.S5 Langmuir isotherm graphs for (a) CD-TFP@cotton, and (b) untreated cotton.

The Freundlich model, which is used for heterogeneous adsorption surfaces without a saturation of adsorption sites, is expressed in the following linear form:

$$Log(q_e) = \frac{1}{n_f}\log(C_e) + \log(K_f) \text{ (eq 3.S2)}$$

Where q_e (mg BPA/g fabric) is the amount of BPA adsorbed per gram of fabric at equilibrium. C_e(mM) is the concentration at equilibrium. n_F is the Freundlich constant associated to the degree of system heterogeneity. K_F ((mg g^{-1})(L $mmol^{-1}$)^{n_F}) is a unit capacity coefficient.

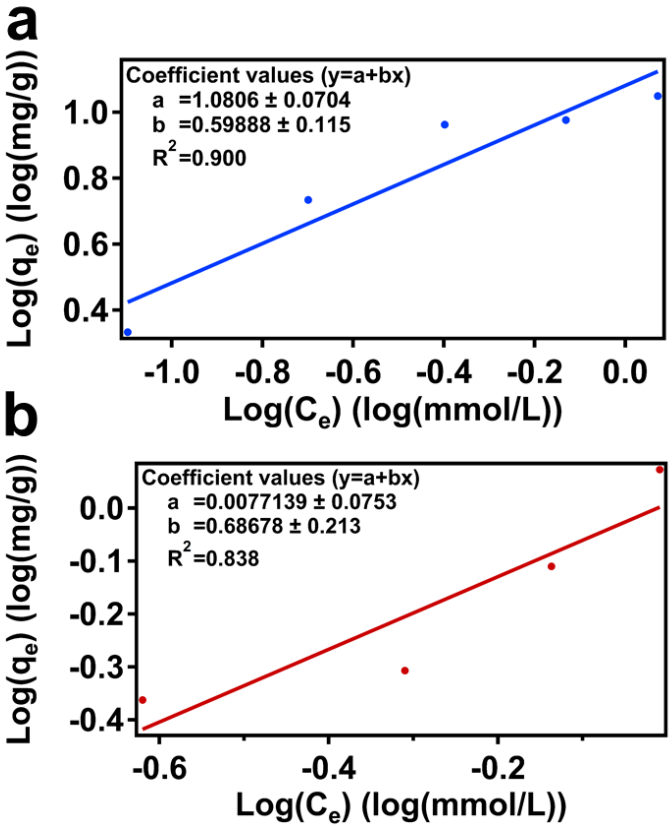

Figure 3.S6 Freundlich isotherm graphs for a. CD-TFP@cotton, and b. untreated cotton.

Table 3.S3 Thermodynamic calculations result of the CD-TFP@cotton and the untreated cotton.

Model	Fabric	$q_{max,e}$ (mg g^{-1})	k_c (mol^{-1})	K_F ((mg g^{-1})(L $mmol^{-1}$)^{nF})	n_F	R^2
Langmuir	CD-TFP@cotton	16.5	4.7			0.975
	Untreated cotton	0.9	6.5			0.691
Freundlich	CD-TFP@cotton			12.0	1.67	0.900
	Untreated cotton			1.0	0.57	0.838

3.7.5 UV-vis Spectra

BPA experiments

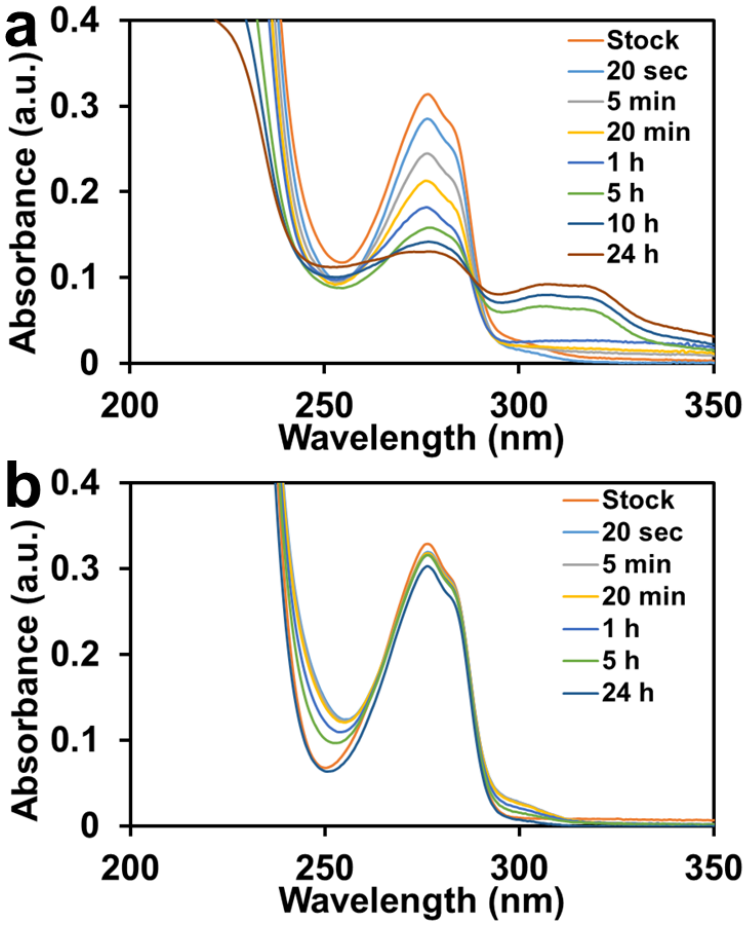

Figure 3.S7 UV-vis spectra of BPA remained in the solution after the removal of the pollutant by the fabrics as a function of time of (a) CD-TFP@cotton and (b) untreated cotton. The trace labeled "Stock" corresponds to the initial concentration of the solution.

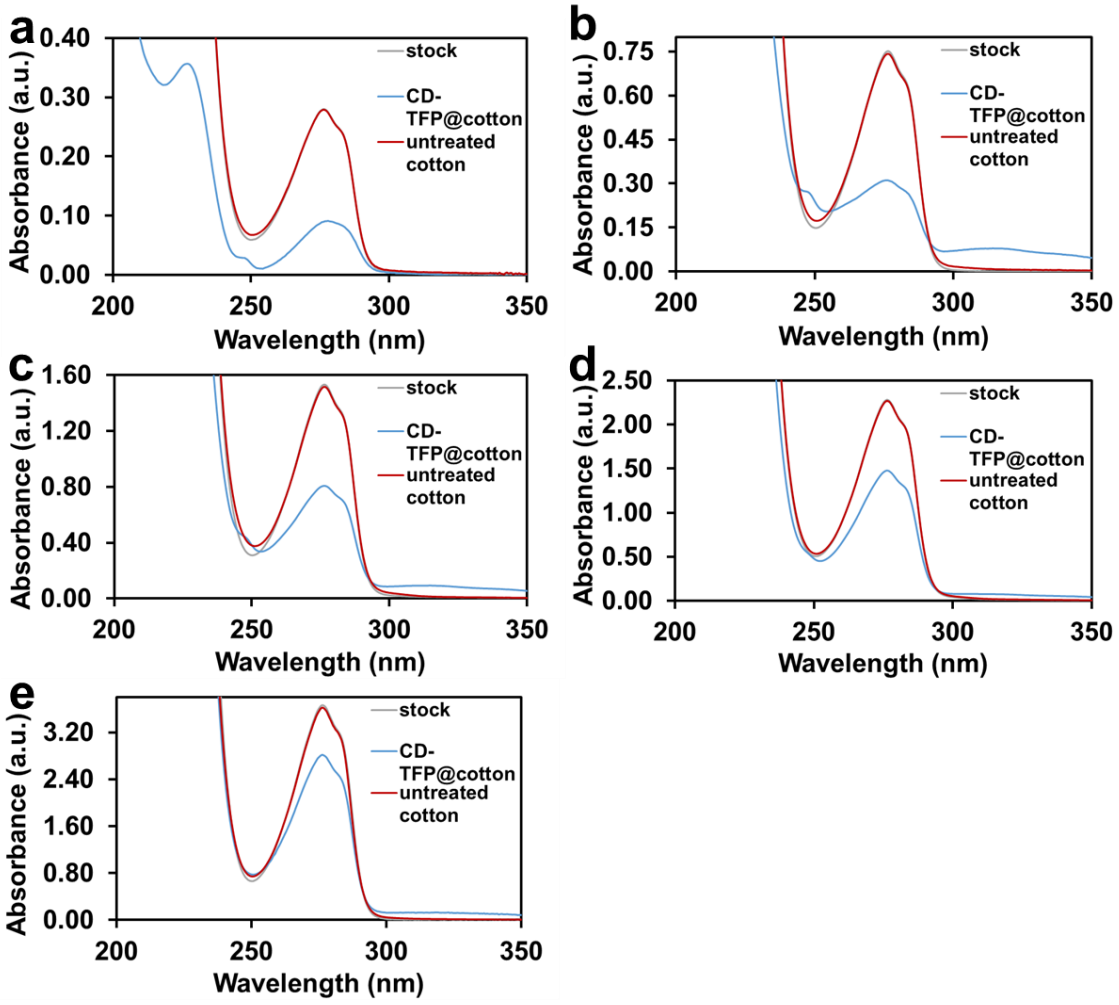

Figure 3.S8 UV-vis spectra of BPA that remained in the solution after the removal of the pollutant by the fabrics as a function of initial BPA concentration: (a) 0.1 mM; (b) 0.125 mM; (c) 0.25 mM; (d) 0.5 mM; (e) 1 mM. The trace labeled "Stock" corresponds to the initial concentration of the solution.

Styrene experiments

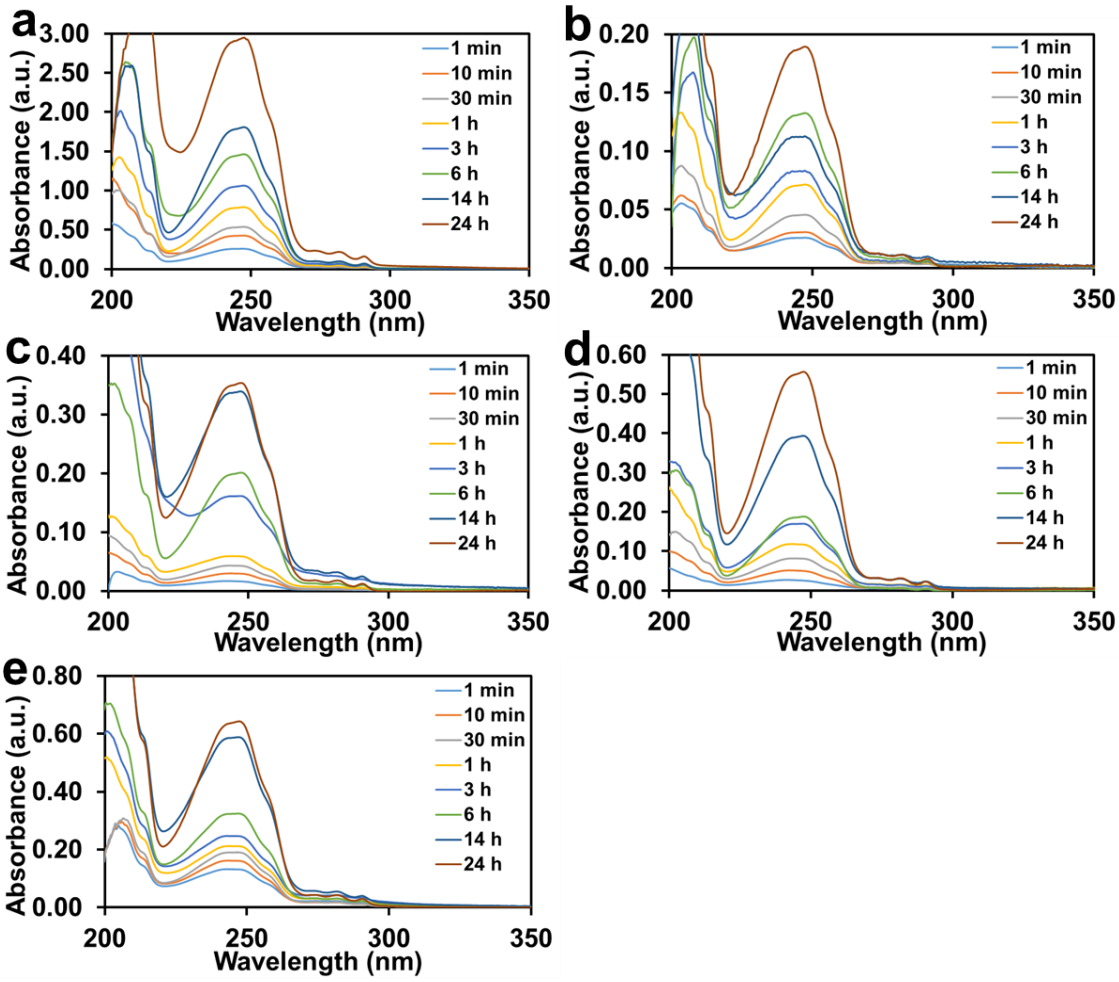

Figure 3.S9 UV-vis spectra of styrene extracted from the fabric samples in the high-concentration vapor phase experiments. The times listed for each spectrum indicate the contact time of the fabric with styrene vapor, with increased contact times generally resulting in increased signal intensity in this experiment. (a) CD-TFP@cotton; (b) untreated cotton; (c) commercial fabric #1; (d) commercial fabric #2; (e) commercial fabric #3.

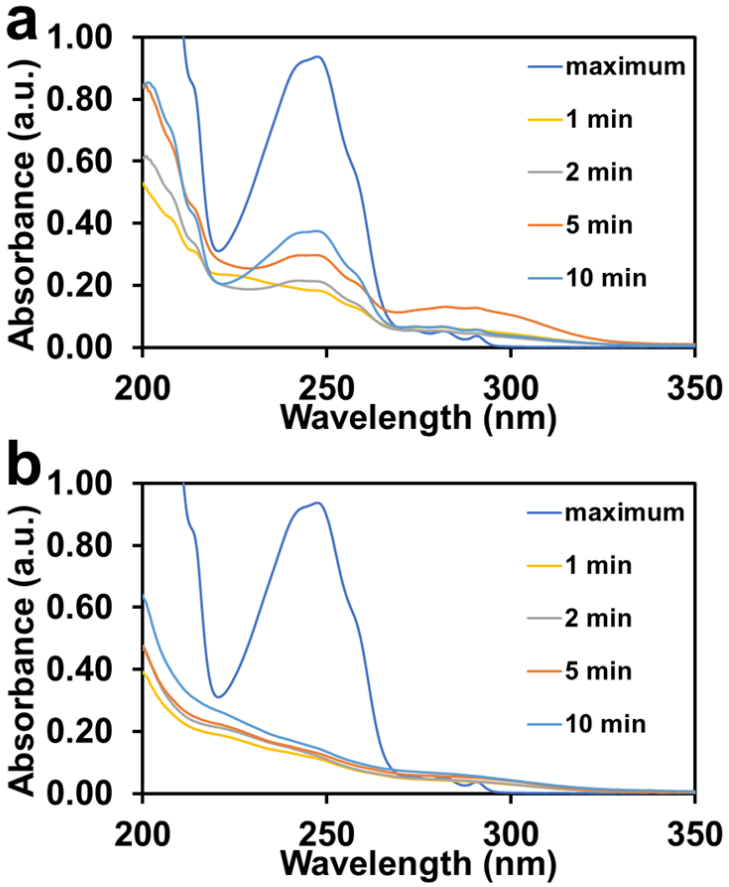

Figure 3.S10 UV-vis spectra of styrene extracted from the fabric samples in the low-concentration vapor phase experiments. The times listed indicate the contact time of the fabric with styrene vapor, such that increased styrene uptake is observed for the CD-TFP@cotton a. over 10 minutes of contact time. In contrast, unmodified cotton b. shows little to no specific styrene uptake under similar conditions. The trace labeled "maximum" corresponds to the response expected that would correspond to 100% adsorption of styrene under the experimental conditions.

Model compound experiments

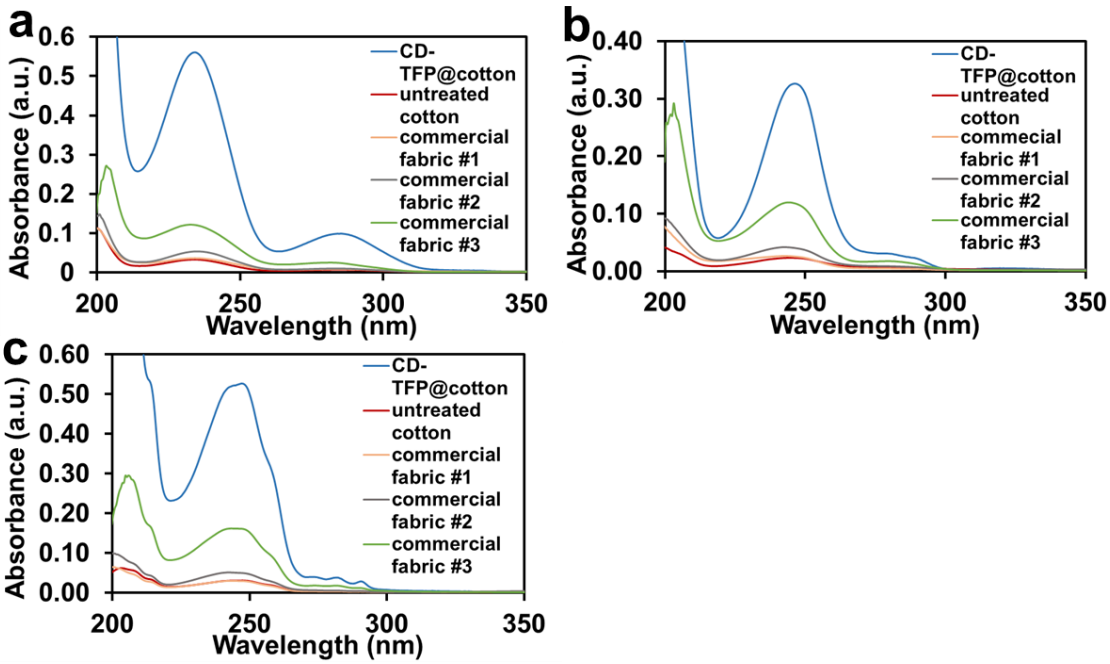

Figure 3.S11 UV-vis spectra of (a) aniline; (b) benzaldehyde; and (c) styrene, extracted at 10 min contact time from each fabric sample in the gas model compound experiments. The CD-TFP@cotton fabric sequesters larger amounts of each compound than untreated cotton and the commercial odor-controlling fabrics.

4. HEAT-PRESS FUNCTIONALIZATION OF COTTON FABRICS WITH A METAL ORGANIC FRAMEWORK FOR SIMULANT NERVE AGENT HYDROLYSIS

4.1 Preface

In this chapter, I show the work done in the expansion of the scope of functional materials and display a novel method to incorporate/fabricate metal organic framework (MOF) on cotton fabrics. Previously, incorporation of active MOFs like UiO-66-NH_2 onto cotton fabrics have been done through deposition of a pre-synthesized MOF and/or solvothermal synthesis. However, both methods use large amounts of solvents and long times in the network synthesis which are not ideal for scaling up. Thus, we aimed to develop an alternative method to integrate UiO-66-NH_2 on a cotton fabric that allows us a fast and easy incorporation of the network. We hypothesized that the heat-pressing technique, highly used in the textile industry and recently employed to deposit MOFs on carbon cloths, is applicable to incorporate UiO-66-NH_2 onto cotton fabrics. We developed a method to produce UiO-66-NH_2 using the heat-press technique by exploring different conditions. Then, we tested the developed method to grow *in-situ* UiO-66-NH_2 on a cotton fabric functionalized with carboxylic acids. We demonstrated that carboxylic groups anchored to the cotton fabric promote the MOF growing, and we further showed that the UiO-66-NH_2 deposited on the fabric is active towards the hydrolysis of a nerve agent simulant. This work was led by Deborah Turetsky and me and was performed in collaboration with Dr. Timur Islamoglu, Megan Wasson and Prof. Omar Farha from the Chemistry Department at Northwestern University.

4.2 Abstract

Chemical warfare agents (CWAs) are a serious threat to our society, therefore, a quick and large scale access to decontamination materials is required. Herein, we describe the development of an easy and scalable heat-pressing method for the solvent-free synthesis of UiO-66-NH_2, and its subsequent incorporation on cotton fabrics for the decontamination of CWAs. Use of pre-formed hexanuclear zirconium benzoate cluster along with 1,8-bis(dimethylamino)naphthale, a non-nucleophilic base, improved the network formation as evidenced by the increase in the surface area and crystallinity of the final MOF material, and showed faster hydrolysis of a nerve agent (NA) simulant. The developed methodology was used to incorporate the MOF in a cotton fabric that contains dangling carboxylic groups. The pre-functionalization of the cotton fabric increased the loading of UiO-66-NH_2 and the catalytic activity towards the hydrolysis of the nerve agent simulant. This fast and easy approach to incorporate UiO-66-NH_2 in cotton fabrics is scalable and compatible with existing textile manufacturing techniques.

4.3 Introduction

The use of chemical warfare agents to attack military soldiers and civilians continues to be a threat for our society.[169] Among the different chemical weapons, organophosphate nerve agents (NAs) like sarin are particularly aggressive, because of their ability to rapidly block acetylcholinesterase, disrupting the message transport between nerves and organs.[170] Therefore, development of materials and technologies capable of degrading NAs are of great interest. Current methods used by the United States Army to destroy large amounts of NAs often employ incineration and

neutralization via alkaline hydrolysis.[171–173] However, neither of them are suitable for rapid decontamination which is needed in the battlefield. Therefore, portable technologies able to remove NA rapidly are being developed.[94]

Materials designed to abate NA should rapidly interact with the substance. Metal–organic frameworks (MOFs) are envisioned as promising candidates.[31] MOFs are highly porous materials, which allows an efficient transport and capture of gases in their pores.[104] Additionally, MOFs are made of inorganic metal-oxo nodes that can hydrolyze NAs,[101] making it ideal for CWAs deactivation.[174] Especially, zirconium-based MOFs (*e.g.* UiO-66) are known to have excellent thermal and hydrolytic stability, and have been demonstrated to catalytically degrade NAs.[175,176,177] Recently, amino functionalized MOF UiO-66-NH_2 has shown to have superior hydrolysis activity as the amino group acts as a proton-transfer agent during the phosphoester bond hydrolysis, being able to hydrolyze a NA simulant with a half-life time of 1 min..[108,178] However, UiO-66-NH_2 is obtained as a powder-like material, which hampers its use in more realistic situations. Therefore, methods to incorporate it into protective garments and fabric-like materials are required.

Deposition of UiO-66-NH_2 onto fabric-like materials have been explored by several groups[179,180]and their catalytic activities toward CWAs have been demonstrated.[112] For instance, Dwyer et al. illustrated that solvothermal growth of UiO-66-NH_2 onto fabrics coated with inorganic surfaces can hydrolyze the NA simulant, dimethyl 4-nitrophenyl phosphate (DMNP).[181] In another report, Lu et al. incorporated a pre-synthesized UiO-66-NH_2 into polyvinylidene fluoride fibers via electrospinning of the composite; the authors also reported the hydrolysis of the NA soman.[182] Although, the functionalized fabrics have high catalytic performance in the

hydrolysis of organophosphates, the MOF synthesis and incorporation onto the fabrics in most of the cases are done by solvothermal methods, which can damage the fabrics and is not ideal for large scale coating of the MOF. Consequently, an alternative and facile approach to incorporate UiO-66-NH_2 on fabric-like materials is desirable.

Recently, a solvent-free heat-pressing method was introduced for the preparation of MOFs. In their report, Chen et al. incorporated seven different MOFs on carbon cloths by pressing the MOF precursors on top of the cloth for 10 min at 200 °C.[183] Subsequently, the method was employed to deposit various MOFs on other substrates due to its robustness and simplicity.[184–186] In this work, we explored the heat-press functionalization of cotton fabrics, which are widely use in the garment industry, with a MOF capable of hydrolyze NAs Initially, we explored conditions of the heat-press machine to synthesize UiO-66-NH_2 and to maximize its catalytic performance. Then, we in-situ synthesized UiO-66-NH_2 onto cotton fabrics functionalized with carboxylic acids using the heat-press method. Finally, we demonstrated that the modified fabric can catalytically hydrolyze the NA simulant DMNP.

4.4 Results and Discussion

4.4.1 Synthesis of the MOF UiO-66-NH_2

Synthesis of the MOF UiO-66-NH_2 was performed by depositing a solid mixture of a zirconium salt with 2-aminoterphthalic acid (BDC-NH_2) and polyethylene glycol (PEG) with a molecular weight of 3000 Da onto aluminum foil and heating the mixture up to 200 °C for 20 min using a heat-press machine (Scheme 4.1). These conditions were adapted from a recent publication where

a heat-pressing method was used for the synthesis of various MOFs.[183] We screened 5 different zirconium precursors, keeping a zirconium/linker molar ratio of 1.1 to increase the probability of network formation. Notably, the hexanuclear zirconium benzoate cluster (Zr_6-node) was the only precursor producing a crystalline material that matches the reported PXRD pattern of UiO-66-NH_2,[177] presumably due to its pre-formed MOF cluster that drives to the network extension just by an interchange of the ligands (Figure 4.S1 and Figure 4.S2b). However, this MOF (UiO-66-NH_2-HP1) had a surface area of 435 m^2/g (Figure 4.S2a), which is inferior to the ones reported for the solvothermal synthesis of UiO-66-NH_2 (1110-1455 m^2/g).[187,188] Additionally, the diffraction peak corresponding to the (111) plane at 7.34º was broad, and the peak corresponding to the (200) plane at 8.45° could be barely seen as a shoulder (Figure 4.S2b). These observations can be related with partial formation of the network under the reaction conditions. Formation of the MOF is done by an interchange of the Zr_6-node benzoic acid (BA) with BDC-NH_2. Therefore, incomplete network formation can be investigated by quantifying and comparing the amounts of BA and BDC-NH_2 in the final material. We digested UiO-66-NH_2-HP1 in concentrated sodium deuteroxide (NaOD) and used calcium formate as an internal standard to quantify the different organic molecules in the framework by ^{1}H-NMR spectroscopy. Herein, we determined the amount of BA, BDC-NH_2, and PEG in the digested solid (Figure 4.S3 and Table 4.S3). UiO-66-NH_2-HP1 still contained BA, and its concentration was 1.5 times higher than the amount of BDC-NH_2, which corroborated the partial formation of the network. Additionally, the network contained 4.4% of PEG that can partially clog the pores of the MOF, reducing its surface area. Therefore, further optimization of the heat-press method is necessary to increase the exchange between BA and BDC-NH_2, which will ultimately improve the properties of the MOF.

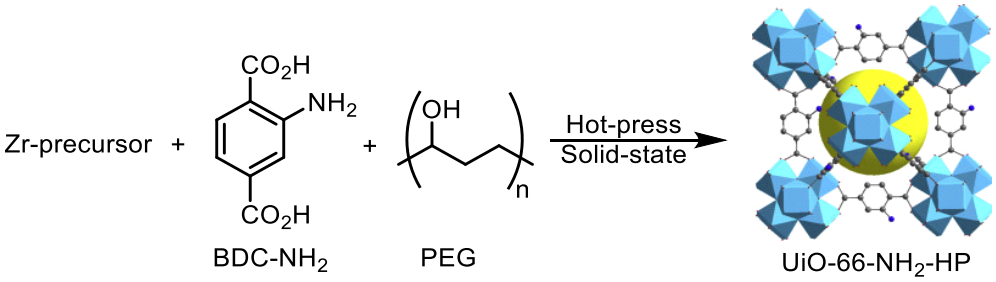

Scheme 4.1 Heat-press procedure for the synthesis of UiO-66-NH_2

In order to increase the reaction between the Zr_6-node and the BDC-NH_2, we added a base to deprotonate the carboxylic groups of the linker, which more readily forms the Zr-O bonds. We used equimolar amounts relative to BDC-NH_2 of the non-nucleophilic base 1,8-bis(dimethylamino)naphthalene (PS) to promote the incorporation of BDC-NH_2, without competing for the coordination sites of the zirconium. After reacting the solid precursors for 20 min at 200 °C in the heat-press machine, we obtained a yellow solid (UiO-66-NH_2-HP2) that was characterized using PXRD, N_2 physisorption isotherms, and ^{1}H-NMR. The PXRD pattern matched the UiO-66-NH_2 synthesized by solvothermal conditions, where the diagnostic (111) and (200) peaks were seen at 7.4º and 8.5º, respectively (Figure 4.1a). Additionally, this MOF had a surface area of 649 m^2/g, which is higher than the surface area of UiO-66-NH_2-HP1 (Figure 4.1b). Moreover, we found that UiO-66-NH_2-HP2 has a DFT pore size distribution with the majority of the pores at 12.7 Å, corresponding to the octahedral pores of the MOF. Additionally, UiO-66-NH_2-HP2 also contained pores at higher sizes corresponding to structure defects caused by missed linkers (Figure 4.S4).[189] Digestion of UiO-66-NH_2-HP2 and NMR analysis of the components showed 1.3 times more BDC-NH_2 compared with the amount of BA, which indicates a more

efficient incorporation of the linker mediated by the base (PS). Although, this MOF contains more PEG compared with UiO-66-NH_2-HP1, no presence of the PS was seen in the ^{1}H-NMR (Figure 4.S5 and Table 4.S3). SEM image of UiO-66-NH_2-HP2 showed indiscernible particle morphology as compared to the expected octahedral morphology observed with solvothermally synthesized UiO-66-NH_2.[188] Presumably, the fast reaction does not allow the complete formation of the MOF crystallites (Figure 4.1c). Furthermore, we evaluated the catalytic activity of the MOFs prepared with and without PS to hydrolyze the phosphoester linkage of DMNP. Better performance in terms of total conversion, and rate of hydrolysis by UiO-66-NH_2-HP2 compared with UiO-66-NH_2-HP1 was observed (Figure 4.1d). Conversion of DMNP reached 99% when UiO-66-NH_2-HP2 was used as a catalyst, in contrast, just 75% DMNP conversion was achieved when UiO-66-NH_2-HP1 was employed. Additionally, using the initial rate method, first order rate constant, k = 0.134 min^{-1} and 0.049 min^{-1}, were obtained for UiO-66-NH_2-HP2 and UiO-66-NH_2-HP1 respectively. The values indicate a faster rate of DMNP hydrolysis for the MOF synthesized in the presence of PS. Moreover, the half-life time decreased from 14.2 min for the MOF synthesized without the PS to 5.2 min for the MOF synthesized in the presence of the PS (see annex for detailed calculation, Figure 4.S6 and Table 4.S4). These findings support the use of PS to promote the incorporation of BDC-NH_2 during the network formation, which ultimately have a positive effect in the performance of the MOF towards the catalytic hydrolysis of DMNP.

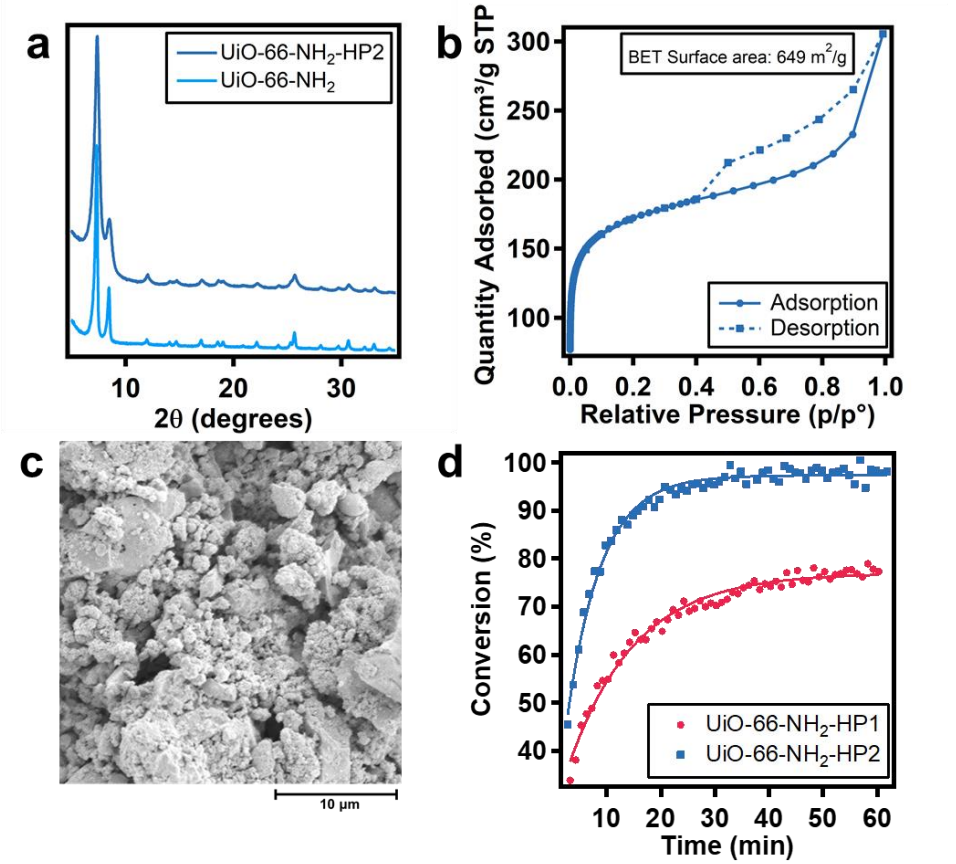

Figure 4.1 a. PXRD pattern comparison of UiO-66-NH_2-HP2 and UiO-66-NH_2 (via solvothermal synthesis) b. Nitrogen adsorption isotherm of UiO-66-NH_2-HP2 c. SEM image of UiO-66-NH_2-HP2 and d. Hydrolysis of DMNP by the MOF synthesized without PS (UiO-66-NH_2-HP1) and with PS (UiO-66-NH_2-HP2).

4.4.2 Functionalization of a cotton fabric with UiO-66-NH_2

Cotton fabrics have been used previously to template MOF growth. However, most methods rely on a solvothermal incorporation, where the fabrics and the MOF precursors are reacted in organic solvents.[190,191] Herein, cotton fabrics were functionalized with UiO-66-NH_2 using the optimized

heat-press method. We started pre-activating the cotton fabric by incorporating carboxylic acid groups, which can serve as nucleation points for MOF growth. The carboxylation of cellulose has been widely explored, with the reaction of chloroacetic acid.[192,193] However, this reaction uses highly concentrated sodium hydroxide solutions at elevated temperatures, which decreases the mechanical properties of the fabrics. Instead, we used succinic anhydride in the presence of 4-dimethylaminopyridine (DMAP) to produce carboxylic acid groups on the cotton fabric with imperceptible damage (Scheme 4.2). The carboxylated fabric (Cotton-COOH) was characterized by ICP-OES, FTIR, SEM and PXRD. Carboxylic acid groups were determined by the exchange of protons with lithium, followed by digestion of the fabric and subsequent quantification of the lithium in solution using ICP-OES. [138] We determined a concentration of 1.29 ± 0.33 mmol of COOH per gram of fabric, which corresponds a functionalization of 7.0 ± 1.8 % of the cellulose hydroxyl groups, assuming the fabric is ~100% cellulose, which indicates that one in every 4 to 5 glucoses in the cellulose has a carboxylic acid group. The FTIR spectrum of Cotton-COOH further confirmed the incorporation of the carboxylic acid groups on the fabric as new absorbance at 1726 cm^{-1} corresponding to the carbonyl C=O stretch appears along with the typical bands for carbohydrates at 1060 cm^{-1} and 3340cm^{-1} (Figure 4.S7 and Figure 4.2a). PXRD of the fabric showed diffraction peaks at 14.6º, 22.5º, and 34.3º, demonstrating no change in the crystalline structure of the cellulose after the reaction (Figure 4.S8, and Figure 4.2b). Finally, SEM images of Cotton-COOH were compared with the SEM images of plain cotton, where a preservation of the fabric structure is depicted (Figure 4.S9 and Figure 4.2c).

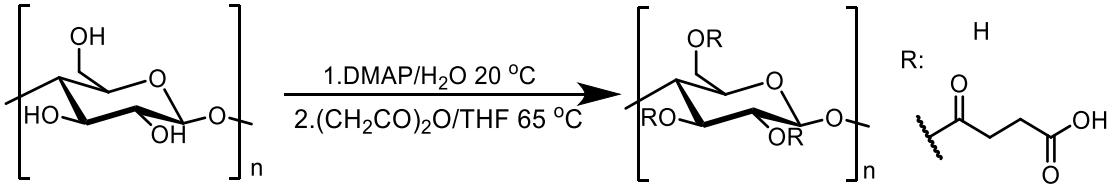

Scheme 4.2 Carboxylation of the cellulose in cotton fabrics using succinic anhydride.

The MOF functionalized fabric was prepared by spreading a mixture of Zr_6-node, BDC-NH_2, PS and PEG in between the Cotton-COOH, that is subsequently packed in aluminum foil. Then the wrapped fabric was heat-pressed at 200 ºC for 20 min (Scheme 4.3). After the reaction, a pale-brown fabric (UiO-66-NH_2@Cotton-COOH), as well as a small amount of a yellow solid were obtained. PXRD characterization of the solid reveal that it is unbound UiO-66-NH_2 (Figure 4.S10). Furthermore, using the same reaction conditions we functionalized a plain cotton fabric (UiO-66-NH_2@Cotton) to address the importance of the fabric pre-activation.

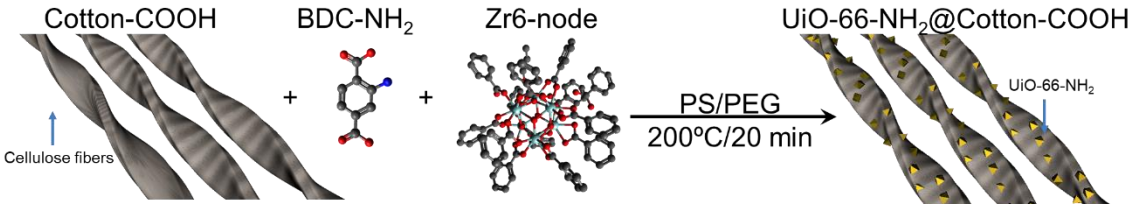

Scheme 4.3 Functionalization of cotton fabrics with UiO-66-NH2 via heat-pressing.

The MOF functionalized fabrics were characterized by PXRD, FTIR, SEM and ICP-OES to determine zirconium content. The FTIR spectra of the fabrics contained the typical carbohydrate peaks located around 1100 cm^{-1}, and new peaks in the 1500 to 1800 cm^{-1} region. A new band at 1650 cm^{-1} was seen in the FTIR spectrum of UiO-66-NH_2@Cotton, which corresponds to the C=O

stretch of the carboxylic acids in the MOF (Figure 4.2d). Moreover, the FTIR spectrum of UiO-66-NH_2@Cotton-COOH contains more than one band in the 1500 to 1800 cm^{-1} region, corresponding to the carboxylic group previously incorporated into the fabric, and the new carboxyl group from the MOF linker (Figure 4.2g). The PXRD patterns also indicated the incorporation of UiO-66-NH_2 into the two fabrics, where the d_{111} peak of UiO-66-NH_2 was seen at 7.4º and 7.2º for UiO-66-NH_2@Cotton and UiO-66-NH_2@Cotton-COOH respectively, along with the typical diffraction peaks of the cellulose at 14.6º, 22.5º, and 34.3º (Figures 4.2e and 4.2h). Additionally, SEM images of the fabrics revealed a poor covering of the MOF on UiO-66-NH_2@Cotton, where few particles were deposited on the cotton fibers (Figure 4.2f). In contrast, the SEM image of UiO-66-NH_2@Cotton-COOH clearly showed a higher coverage of the cotton fibers by UiO-66-NH_2, which is due to the incorporation of nucleation points that facilitate the growth of the MOF on the fabric (Figure 4.2i). Finally, the amount of zirconium was determined after acid digestion of the fabric and subsequent ICP-OES quantification. MOF incorporation was determined to be 3.1 ± 0.5 and 7.9 ± 1.9 g UiO-66-NH_2/100 g fabric for UiO-66-NH_2@Cotton and UiO-66-NH_2@Cotton-COOH respectively. A higher incorporation of UiO-66-NH_2 in the fabric with carboxylic acid groups demonstrated that the carboxylic acid groups promote the formation and attachment of the MOF on the fabric. These combined results illustrate the viability of using the heat-press method to incorporate UiO-66-NH_2 in cotton fabrics.

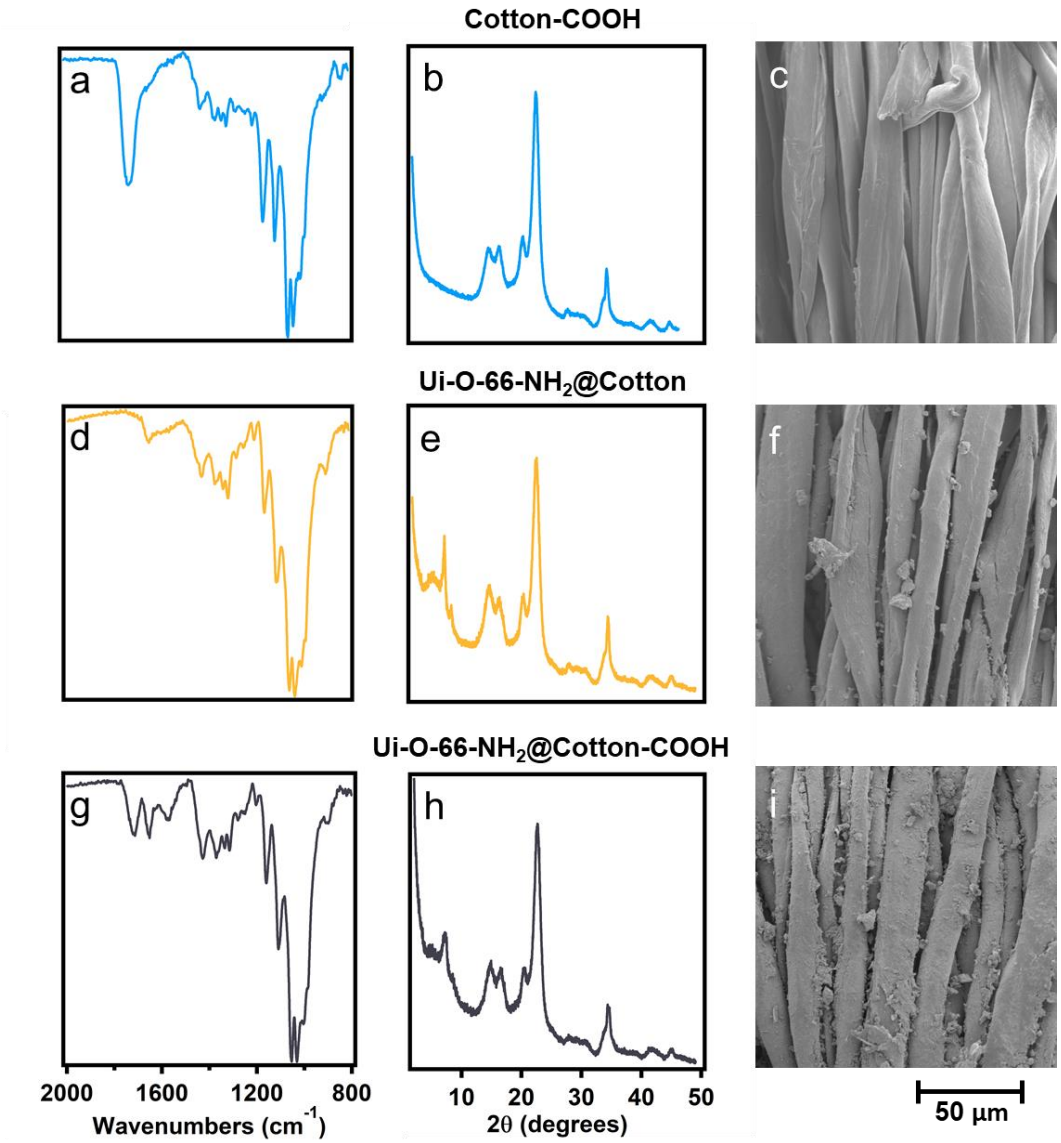

Figure 4.2 a. FTIR spectrum, b. PXRD pattern and c. SEM image of Cotton-COOH. d. FTIR spectrum, e. PXRD pattern and f. SEM image of UiO-66-NH_2@Cotton. g. FTIR spectrum, h. PXRD pattern and i. SEM image of UiO-66-NH_2@Cotton-COOH.

4.4.3 Hydrolysis of DMNP with the functionalized fabric

The catalytical performance of the fabrics was tested following the same method used for evaluating DMNP hydrolysis with MOF powder samples, UiO-66-NH_2-HP. We immersed the fabrics in a solution containing DMNP, and monitored its hydrolysis using UV-Vis spectroscopy. However, we tuned the mass of fabrics to keep the final amount of UiO-66-NH_2 constant in all the experiments. UiO-66-NH_2@Cotton-COOH displayed the highest catalytical activity of any of the fabrics tested under these conditions, having a hydrolysis rate constant of 0.012 min^{-1}. In contrast, UiO-66-NH_2@Cotton hydrolyzed DMNP slowly with a rate constant of 0.0065 min^{-1}, which represents a half-life time of 59.9 min and 107.3 min for UiO-66-NH_2@Cotton-COOH and UiO-66-NH_2@Cotton, respectively (Figure 4.S11 and Table 4.S5). Moreover, UiO-66-NH_2@Cotton-COOH reached a maximum hydrolysis of 68.3%, which is almost 1.5 times higher than the maximum hydrolysis of UiO-66-NH_2@Cotton (47.1%). Finally, Cotton-COOH showed no significant catalytic activity towards the hydrolysis of DMNP, having conversions below 10% (Figure 4.3). These results show that UiO-66-NH_2 anchored to the Cotton-COOH is more active compared with the one attached to plain cotton, which adds up an additional benefit of using the pre-activated fabric.

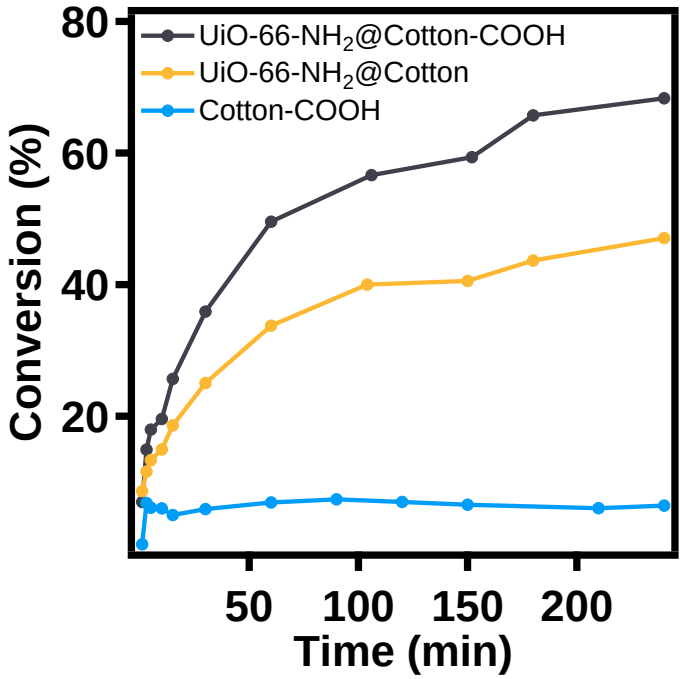

Figure 4.3 Hydrolysis of DMNP by the fabrics UiO-66-NH_2@Cotton-COOH, UiO-66-NH_2@Cotton and Cotton-COOH.

4.5 Conclusions

Heat-press technique was used as an easy, quick and solvent-free way to obtain UiO-66-NH_2. Use of a pre-formed zirconium node and a non-nucleophilic base enhances MOF formation, producing a material with a higher catalytical activity towards the hydrolysis of a nerve agent simulant. The developed heat-press method was used to further anchor UiO-66-NH_2 to cotton fabrics. Pre-activated cotton fabric with carboxylic acid was efficiently prepared using succinic anhydride. Higher loading and more homogeneous MOF distribution was observed when the pre-activated cotton fabric was used instead of the plain cotton. UiO-66-NH_2 deposited on the fabric is active

and effectively hydrolyzed the NA simulant DMNP. The technique described in this manuscript shows an accessible way to deposit MOFs on cotton fabrics that can be easily incorporated into traditional textile manufacturing processes.

4.6 Acknowledgments

This work was supported by the National Science Foundation (NSF) through the Center for Sustainable Polymers (CHE-1413862). This work made use of the IMSERC, QBIC and NUANCE facilities at Northwestern University, which have received support from the Soft and Hybrid Nanotechnology Experimental (SHyNE) Resource (NSF ECCS-1542205); the State of Illinois and International Institute for Nanotechnology (IIN).

4.7 Chapter 4 Appendix

4.7.1 Materials and Instrumentation

Reagents: Polyethylenglycol (3000 g/mol), 2-aminoterphthalic acid (99%), 1,8-bis(dimethylamino)naphthale (99%), zirconium(IV) chloride (99.5%), zirconium (IV) oxychloride octahydrate (99.5%), zirconium(IV) acetylacetonate (97%), zirconium(IV) oxynitrate hydrate (99%), succinic anhydride (≥99%), dimethylaminopyridine (≥99%), deuterium oxide (99.9 atom % D), sodium deutoroxide (40% in D2O, 99.5 atom % D), N-ethylmorpholine (97%), N,N-dimethylformamide (≥99%), acetone (99.5%), and tetrahydrofuran (≥99%) were purchased from Sigma Aldrich and used without further purification. Cotton fabric (cotton-400) was purchased from testfabrics, and the zirconium node was synthesized as previously described.[194] Dimethyl 4-nitrophenyl phosphate was synthesized according to the reported literature procedure.[195]

Instrumentation: Heat pressing was done in a Fancierstudio 9X12 Blue Black heat press machine. Infrared spectroscopy was performed on a Thermo Nicolet iS10 with a diamond ATR attachment. Scanning electron microscopy was performed on a Hitachi S-3400N-II spectrometer operating at 5.00 kV and a working distance of 10 mm with an aperture size of 20 μm. Samples were prepared by adhesion to carbon tape on a flat aluminum platform sample holder and coated with gold/palladium at 40 mA in a Denton Desk III TSC sputter coater. Powder X-ray diffraction was performed on a Stoe STADI-MP diffractometer using Cu Kα radiation in transmission mode. Solution nuclear magnetic resonance (^{1}H-NMR) were recorded in a Varian Inova 500 MHz system. Surface area measurements were conducted on a Micromeritics ASAP-2040 Accelerated Surface Area and Porosimetry Analyzer. Each sample was degassed at 120 °C until the rate of degassing was lower than 2 μm Hg/min, and then backfilled with N_2. Ultraviolet/visible (UV/vis) spectroscopy was performed on a Cary 5000 Varian UV/vis spectrometer. UV/vis spectra were recorded at RT over the range 300–500 nm, corrected against an appropriate background spectrum, and normalized to zero absorbance at 500 nm. Inductively coupled plasma optical emission spectroscopy (ICP-OES) was performed in an iCAP^{TM} 7600 analyzer.

4.7.2 Experimental Protocols

Synthesis of UiO-66-NH_2-HP: The procedure for the synthesis of UiO-66-NH_2 using the heat-press machine was the same for all the zirconium precursors, and the amounts are related in Table S.4.1. As an example, $ZrCl_4$ (300 mg, 1.3 mmol), BDC-NH_2 (210 mg, 1.2 mmol) and PEG (190 mg, 63 μmol) were mixed using a mortar and pestle until a homogenous solid mix was obtained. The solid was loaded onto aluminum foil covering an area of approximately 6 cm^2. Then, the

wrapped solid was put into the heat-press machine preheated at 200 ºC. After 20 min, the wrapped solid was removed from the heat-press machine and it was transferred into a conical centrifuge tube with DMF (10 mL). The suspension was stirred with an oscillator for 2 h. Then, the solvent was removed via centrifugation, fresh DMF (10 mL) was added to the solid, and the suspension was mixed using the oscillator for other 2 h. Afterwards, the DMF was removed via centrifugation, acetone (10 mL) were added to the solid, and the suspension was mixed in the oscillator for 10 h. Then, the acetone was removed using centrifugation, acetone (10 mL) were added to the solid and mixed using the oscillator for 2 h. Finally, the acetone was removed via centrifugation, and the solid was dried in a vacuum oven for 2 h (90 ºC, 60 torr) to give a dark-brown solid (226.5 mg).

Table 4.S 1 Different Zirconium source screened, and amounts used in the heat-press for the synthesis of UiO-66-NH_2

Zirconium source	Amount (mg, mmol)	BDC-NH_2 (mg, mmol)	PEG (mg, μmol)
$ZrO(NO_3)_2$	350, 0.9	149, 0.8	91, 30.3
$ZrCl_4$	300, 1.3	210, 1.2	91, 30.3
$Zr(acac)_4$	370, 0.8	131, 0.7	89, 29.8
$ZrOCl_2$	25, 1.5	250, 1.4	90, 30.1
$Zr_6O_4(OH)_4(C_6H_5COO)_{12}$	179, 0.04	81, 0.4	91, 30.5
$Zr_6O_4(OH)_4(C_6H_5COO)_{12}$*	350, 0.08	160, 0.9	189, 63.1

*Addition of PS (195.0 mg, 0.91 mmol) to the solid mixture

Synthesis of Cotton-COOH: DMAP (2 g, 1.64 mmol) was dissolved in water (38 mL) at 20 ºC. Then, cotton fabric (1.975g) was soaked in the solution for 15 min. Then, the fabric was removed from the solution, pat-dried, and placed in an oven at 85 ºC for 15 min, until dryness. In a 350 mL high-pressure vessel, succinic anhydride (20 g, 199.8 mmol) was dissolved in THF (80 mL). The

fabric was added to this solution, and then the vessel was closed and heated to 65 ºC overnight. Afterwards, the system was cooled down to 20 ºC and the fabric was removed from the THF solution. The activated fabric was washed with THF (20 mL, 3X), water (20 mL, 3X) and finally air dried, to give a white fabric (2.270 g).

Synthesis of UiO-66-NH_2@Cotton: The procedure for the functionalization of cotton and Cotton-COOH was the same, and the amounts are related in Table S4.2. As an example, Zr_6-node (160 mg, 36 μmol), BDC-NH_2 (73 mg, 0.4 mmol), PEG (86 mg, 29 μmol) and PS (88 mg, 0.4 mmol) were mixed using a mortar and pestle until a homogenous solid mix was obtained. Then, cotton fabric (319 mg, 25 cm^2) was located on top of a sheet of aluminum foil. The solid was loaded onto the fabric and spread out uniformly covering half of the total area of the fabric. Then, the uncovered half of fabric was folded to cover completely the powder mixture. Afterwards, it was wrapped with the aluminum foil and put into a heat-press machine preheated at 200 ºC. After 10 min, the wrapped fabric was flipped and heated for another 10 min. Then, the aluminum foil was removed from the heat-press machine, the fabric was unwrapped, opened, and the unbound solid was transferred into a conical centrifuge tube with DMF (10 mL). The suspension was stirred with an oscillator for 2 h. Then, the solvent was removed via centrifugation, fresh DMF (10 mL) was added to the solid, and the suspension was mixed using the oscillator for other 2 h. Afterwards, the DMF was removed via centrifugation, acetone (10 mL) were added to the solid, and the suspension was mixed in the oscillator for 10 h. Then, the acetone was removed using centrifugation, and acetone (10 mL) were added to the solid and mixed using the oscillator for 2 h. Finally, the acetone was removed via centrifugation, and the solid was dried in a vacuum oven for 2 h (90 ºC, 60 torr) to give a dark-

yellow solid (29 mg). Simultaneously, the fabric was put in another conical centrifuge tube, and the same washing procedure of the solid was applied. Obtaining a light brown fabric (304 mg).

Table 4.S 2 Amounts used for the heat-press modification of the cotton fabrics with UiO-66-NH_2.

	Fabric (mg)	Zr_6-node (mg, μmol)	BDC-NH_2 (mg, mmol)	PEG (mg, μmol)	PS (mg, mmol)
UiO-66-NH_2@Cotton	318	160, 36.4	72, 0.40	86, 28.7	88, 0.41
UiO-66-NH_2@Cotton-COOH	310	151, 34.4	69, 0.38	82, 27.3	85, 0.40

Scanning electron microscopy: UiO-66-NH_2-HP2 (5 mg) was suspended in methanol (0.5 mL). The solution was sonicated for 5 min, and then a 10 μL aliquot was taken and deposited in a holder covered with carbon tape, and the methanol was allowed to evaporate overnight. The fabrics were deposited directly onto a holder covered with carbon tape. Afterwards, both the powder and the fabric were coated with a 10 nm gold/palladium layer. The samples were transferred to the microscope and SEM images were recorded using a working distance of 10 mm, with a charge voltage of 5 kV.

Sodium deuterium oxide digestion: The following procedure was used for all the synthesized UiO-66-NH_2. UiO-66-NH_2-HP1 (5 mg) was suspended in NaOD (0.1 mL 0.1 M) and sonicated for 5 min. Then, calcium formate in D_2O (0.4 mL, 1.0%) was added, then the suspension was centrifugated, the solution was transferred to an NMR tube, and ^{1}H-NMR was recorded.

Carboxylic acid amount determination: Cotton-COOH (5 mg) were suspended in saturated Li_2CO_3 (1 mL, 17 M) for 20 minutes at 20 ºC. Then, the fabric was removed and washed with 5

mL (2 mL, then 3 mL) of water to remove the excess of Li_2CO_3. The sample was placed in a vacuum oven for 15 minutes to dry. Afterwards, the fabric was digested in HNO_3 (0.5 mL, 70%) in a heat bath for 3 h at 70 ºC, then DI water (9.5 mL) was added to the solution, and ICP-OES was used to determine the amount of lithium in solution. This experiment was done in triplicate.

Zirconium amount determination: The following procedure was used for all the functionalized fabrics. UiO-66-NH_2@Cotton (10 mg) was digested in HNO_3 (1 mL, 70%) for 3 h at 70 ºC. Then, 0.1 mL of the solution were diluted to 10 mL with HNO_3 (3%) and ICP-OES was used to determine the amount of zirconium in solution. This experiment was done in triplicate.

DMNP hydrolysis by the MOF powders: Hydrolysis experiments were carried out at room temperature and was the same for all the MOFs. A solid sample of UiO-66-NH_2-HP1 (3 mg, 6 mol %, 0.0015 mmol Zr_6) was added to an aqueous buffered solution containing *N*-ethylmorpholine (1.0 mL, 0.45 M) in a 1.5 mL Eppendorf vial. The resulting mixture was stirred for 15 min to finely disperse the MOF powder. DMNP (4.0 μL, 6.2 mg, 0.025 mmol) was then added to this suspension. Periodic monitoring of the hydrolysis reaction was carried out by removing a 20 μL aliquot from the reaction mixture and diluting it with an aqueous solution of N-ethylmorpholine (10 mL, 0.15 M) prior to UV-vis measurements. Progress of the reaction was monitored by following the *p*-nitrophenoxide (degradation byproduct) absorbance at 403 nm, which avoids overlapping absorption bands from other species (*e.g.*, DMNP).

DMNP hydrolysis by the functionalized fabrics: Hydrolysis experiments were carried out at room temperature and was the same for all the fabrics. A solid sample of the fabrics (33 mg of

UiO-66-NH_2@Cotton-COOH, 84 mg of UiO-66-NH_2@Cotton and 80 mg of Cotton-COOH) was added to an aqueous buffered solution containing *N*-ethylmorpholine (1.0 mL, 0.45 M) in a 1.5 mL Eppendorf vial. DMNP (4.0 µL, 6.2 mg, 0.025 mmol) was then added to this suspension and stirred. Periodic monitoring of the hydrolysis reaction was carried out by removing a 20 µL aliquot from the reaction mixture and diluting it with an aqueous solution of N-ethylmorpholine (10 mL, 0.15 M) prior to UV-vis measurements. Progress of the reaction was monitored by following the *p*-nitrophenoxide absorbance at 403 nm, which avoids overlapping absorption bands from other species (*e.g.*, DMNP).

4.7.3 Additional Characterization

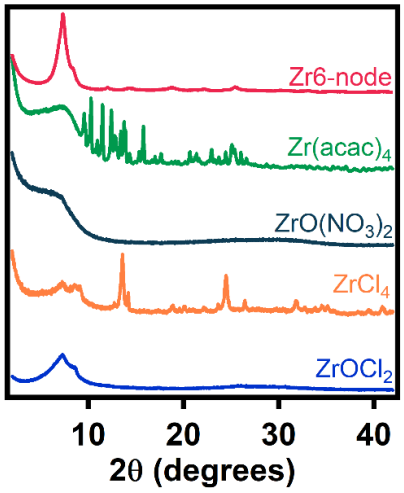

Figure 4.S1 PXRD patterns of the solids obtained using the heat press machine by employing different salts as zirconium sources.

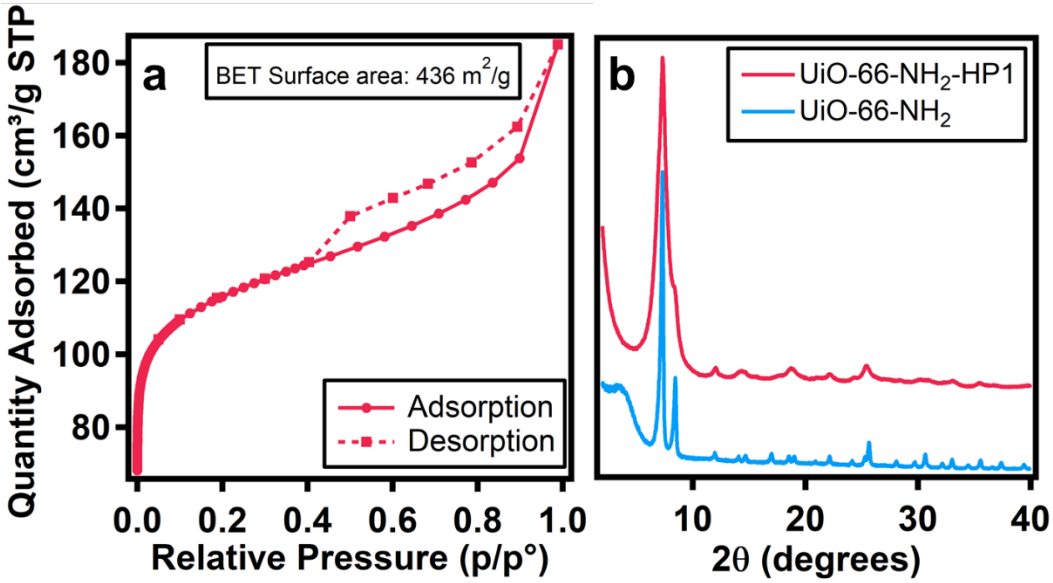

Figure 4.S2 a. Nitrogen adsorption isotherm of UiO-66-NH_2-HP1 and b. PXRD pattern comparison of UiO-66-NH_2-HP1, and UiO-66-NH_2 (via solvothermal synthesis).

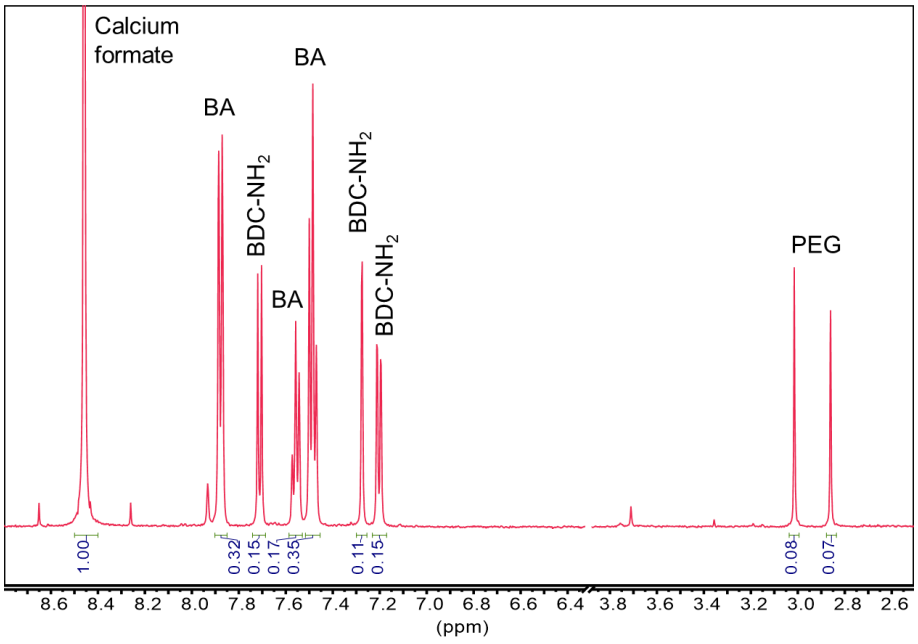

Figure 4.S3 ^{1}H-NMR spectrum of the digested UiO-66-NH_2-HP1**.**

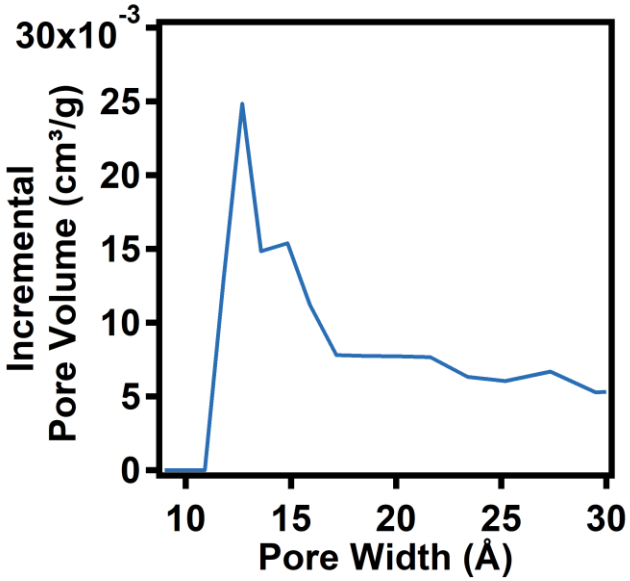

Figure 4.S 4 Pore size distribution of UiO-66-NH_2-HP2.

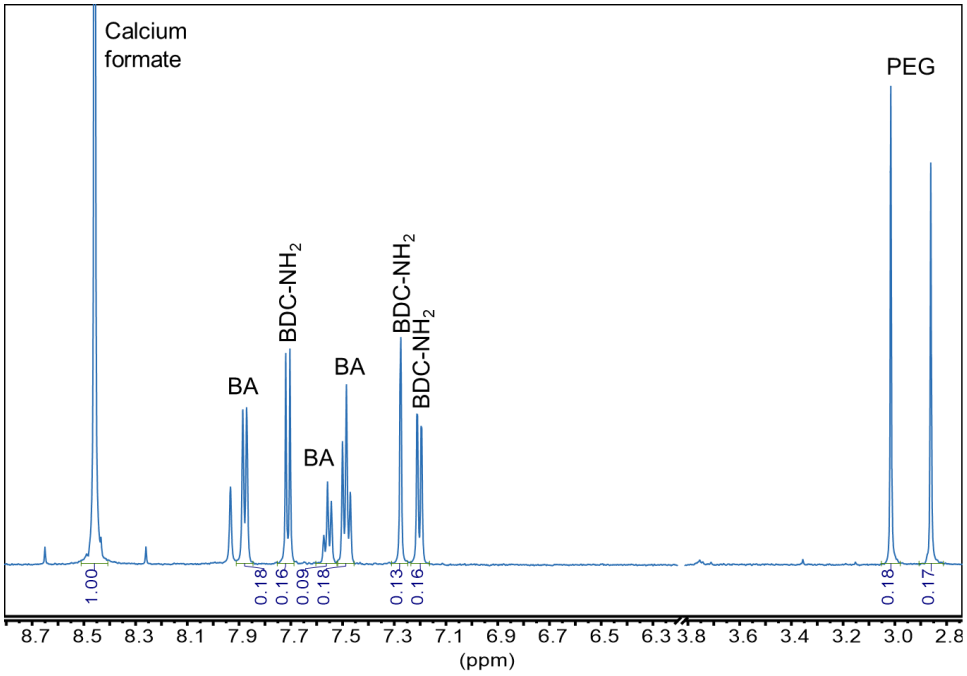

Figure 4.S5 ^{1}H-NMR spectrum of the digested UiO-66-NH_2-HP2**.**

Table 4.S3 Amount of benzoic acid (BA), 2-aminoterphthalic acid (BDC-NH_2) and polyethyleneglycol (PEG) obtained from the alkaline digestion of the MOFs.

MOF	BA (%)	BDC-NH_2 (%)	PEG (%)	PS (%)
UiO-66-NH_2-HP1	34.4	23.9	4.4	0
UiO-66-NH_2-HP2	17.0	22.4	8.6	0

Conversion rate calculations

The hydrolysis of DMNP to produce p-nitrophenol is a reaction with a first order rate law. Therefore, we used the following expressions to calculate the rate constant and half-life time.

Rate constant:

$$Ln(Consumption) = Ln\left(\frac{[DMNP]}{[DMNP]_0}\right) = -kt \quad \text{(eq 4.S1)}$$

Half-life time:

$$t_{1/2} = \frac{0.693}{k} \quad \text{(eq 4.S2)}$$

To determine the rate constant (k) we used the initial rate approximation, where just the initial linear region of the Ln(consumption) vs time is considered to fit a straight line.[196]

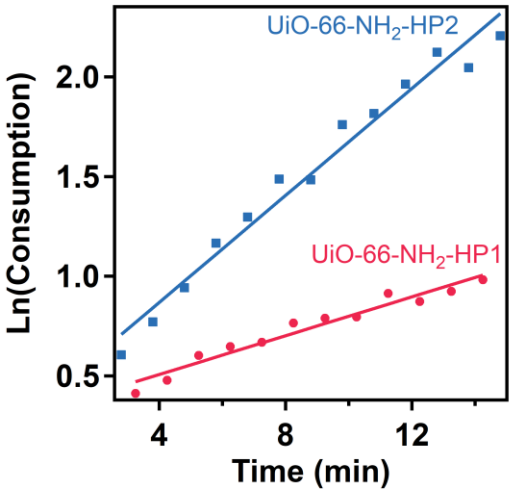

Figure 4.S6 First order reaction fitting for the DMNP hydrolysis by UiO-66-NH_2-HP1 and UiO-66-NH_2-HP2.

Table 4.S 4 Kinetic parameters of the catalytic hydrolysis of DMNP by the MOFs.

MOF	Rate constant(min^{-1})	Half-life time (min)	Maximum conversion (%)
UiO-66-NH_2-HP1	0.049	14.2	75
UiO-66-NH_2-HP2	0.134	5.2	99

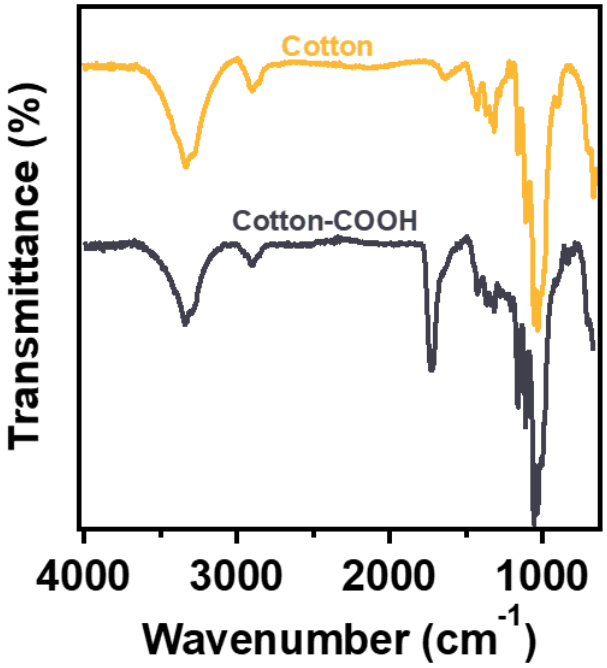

Figure 4.S7 FTIR spectra of the cotton fabric before (Cotton) and after the reaction with succinic anhydride (Cotton-COOH).

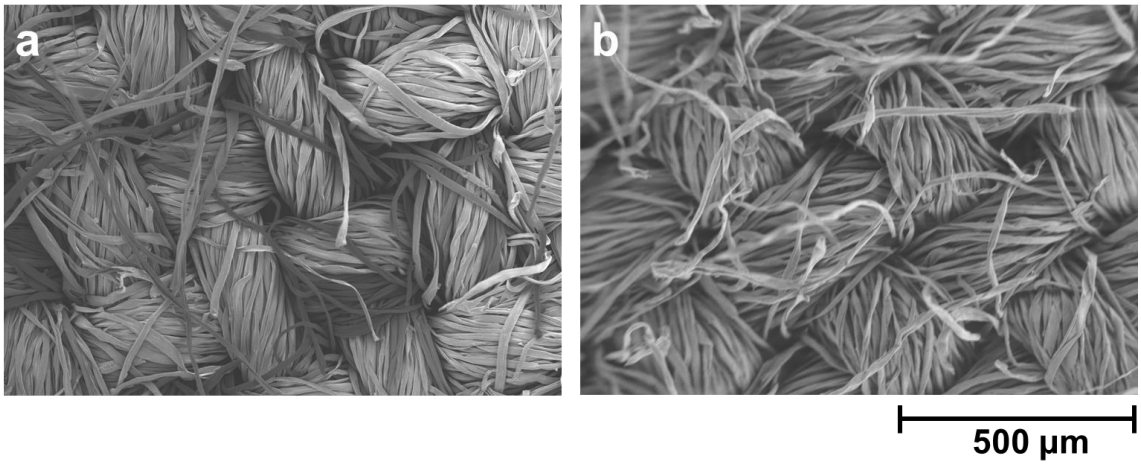

Figure 4.S8 SEM images of a. Cotton-COOH and b. Cotton.

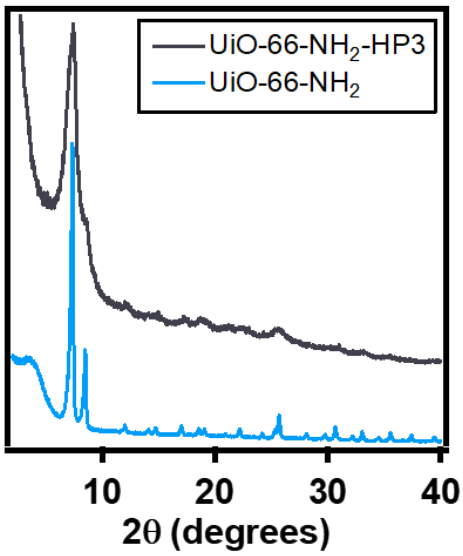

Figure 4.S9 PXRD pattern comparison of the solid recovered from the cotton fabric functionalization (UiO-66-NH_2-HP3), and UiO-66-NH_2 obtained via solvothermal synthesis.

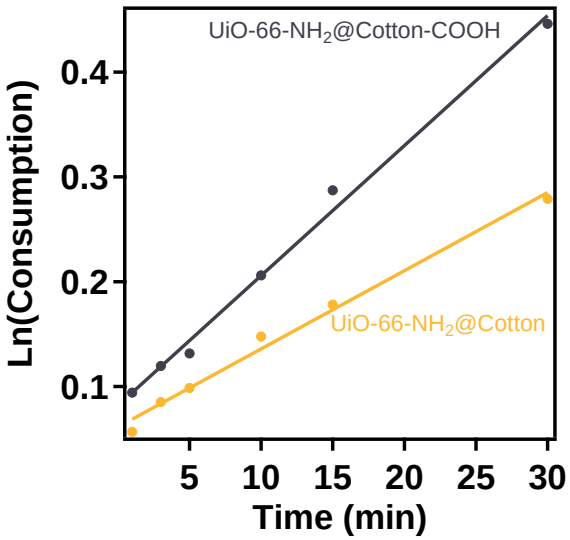

Figure 4.S10 First order reaction fitting for the DMNP hydrolysis by UiO-66-NH_2@Cotton and UiO-66-NH_2-HP@Cotton-COOH.

Table 4.S5 Kinetic parameters of the catalytic hydrolysis of DMNP by the fabrics.

Fabric	Rate constant (min^{-1})	Half-life time (min)	Maximum conversion (%)
UiO-66-NH_2@Cotton-COOH	0.012	59.9	68.3
UiO-66-NH_2@Cotton	0.0065	107.3	47.1

5. SACCHARIDE DOUBLE NETWORK HYDROGELS DERIVED FROM DYNAMIC IMINE LINKAGES

5.1 Preface

In this chapter, I show a different approach to use β-CD in the construction of functional polymers that contain dynamic networks. Herein, we expanded the scope of β-CD beyond its host-guest chemistry by taking advantage of its multiple primary alcohols. We demonstrated that selective oxidation of β-CD can be accomplished, producing per-formyl β-CD, which was used as a crosslinker in the generation of hydrogels with chitosan via imine linkages. Moreover, we used the dynamic chitosan/β-CD network in combination with a flexible polyacrylamide in the construction of a double network hydrogel. The combination of the two networks improved the mechanical properties of the final material and imparted an additional dynamic characteristic that has not been reported yet in these type of structures. This work is an example of the β-CD versatility, where we demonstrated that it can be used not just to form host-guest complexes, but also as a crosslinker in the synthesis of materials with interesting properties.

5.2 Abstract

Toughness and flexibility are desirable characteristics in hydrogels for use in biological applications, yet most hydrogels are weak and brittle. Recently, double network hydrogels have been developed as a new class of tough and flexible hydrogels, which outperform the mechanical properties of classic hydrogels. However, developed double network hydrogels lack fatigue resistance, which detriments their mechanical properties after several stress cycles. In the

presented research, we developed a novel double network hydrogel that contains covalent dynamic bonds, which dissipates the stress without losing its mechanical properties. We first developed the synthesis of the dynamic network by crosslinking the amino groups of chitosan with a formyl-functionalized β-cyclodextrin via imine condensation, after which we combined the dynamic network with a loosely crosslinked polyacrylamide network, producing the double network hydrogel. The novel hydrogel is stiff and flexible, and the presence of the dynamic bonds allows it to dissipate strain without losing its initial mechanical properties.

5.3 Introduction

Hydrogels made out of hydrophilic polymers are considered as biological tissue alternatives, mainly due to their inherent high water content and the tunability of their mechanical properties.[197,198] Hydrogels have found applications in diverse areas like tissue engineering, drug delivery, sensors and actuators.[199–201] However, their poor mechanical properties limits their use in most applications. Most hydrogels are soft, weak and brittle.[202] For example, polyacrylamide hydrogels have modulus of elasticity in the order of kPa.[203] In contrast, biological soft tissues like cartilage, can bear stresses of 36 MPa before failing.[204] Different approaches have been proposed to improve the mechanical properties of hydrogels. For example, hydrogels with sliding crosslinking points are highly stretchable due to the dissipation of stress via reorganization of the crosslinking points in the network.[205] Another alternative is the use of fillers in the hydrogel network, these composites hold high mechanical strength due to the reinforcement of the network with materials like nanoclay or cellulose nanocrystals, which have Young's modulus in the order

of tens of GPa.[206,207] However, the combination of both high stretchability and mechanical strength, seeing in biological scaffolds, can not be obtained by using these approaches.

Hydrogels with high mechanical stress and high stretchability have been explored through the combination of brittle polyelectrolytes with flexible polymers, and are known as double network (DN) hydrogels.[208] The high toughness of DN hydrogels comes from the synergistic effect of combining two networks, which effectively dissipates the energy applied to the system during mechanical stress.[209] Under optimized conditions, DN hydrogels with a water content higher than 90% can bare tensile stress in the order of tens of megapascals, and can be stretched up to 1000% before fracturing, which approach the mechanical properties of cartilages.[210] However, the high toughness of DN hydrogels comes from the dissipation of energy via breaking of the brittle polyelectrolyte bonds, which produces permanent damage to the network. As a consequence, a decrease in the mechanical properties of the hydrogel after several loadings is observed.[211] Alternatives to produce DN hydrogels with high fatigue resistance rely in the use of ionic bonds, recoverable sacrificial bonds, and physical crosslinking.[212,213]

Hydrogels with dynamic bonds *e.g.* imine, boronate ester, and disulfide linkages have been extensively studied.[214] Due to the dynamic properties of the network, these hydrogels have founds some use in applications where self-recovery and self-healing are needed.[215] Inclusion of dynamic covalent bonds into DN hydrogels will increase their fatigue resistance without decreasing the toughness of the material. However, DN hydrogels containing dynamic bonds are not being explored yet.[216] Imine linkages have been used in the synthesis of hydrogels with self-healing and cargo-delivery properties.[217] However, most studies focus in the ability of the gels to self-heal,

release cargos and cell viability, but do not include a study of the mechanical properties of the networks. In this regard, we hypothesize that the incorporation of imine bonds in the polyelectrolyte network of DN hydrogels can prevent their fatigue under constant loading while keeping high mechanical strength.

Reports have shown the use of crosslinked polysaccharides as the primary (brittle) network in hydrogels.[218,219] Sun et. al. reported the synthesis of a DN hydrogel of alginate/polyacrylamide, where the primary network is crosslinked with calcium ions and the second network is crosslinked via covalent bonds. The authors demonstrated that high stretchability and toughness are obtained due to the two types of linkages of the hydrogel.[210] Chitosan, a polysaccharide derived from the skeleton of shellfish that contains a dangling amino groups, can be used to incorporate dynamic bonds in the primary network of DN hydrogels.

Chitosan has been widely used in the synthesis of bio-compatible hydrogels,[220] and its use as a crosslinker in imine linkages has also being reported.[221] Therefore, the use of a multifunctional aldehyde to crosslink chitosan by combining it with a flexible network would constitute the synthesis of a dynamic DN hydrogel. In order to crosslink chitosan via imine linkages, we envision the use of β-CD-based moieties. Although, β-CD does not contain formyl groups in its structure, reports have demonstrated that the primary alcohols of saccharides can be selectively oxidized to aldehydes.[222] Therefore, through a controlled oxidation of β-CD it is possible to form a new β-CD-based crosslinker that contains formyl groups and it is capable of reacting with the amino groups of chitosan. Moreover, because the internal cavity of the β-CD is not used for the synthesis of the

hydrogel, it is possible to incorporate additional functionality to the network, including cargo-delivery.

In this work, we show the controlled oxidation of all seven primary alcohols of β-CD through the use of trychloroisocyanuric acid (TCCA) with 2,2,6,6-Tetramethylpiperidin-1-yl)oxy (TEMPO). Additionally, we demonstrate the formation of dynamic hydrogels when the formyl-β-CD is reacted with chitosan. Finally, we show the synthesis and mechanical properties of a tough and dynamic DN hydrogel by combining the chitosan/β-CD network with a loosely crosslinked polyacrylamide polymer.

5.4 Results and Discussion

5.4.1 Synthesis of the per(5-formyl-5-dehydroxymethyl)-β-cyclodextrin (β-CD-CHO)

Oxidation of the β-CD primary alcohols was adopted based on a previously reported oxidation of unprotected saccharides under weakly basic conditions using TCCA and TEMPO as mild oxidant and catalyst, respectively (Scheme 5.1).[222] The first attempt to oxidize all the primary alcohols of β-CD was done by using 5.3 equivalents of TCCA and 0.2 equivalents of TEMPO per equivalent of β-CD, which corresponds to 2.3 equivalents of oxidantant and 2.5mol% of catalyst per primary alcohol (seven in total). The reaction was monitored with MALDI-TOF by mixing the filtered reaction solution with a methanolic solution of 2,5 dihydroxybenzoic acid in a β-CD/matrix mass ratio of 1/100. We expected to observe a mass decrease of the β-CD as the reaction continues. However, after 10h, we primarily observed a peak located at 1157 m/z, corresponding to $[\beta\text{-CD}+Na]^+$, which indicates no oxidation of the alcohols. However, a small signal at 1155 m/z was

also seen corresponding to the mono-formylation of the β-CD (Figure 5.S1). The presence of this oxidation product encouraged us to optimize the reaction whereby we increase the amount of formyl groups in β-CD.

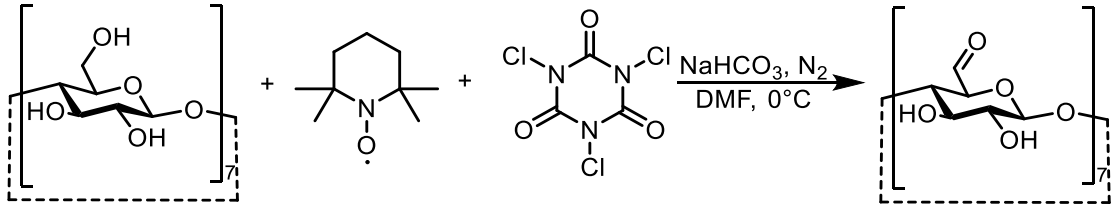

Scheme 5.1 Reaction scheme for the oxidation of β-CD primary alcohols.

We hypothesized that the conversion to formyl groups in β-CD can be promoted by increasing the reaction temperature. Therefore, we performed the reaction at two higher temperatures on top of the previously used one (0 °C). From the MALDI-TOF spectra, we saw that reactions at 20 °C and 40 °C had the same molecular weight distribution than the reaction at 0 °C, with primarily presence of $[\beta\text{-CD+Na}]^+$ and a small peak corresponding to the mono-formylation of β-CD. Surprisingly, the 1155 m/z peak, corresponding to monoformyl-β-CD, was the lowest in the 40 °C reaction compared to the other two temperatures (0 °C and 20 °C), which indicates that increasing the temperature was not beneficial for the oxidation of β-CD (Figure 5.S2). Continuing with the optimization of the reaction, we next tested the amount of secondary oxidant needed to promote further conversion. We increased two and ten times the amount of TCCA, but we did not obtain the heptaformyl β-CD either. Increasing two times the equivalents of TCCA, enhanced the oxidation of β-CD, where the signal at 1155 m/z was at least half of the signal at 1157 m/z, also a

new peak at 1153 m/z, corresponding to the di-formylation of β-CD was also seen. Yet, increasing the amount of TCCA ten times did not produce the desired product. In fact, this reaction did not contain any of the signals corresponding to β-CD moieties, which indicates a possible degradation of the saccharide under this reaction conditions (Figure 5.S3). Subsequently, we tested the influence of the catalyst in the reaction. We increased the concentration of the amount of catalyst (TEMPO) by 2, 5 and 10 times. Doubling the among of catalyst produced the monoformyl-β-CD, and a very small amount of diformyl-β-CD. Addition of five times more TEMPO increased the amount of monoformyl-β-CD, along with formation of di and tri-formyl-β-CD. Finally, addition of 10 times the amount of initial catalyst completely formed per-formyl-β-CD (1143 m/z), without the presence of the starting material (β-CD) (Figure 5.S4). These combined observations demonstrate that oxidation of the seven primary alcohols in β-CD can be accomplished by increasing the amount of catalyst employed during the reaction.

Based on the results obtained from the optimization, we scaled up the reaction by 10 times. After purification of per(5-formyl-5-dehydroxymethyl)-β-cyclodextrin (β-CD-CHO), we characterized the final product by FTIR, NMR and mass spectrometry. FTIR spectrum of the solid exhibited typical bands for carbohydrates (O-H stretching and C-O stretching at 3360 and 1016 cm^{-1}, respectively), in addition to a band located at 1730 cm^{-1} corresponding to the C=O stretch of the formyl groups in β-CD-CHO (Figure 5.S5). The ^{1}H-NMR of the solid dissolved in DCl (0.1 M in D_2O) showed the expected signals for a β-CD derivative. Protons attached to the C2, C3, C4 and C5 can be assigned to the signals at 3.43, 3.75, 3.36 and 3.63 ppm respectively. Additionally, the

anomeric proton (C1) can be seen as a doublet at 4.90 ppm. Moreover, the signal corresponding to primary alcohol (C6) disappeared from the region of 3.83-3.71 ppm, and a new signal at 5.32 ppm corresponding to the hydrate of the formyl group can be observed (Figures 5.S6 and 5.S7). ^{13}C-NMR spectrum also corroborates the oxidation of the β-CD. On top of the signals corresponding to C1 at 101.9 ppm and the signals for, C2, C3, C4 and C5 at 82.1, 72.8, 72.0 and 71.4 ppm, a new peak corresponding to the aldehyde hydrate is observed at 86.8 ppm (Figures 5.S8 and 5.S9). The mass spectrum of the dissolved solid showed a mass centered at 1269 m/z, which is higher than the expected mass of $[\beta\text{-CD-CHO+Na}]^+$ (1143 m/z). The increase in the mass is due to the preference of the compound to be as a covalent hydrate in solution,[223] where the 1264 m/z peak corresponds to the hydration of all the aldehyde groups of β-CD-CHO (Figure 5.S10). The spectroscopic characterization of the reaction product proves that the current protocol can be used to incorporate seven formyl groups in β-CD.

As a side note, in one of our optimization attempts to access a higher amount of β-CD-CHO more efficiently, we increased the concentration of all the reagents in the reaction solution 10 times. From the mass spectrum of the reaction mixture, we observed a peak at 1250 m/z, which did not correspond to any of the expected formyl products. After purification of the new β-CD derivative, we characterized the isolated product by FTIR, NMR and mass spectroscopy. The FTIR showed presence of saccharide moieties, where the bands corresponding to the O-H and C-O stretching can be observed at 3310 and 1027 cm^{-1}, respectively. Additionally, it contained an extra band located at 1602 cm^{-1} corresponding to a C=O stretch, which differs in terms of position and intensity from the C=O band of β-CD-CHO (Figure 5.S11). ^{1}H-NMR of the solid dissolved in DCl

(0.1 M in D_2O) showed the expected β-CD signals of the protons attached to the carbons C1, C2, C3, C4 and C5 at 4.98, 3.58, 3.86, 3.60 and 4.25 ppm, respectively. However, no additional proton signals are observed in the spectrum, indicating that the obtained product corresponds to the over oxidation of C6 from alcohol to carboxylic acid (Figures 5.S12 and 5.S13). ^{13}C-NMR spectrum also corroborates the presence of an overoxidized C6 by depicting a signal at 150.9 ppm, on top of the signals of the carbons in the glucopyranose unit at 101.9, 82.6, 71.8, 71.2 and 71.1ppm for C1, C2, C3, C4 and C5, respectively (Figures 5.S14 and 5.S15). Finally, as seen from the reaction mixture, the mass obtained of the purified solid is centered at 1250 m/z, corresponding to the hepta-carboxylation of the β-CD (Figure 5.S16). Based on the spectroscopic characterization, we conclude the obtained β-CD derivative is the per(5-carboxy-5-dehydroxymethyl)-β-cyclodextrin (β-CD-CO_2H). These results demonstrate that we can selectively access two types of per-oxidized β-CD by only changing the reaction concentration (Figure 5.1).

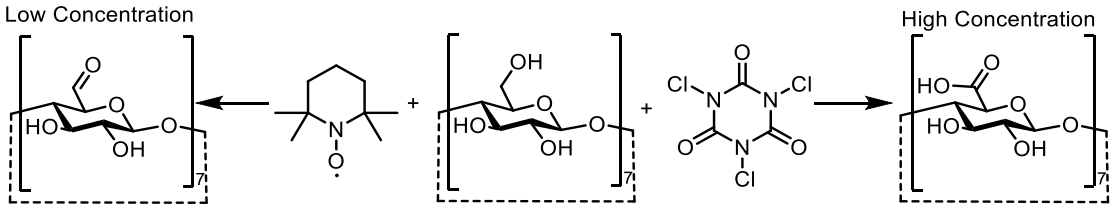

Figure 5.1 Synthesis of β-CD-CHO and/or β-CD-CO_2H by changing the reaction concentration.

5.4.2 Synthesis of the chitosan/cyclodextrin hydrogel (β-CD-CHO-CS)

After the synthesis of β-CD-CHO, we explored different conditions to crosslink it with chitosan (CS). We used acetic acid to solubilize both CS and β-CD-CHO, as well as to facilitate the imine

formation between the formyl groups of β-CD-CHO and the amino groups of CS. We used 2% acetic acid, which was enough to facilitate the solubilization of chitosan and β-CD-CHO. We also employed an equimolar ratio of aldehyde to amine functional groups, and room temperature for the formation of the crosslinked polymer. We initially tried four different polymer concentrations and evaluated the gel formation by tilting the solutions. From this experiment, we immediately observed gel formation when a polymer concentration higher than 40 mg/mL was used. These gels did not present a visual significant change after six hours of reaction (Figure 5.S17).

We optimized the formation of the hydrogel by tuning temperature, reaction time and amount of crosslinker, and we evaluated the quality of the hydrogels by measuring their complex viscosity using a rheometer. Initially, we evaluated the crosslinking reaction at different temperatures, using a polymer concentration of 40 mg/mL. The hydrogel obtained at 25 °C after 6 hours of reaction has a complex viscosity of 63.8 ± 1.8 Pa and this value increased when higher temperatures were used, reaching a value of 332.7 ± 13.5 Pa with a temperature of 80 °C. However, the reaction held at 80 °C had a deep dark color with presence of liquid water, which indicates degradation of the hydrogel. In contrast, the hydrogel prepared at 60 °C had a brown color, with no visual presence of liquid water and a complex viscosity of 233.2 ± 9.9 Pa (Figure 5.S18). Next, we evaluated the gelation time at 60 °C as a function of time. We found that the reactions held at 4 h and 6 h had complex viscosities of 199.7 ± 1.3 and 233.2 ± 9.9 Pa, respectively. The reaction run for 8h had a higher viscosity (935.2 ± 15.4 Pa). However, like in the case of the reaction held at 80 °C for 6 h, a brown dark hydrogel and liquid water was observed in this sample (Figure 5.S19). Therefore, we selected 4 h of reaction at 60 °C as the optimal conditions to synthesize the β-CD-CHO/CS

hydrogel. Final optimization of the hydrogel was done by changing the amount of β-CD-CHO in the network. We found that use of half of the initial amount of the crosslinker produced a hydrogel with a complex viscosity of 243.1 ± 2.2 Pa, which is similar to the viscosity obtained with the initial amount of crosslinker (Figure 5.S20). From these optimization experiments, we found that synthesis of the CS/ β-CD-CHO hydrogel is accomplished after 4 h at 60 ºC with an aldehyde/amine ratio of 1/2 (Scheme 5.2).

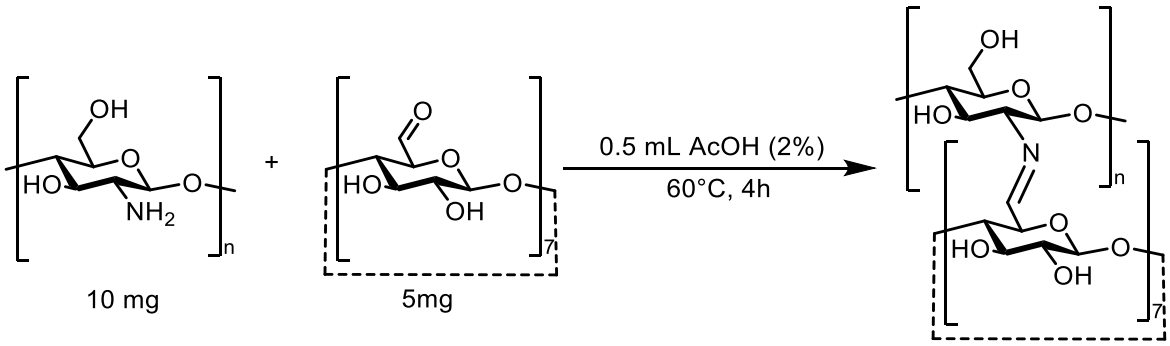

Scheme 5.2 Synthesis of the β-CD-CHO /CS hydrogel.

We prepared the hydrogel in a larger scale (10X) using the optimized reaction conditions, after which we removed the water and the acetic acid via lyophilization, obtaining a brown solid (Figure 5.S21a). Then, we characterized the solid using FTIR, solid state NMR, XPS and SEM. The FTIR showed the typical bands for carbohydrates at 3250 and 1075 cm^{-1} indicating the preservation of the carbohydrate functionalities after the reaction. Moreover, comparison of the spectrum with the precursor revealed differences in the FTIR range between 1800 to 1200 cm^{-1}. We observed the disappearance of the band corresponding to the aldehyde C=O stretch at 1730 cm^{-1}, along with the presence of two new intense bands at 1560 and 1404 cm^{-1}. The absorption band at 1560 cm^{-1} can

be attributed to the new C=N stretching coming from the imine linkages, and the absorption at 1404 cm^{-1} couldn't be assigned to a particular bond, but it reflects a change in the environment of the CH_2OH groups in both chitosan and β-CD (Figure 5.2a).[224] The solid state ^{13}C-NMR of the polymer is a combination of the signals of CS and β-CD-CHO, where the signal corresponding to carbons in the glycosidic moiety were observed between 50 and 120 ppm. Moreover, the signal corresponding to the carbon in the aldehyde moiety at 197 ppm was not observed in the final polymer, and a new signal corresponding to the carbon of the imine moiety was observed at 181 ppm (Figure 5.2b).

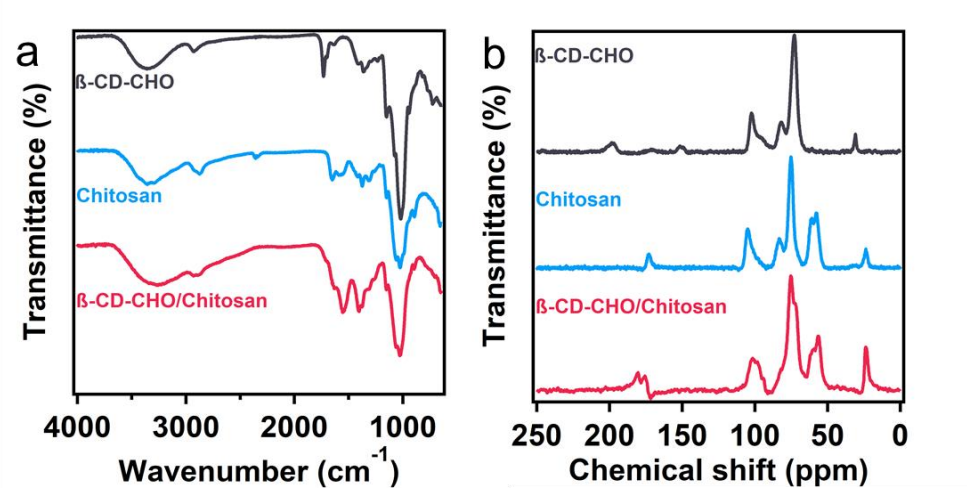

Figure 5.2 a. FTIR and b. ^{13}C solid state NMR spectra of the precursors (β-CD-CHO and chitosan) and the final crosslinked polymer (β-CD-CHO/CS).

N1s and C1s XPS scans revealed new binding bands for the crosslinked polymer. The N1s spectrum of CS showed a signal at 398.3 eV corresponding to the amino group. In contrast, the N1s spectrum of the CS/β-CD-CHO polymer was composed of two signals that can be

deconvoluted into two peaks with maximums at 398.7 eV and 401.1 eV corresponding to the C-NH_2 and C=N groups, however due to the proximity of the binding energies of amine and imine groups, it was not possible to unambiguously assign the peaks (Figure 5.3a).[225] The C1s spectrum of the CS/β-CD-CHO polymer also presented significant differences with the C1s spectra of the precursors. The C1s spectrum of β-CD-CHO was composed by two peaks at 287.5 eV and 285.9 eV corresponding to the C=O group and C(sp^3), respectively. In contrast, CS only shows the peak corresponding to C(sp^3) at 285.4 eV. Furthermore, the C1s spectrum of the CS/β-CD-CHO polymer was composed of two signals with maximums at 285.7 eV and 283.7 eV, which correspond to the C(sp^3) and C=N bond, respectively (Figure 5.3b). The SEM of the crosslinked polymer had a flake-like structure with no visible presence of macropores (Figure 5.S21b). These combined results support the formation of a crosslinked polymer between CS and β-CD-CHO via imine linkages.

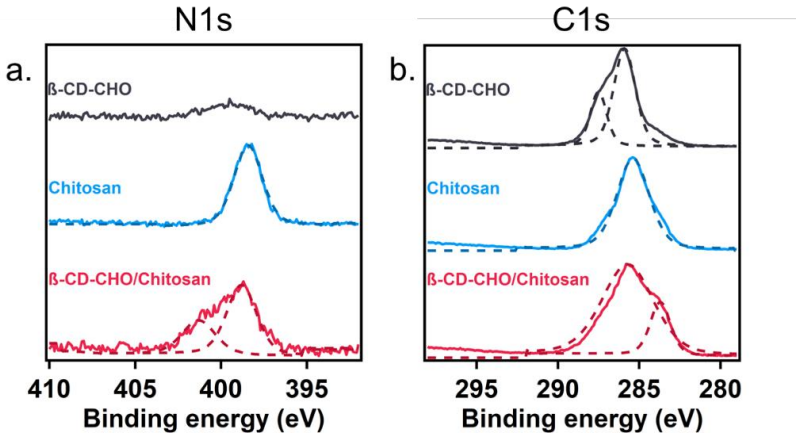

Figure 5.3 N1s and C1s XPS spectra of the precursors (β-CD-CHO and chitosan) and the final crosslinked polymer (β-CD-CHO/CS).

5.4.3 Synthesis of the chitosan/cyclodextrin/polyacrylamide double network hydrogel (β-CD/CS/PAAm)

Combination of the crosslinked β-CD-CHO/CS polymer with a ductile and poorly crosslinked polymer would produce a dynamic double network hydrogel with high toughness. Polyacrylamide (PAAm) was selected as the ductile polymer based on several reports that have shown its effective use in the development of DN hydrogels.[216] In our approach, we simultaneously synthesized the two polymers by combining the monomers in a single batch. We formed the DN hydrogel at 60 ºC for 4 h, using a one (β-CD-CHO/CS) to five (PAAm) ratio. For the β-CD-CHO/CS network, we already demonstrated that the reaction conditions produced a hydrogel based in the imine bonds between β-CD-CHO and CS. Furthermore, the PAAm network was synthesized via heat-initiated radical polymerization using 1.4 X 10^{-4} equiv of N,N,'-methylenbis(acrylamide) as the crosslinker and 9.8 X 10^{-4} equiv of ammonium persulfate as the initiator. As a result of this dual reaction, we obtained a stiff and flexible yellow hydrogel with a water content of 84.7% (Figure 5.4).

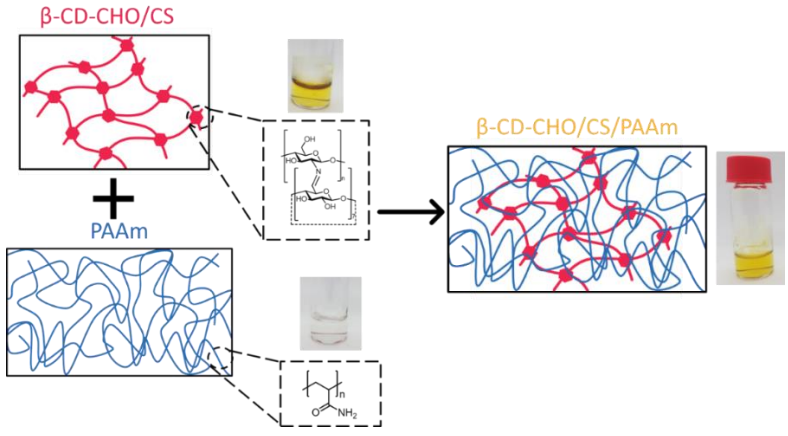

Figure 5.4 Formation of the β-CD-CHO/CS/PAAm double network hydrogel.

5.4.4 Mechanical properties study of the hydrogels

The mechanical properties of the DN hydrogel (β-CD-CHO/CS/PAAm) as well as the SN hydrogels (β-CD-CHO/CS and β-CD-CHO/PAAm) were tested using rheology experiments. For this purpose, we performed amplitude sweep, frequency sweep, and stress-relaxation tests of the three networks using a rheometer with a parallel plate fixture. The amplitude sweep experiments showed a storage modulus (G') in the order of 1 kPa for the SN hydrogels along the strain tested. In contrast, the loss modulus (G'') of the β-CD-CHO/CS hydrogel was two orders of magnitude lower than the loss modulus of the β-CD-CHO/PAAm hydrogel, demonstrating that the β-CD-CHO/CS has a more elastic character. The β-CD-CHO/CS/PAAm hydrogel had the highest storage modulus (5.4 kPa), and it was four times higher than the storage modulus of β-CD-CHO/PAAm hydrogel (1.3 kPa), which indicates a synergistic effect when the two networks are combined. Additionally, detriment in the viscoelastic properties of the β-CD-CHO hydrogel was observed when a strain higher than 50% was applied to the material. Yet, the β-CD-CHO/CS/PAAm hydrogel did not present this behavior, demonstrating that combination of the single networks keeps the viscoelastic properties of the network beyond 100% strain (Figure 5.5a). Frequency sweep experiments were also performed to study the difference in the time-dependent behavior of the hydrogels. We obtained the same trend in the frequency sweep experiments, where the material with the higher mechanical properties was the DN hydrogel. Moreover, a G' value of 0.1 rad/s was used to evaluate the difference in the stiffness of the hydrogels. β-CD-CHO/CS/PAAm had a storage modulus of 5.7 kPa. In contrast, β-CD-CHO/CS and β-CD-CHO/PAAm had storage modulus of 0.7 kPa and 1.2 kPa, respectively, which confirms the higher stiffness of the DN

hydrogel (Figure 5.5b). These combined results show that the β-CD-CHO/CS/PAAm hydrogel is a flexible and stiff material due to the synergistic effect of the combination of a highly crosslinked β-CD-CHO/CS hydrogel with a loosely crosslinked PAAm hydrogel.

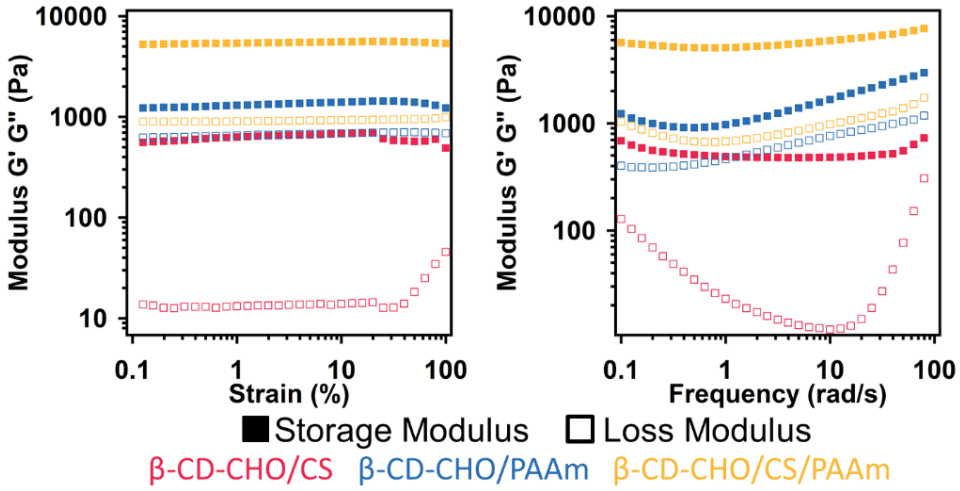

Figure 5.5 a. Amplitude sweep of the three hydrogels performed at a frequency of 10 rad/s. b. Frequency sweep of the three hydrogels performed at a strain of 10%.

Following with the mechanical characterization of the hydrogel, we performed stress-relaxation experiments to corroborate the dynamicity of the imine linkages incorporated in the primary network of the DN hydrogel. After application of 10% strain to the gels, we evaluated the relaxation modulus as a function of time. β-CD-CHO/CS can release stress very efficiency, due to the presence of imine linkages, with a relaxation time τ* of 151 s. β-CD-CHO/PAAm seems to relax faster (τ* = 12 s) but it cannot completely relax all the initial tension, leveling off at 25%. In contrast, β-CD-CHO/CS/PAAm had a much faster relaxation time (τ* = 45 s) than β-CD-CHO/CS,

and a better stress release (levels off at 15%) than β-CD-CHO/PAAm, which indicates the DN hydrogel can effectively release stress in short times, proving the advantage of incorporating dynamic linkages in DN hydrogels (Figure 5.6).

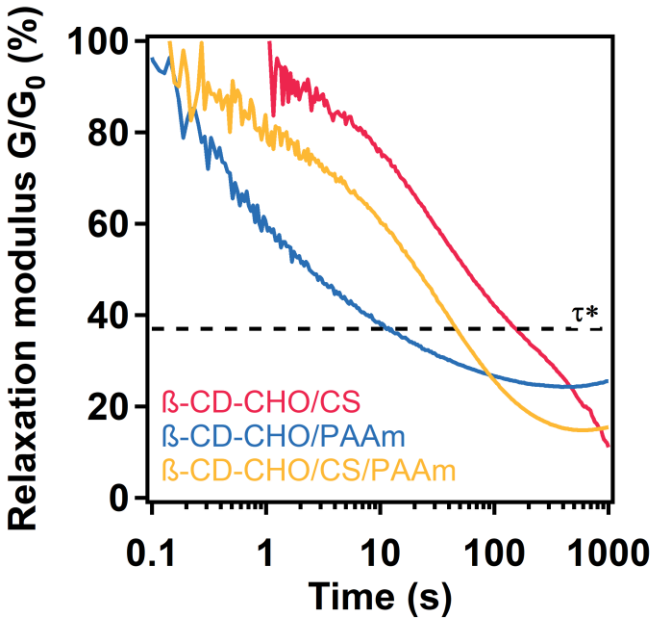

Figure 5.6 Stress relaxation of the three hydrogels performed with an initial strain of 10%.

5.5 Conclusions

In this work, we initially showed a method to selectively oxidize all the primary alcohols of β-CD into aldehyde groups. This new β-CD scaffold was employed as a crosslinker in the synthesis of a dynamic hydrogel, by reacting it with chitosan. We optimized the reaction conditions and corroborated the presence of the imine bonds in the new network. Moreover, we employed the developed dynamic network in the construction of a double network hydrogel with polyacrylamide. Through rheological characterizations we demonstrated that the double network

hydrogel is stiffer and more flexible than the separated networks, which corroborates the synergistic effect of combining highly with lightly crosslinked networks. Finally, we demonstrated that the dynamicity of the imine bonds is present in the double network hydrogel, which supports the ability of the network to relax stress without losing its mechanical properties.

5.6 Acknowledgments

This work was supported by the National Science Foundation (NSF) through the Center for Sustainable Polymers (CHE-1413862). This work made use of the IMSERC, MatCI, Keck biophysics and NUANCE facilities at Northwestern University, which have received support from the Soft and Hybrid Nanotechnology Experimental (SHyNE) Resource (NSF ECCS-1542205); the State of Illinois and International Institute for Nanotechnology (IIN).

5.7 Chapter 5 Appendix

5.7.1. Materials and Instrumentation

Reagents: β-CD (>97%), TEMPO (98%), TCCA (≥95%), sodium bicarbonate (≥99.7), chitosan low molecular weight, acrylamide (≥ 99%), ammonium persulfate (≥98%), N,N,'-methylenbis(acrylamide) (99%), TEMED (≥ 99%), deuterium oxide (99.9 atom % D), deuterium chloride (35% in D_2O, ≥99 atom % D), methanol (≥99.8%), acetic acid (≥99.7), N,N-dimethylformamide (≥99%), acetone (99.5%), dicholoromethane (>99.8%), and acetonitrile (99.8%) were purchased from Sigma Aldrich and used without further purification.

Instrumentation: Infrared spectroscopy was performed on a Thermo Nicolet iS10 with a diamond ATR attachment. Scanning electron microscopy was performed on a Hitachi S-3400N-II spectrometer operating at 5.00 kV and a working distance of 10 mm with an aperture size of 20 μm. Samples were prepared by adhesion to carbon tape on a flat aluminum platform sample holder and coated with gold/palladium at 40 mA in a Denton Desk III TSC sputter coater. Solution nuclear magnetic resonance was recorded in a Bruker Avance III 500 MHz system. Solid nuclear magnetic resonance was recorded in a 400MHz Bruker Avance III HD system. Rheological parameters were recorded in an Anton Paar MCR 302 compact rheometer at 25 °C with a parallel feature. Lyophilization was done with a FreeZone 4.5 liter cascade benchtop freeze dry system.

5.7.2 Experimental Protocols

Synthesis of β-CD-CHO: Oxidation of β-CD was performed by variation of a reported unprotected synthesis of dialdo-glycosides.[222] A 500 mL round bottom flask equipped with a magnetic stir bar was charged with β-CD (500 mg, 0.4 mmol), $NaHCO_3$ (7.628 g, 91 mmol) and TEMPO (125 mg, 0.8 mmol), then DMF (500 mL) were added and the solution was cooled down to 0 °C, stirred and bubbled with N_2 for one hour. After the suspension was at 0 °C, TCCA (548 mg, 2.3 mmol) were added. Subsequently, the N_2 inlet was removed, the flask was sealed with a septum, and the mixture was stirred at 500 rpm at 0 °C for 14 h. The red suspension was then warmed up to room temperature, filtered, and the DMF was removed via rotaevaporation. The residual solid was washed with methanol (100 mL) for 1 h at 20 °C. The yellow solid was re-dissolved in water (5 mL) and it was recrystallized by addition of acetone to the water solution. Obtaining a cream solid (282 mg, 57.0%). ^{1}H NMR (500 MHz, DCl, 0.1 M) δ 5.32 (s, 1H), 4.90

(d, *J* = 3.8 Hz, 1H), 3.75 (t, *J* = 9.5 Hz, 1H), 3.63 (d, *J* = 10.1 Hz, 1H), 3.43 (dd, *J* = 9.9, 3.6 Hz, 1H), 3.36 (t, *J* = 9.5 Hz, 1H). ^{13}C NMR (126 MHz, DCl, 0.1 M) δ 101.87, 101.65, 86.81, 86.58, 82.07, 72.78, 71.98, 71.40. MS: 1264 m/z.

Synthesis of β-CD-CO$_2$H: Oxidation of β-CD was performed by variation of a reported unprotected synthesis of dialdo-glycosides.[222] A 100 mL round bottom flask equipped with a magnetic stir bar was charged with β-CD (500 mg, 0.4 mmol), $NaHCO_3$ (3.815 g, 45.4 mmol) and TEMPO (127 mg, 0.8 mmol), then DMF (50 mL) were added and the solution was cooled down to 0 °C, stirred and bubbled with N_2 during a one hour. After the suspension was at 0 °C, TCCA (551 mg, 2.4 mmol) were added. Subsequently, the N_2 inlet was removed, the flask was sealed with a septum, and the mixture was stirred at 500 rpm at 0 °C for 14 h. The red suspension was then warmed up to room temperature, filtered, and the DMF was removed via rotaevaporation. The residual solid was washed with acetonitrile/HCl (0.1 M), 1/1 (100 mL). The yellow solid was re-dissolved in water (5 mL), and the pH was adjusted to 8. Then the water solution was washed with dichlorometathane, and the solid was recrystallized by addition of acetonitrile to the water solution. Obtaining a cream solid (277 mg, 50.8%). ^{1}H-NMR (500 MHz, DCl, 0.1 M) δ 4.98 (d, J = 4.0 Hz, 1H), 4.25 (d, J = 9.9 Hz, 1H), 3.86 (t, J = 9.5 Hz, 1H), 3.70 – 3.50 (m, 2H). ^{13}C-NMR (126 MHz, DCl, 0.1 M) δ 151.05, 101.50, 82.59, 71.81, 71.20, 71.06. MS: 1250m/z.

Optimization of β-CD-CHO/CS hydrogel: Synthesis of the single network hydrogel was done using the same procedure for all the optimization reactions. β-CD-CHO (5 mg, 5 μmol) was dissolved in AcOH (2%, 2.5mL). In a separated vial, CS (10 mg) was dissolved in AcOH (2%, 2.5

mL). Then, the β-CD-CHO solution was added dropwise to the CS solution and mixed for 1 min with a benchtop mixer. Finally, the solution was heated up at 60 ºC for 4 h. Obtaining a yellow hydrogel.

Synthesis of β-CD-CHO/CS/PAAm double network hydrogel: β-CD-CHO (5 mg, 5 μmol) and acrylamide (70 mg, 1 mmol) were dissolved in AcOH (2%, 0.22 mL). In a separated vial, chitosan (10 mg) was dissolved in AcOH (2%, 0.25 mL). In separated vials, ammonium persulfate (22 mg, 0.1 mmol), N,N,'-methylenbis(acrylamide) (2.1 mg, 13.6 μmol) and TEDEM (3.5 mg, 30.1 μmol) were dissolved in water (1.0, 1.0, and 2.0 mL, respectively). Then, the ammonium persulfate (10 μL) and the N,N,'-methylenbis(acrylamide) (10 μL) solutions were added to the β-CD-CHO-acrylamide solution, and the TEMED solution was diluted 10 times with water. The β-CD-CHO/acrylamide solution was added dropwise to the chitosan solution and mixed for 1 min with a benchtop mixer. Then, the β-CD-CHO/acrylamide/chitosan and TEMED solutions were freeze-dried using liquid nitrogen and vacuum for 1 h. Afterwards, the solutions were thawed and purged with N_2 gas, and the TEMED solution (10 μL) was added to the β-CD-CHO/acrylamide/chitosan solution. Finally, the reaction solution was purged with N_2 and heated up at 60 ºC for 4 h. Obtaining a yellow hydrogel.

Synthesis of β-CD-CHO/CS single network hydrogel: β-CD-CHO (5 mg, 5 μmol) was dissolved in AcOH (2%, 0.25 mL). In a separated vial, CS (10 mg) was dissolved in AcOH (2%, 0.25 mL). The β-CD-CHO solution was added dropwise to the chitosan solution and mixed for 1 min with a benchtop mixer. Then, the final solution was freeze-dried using liquid nitrogen and vacuum for

1h. Afterwards, the solution was thawed and purged with N_2 gas. Finally, the reaction solution was purged with N_2 and heated up at 60 ºC for 4 h. Obtaining a yellow hydrogel.

Synthesis of β-CD-CHO/PAAm single network hydrogel: β-CD-CHO (5 mg, 5 μmol) and acrylamide (70 mg, 1 mmol) were dissolved in AcOH (2%, 0.47 mL). In separated vials, ammonium persulfate (22 mg, 0.1 mmol), N,N,'-methylenbis(acrylamide) (2.1 mg, 13.6 μmol) and TEDEM (3.5 mg, 30.1 μmol) were dissolved in water (1.0, 1.0, and 2.0 mL, respectively). Then, the ammonium persulfate (10 μL) and N,N,'-methylenbis(acrylamide) (10 μL) solutions were added to the β-CD-CHO/acrylamide solution, and the TEMED solution was diluted 10 times with water. Then, the β-CD-CHO/acrylamide and TEMED solutions were freeze-dried using liquid nitrogen and vacuum for 1 h. Afterwards, the solutions were thawed and purged with N_2 gas, and the TEMED solution (10 μL) was added to the β-CD-CHO/acrylamide solution. Finally, the reaction solution was purged with N_2 and heated up at 60 ºC for 4 h. Obtaining a transparent hydrogel.

Lyophilization: The CS/β-CD-CHO/PAAm hydrogel (5.15 g, 5mL) was put in a centrifuge tube and frozen overnight in a freezer at -20 ºC. Then, the tube was transferred to a dewar with liquid nitrogen, allowed to stabilize for 10 min and finally transferred to a lyophilizer, and the samples was evacuated for 14 h. Obtaining a dark-brown solid (146 mg).

Rheology: Hydrogels were scooped on the rheometer plate and analyzed by using a 15 mm in diameter parallel fixture at 25 ºC. The gap between the fixture and the peltier plate was tuned in order to produce a constant force of less than 1 N for all the hydrogels tested. Complex viscosity

experiments were done with an amplitude of 10% and a frequency of 6.28 rad/s, and the viscosity was monitored for 300 s. Amplitude sweep experiments were done with a strain range from 0.01% to 100%, and by employing an angular frequency of 10 rad/s. Frequency sweep experiments were done with an angular frequency of 0.1 rad/s to 100 rad/s and by employing a strain of 10%. Stress relaxation experiments were done with an initial strain of 10% and monitoring of the modulus relaxation for 1000 s. Analysis of amplitude sweep, stress-relaxation and frequency sweep were done consecutively without removing the sample from the instrument.

5.7.3 Additional spectra

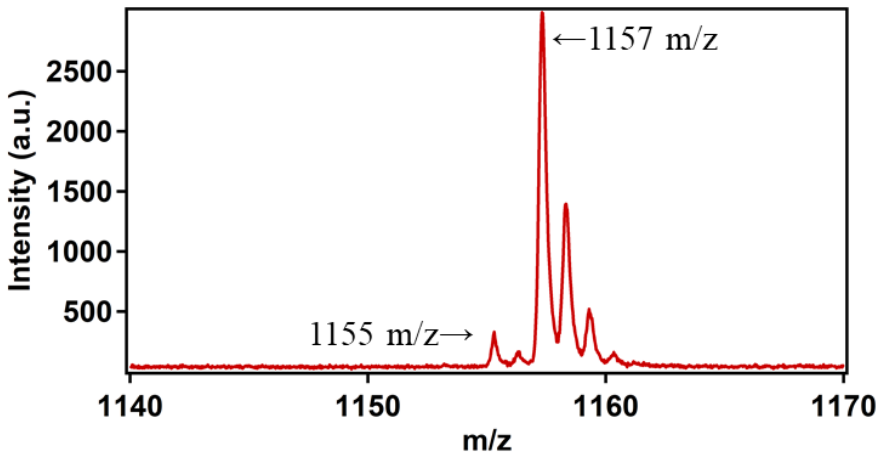

Figure 5.S1 MALDI-TOF spectrum of the crude oxidation reaction of β-CD after 14h of reaction.

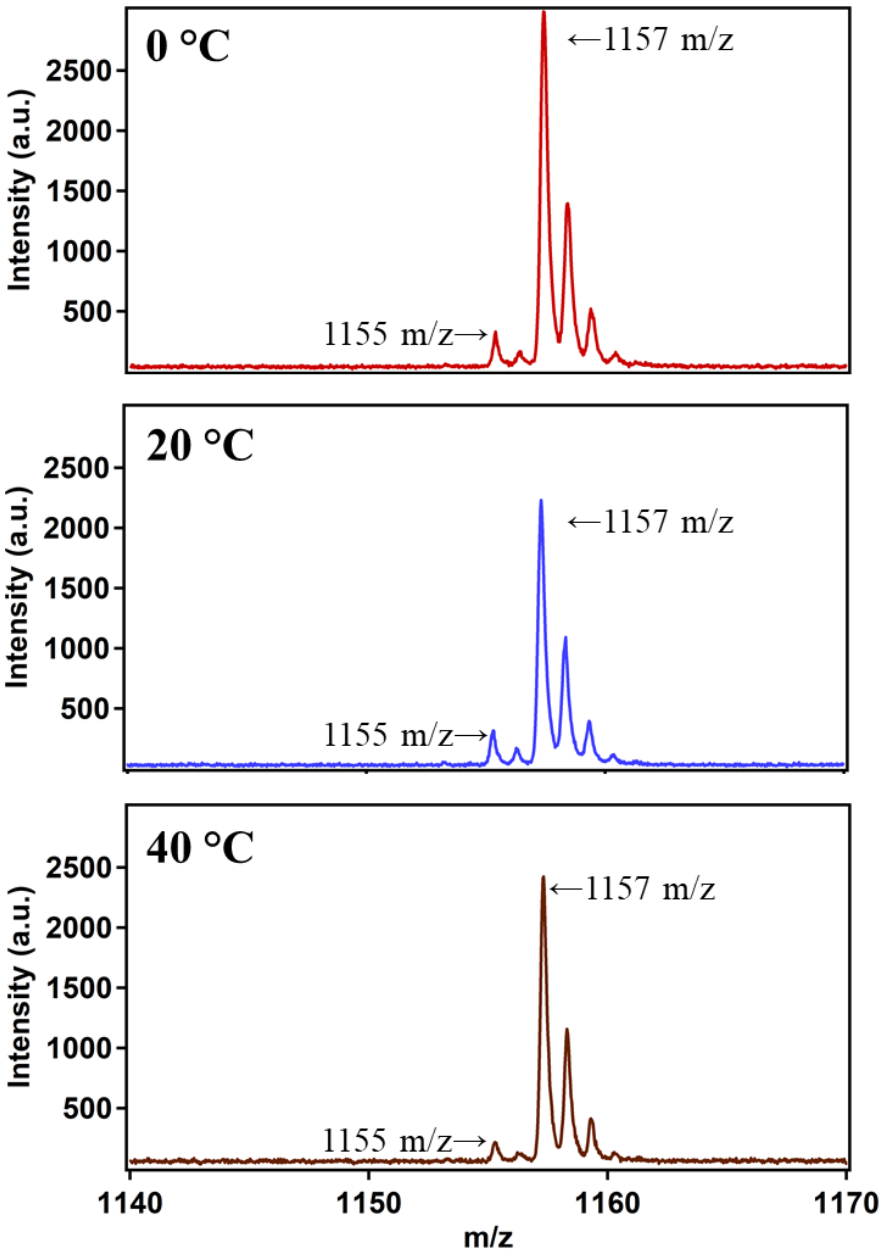

Figure 5.S2 MALDI-TOF spectra of the crude oxidation reaction of β-CD after 14h of reaction at different temperatures.

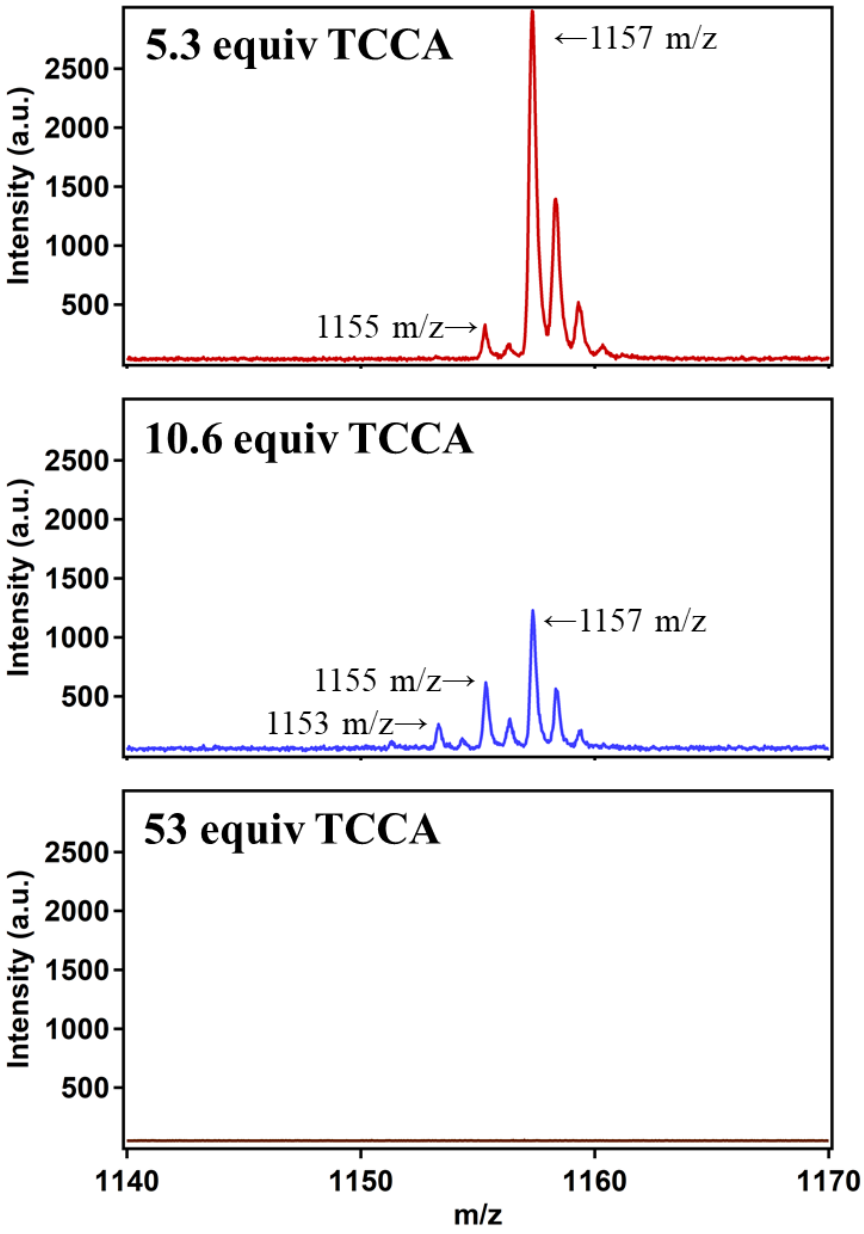

Figure 5.S3 MALDI-TOF spectra of the crude oxidation reaction of β-CD after 14h of reaction with different amounts of TCCA.

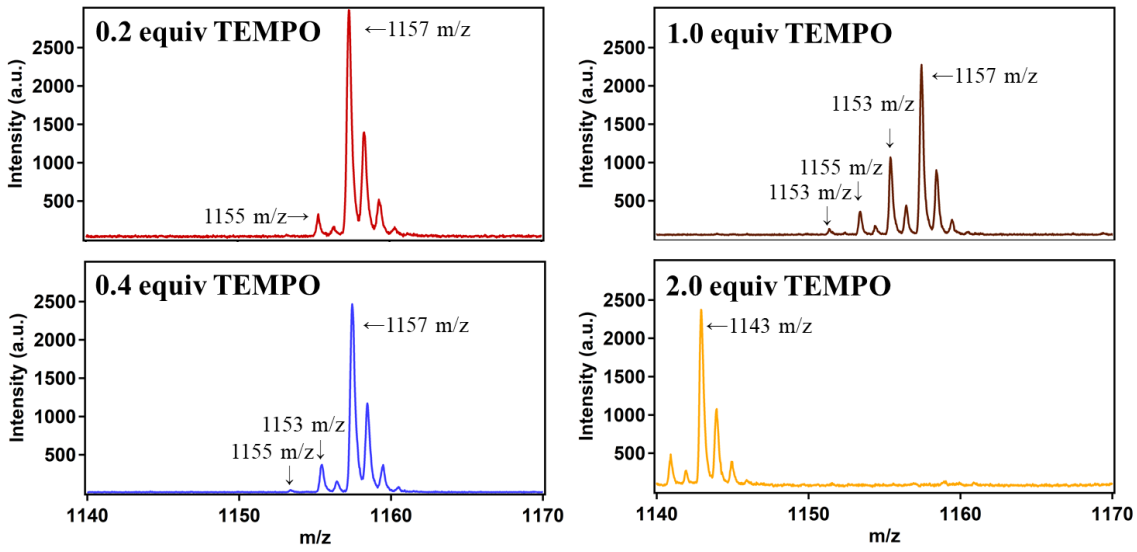

Figure 5.S4 MALDI-TOF spectra of the crude oxidation reaction of β-CD after 14h of reaction with different amounts of TEMPO.

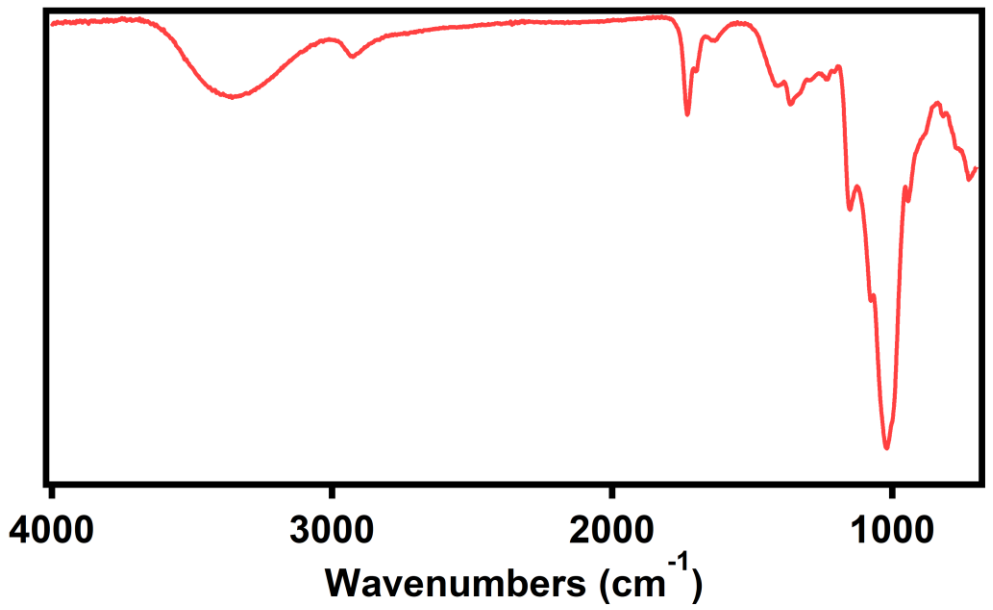

Figure 5.S5 FTIR spectrum of β-CD-CHO.

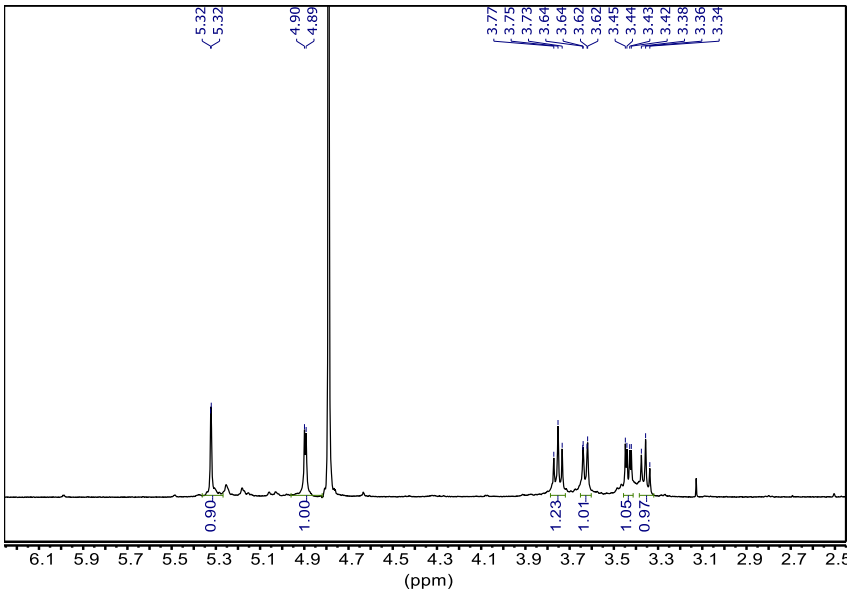

Figure 5.S6 ^{1}H-NMR spectrum of β-CD-CHO.

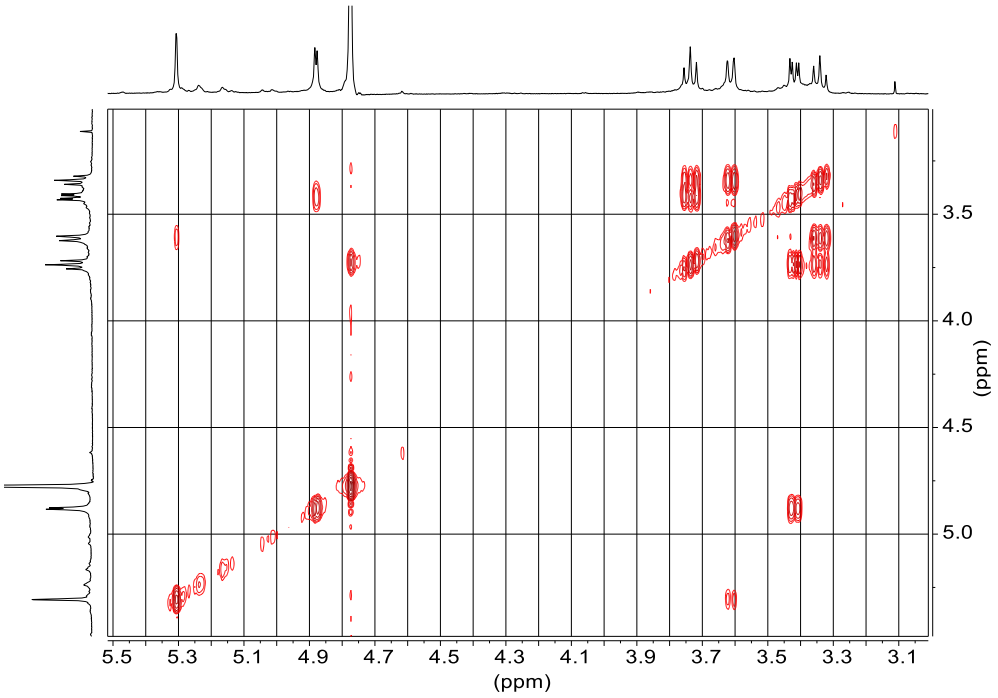

Figure 5.S7 COSY-NMR spectrum of β-CD-CHO.

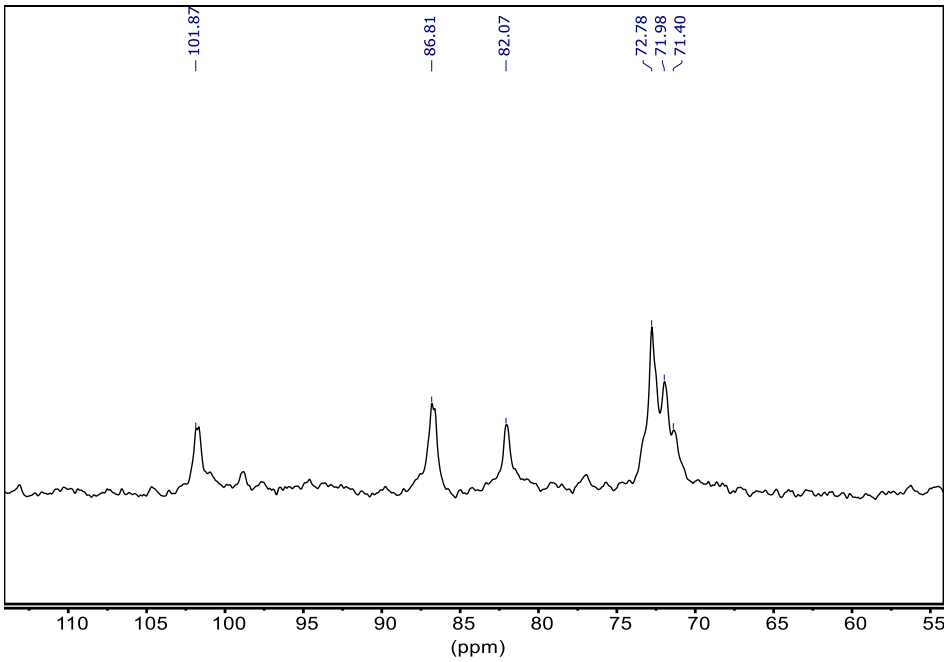

Figure 5.S8 ^{13}C-NMR spectrum of β-CD-CHO.

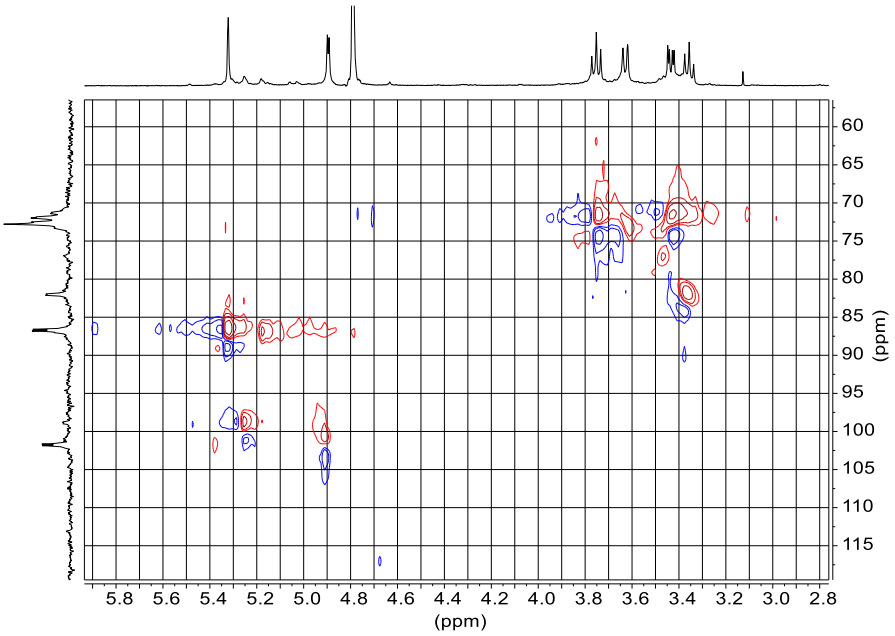

Figure 5.S9 HSQC-NMR spectrum of β-CD-CHO.

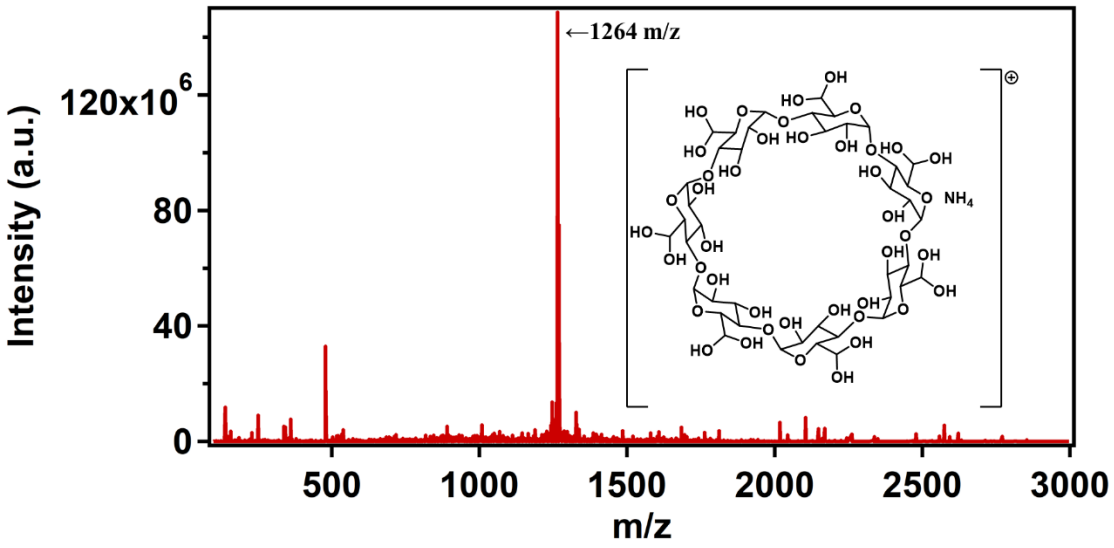

Figure 5.S10 MS spectrum of β-CD-CHO.

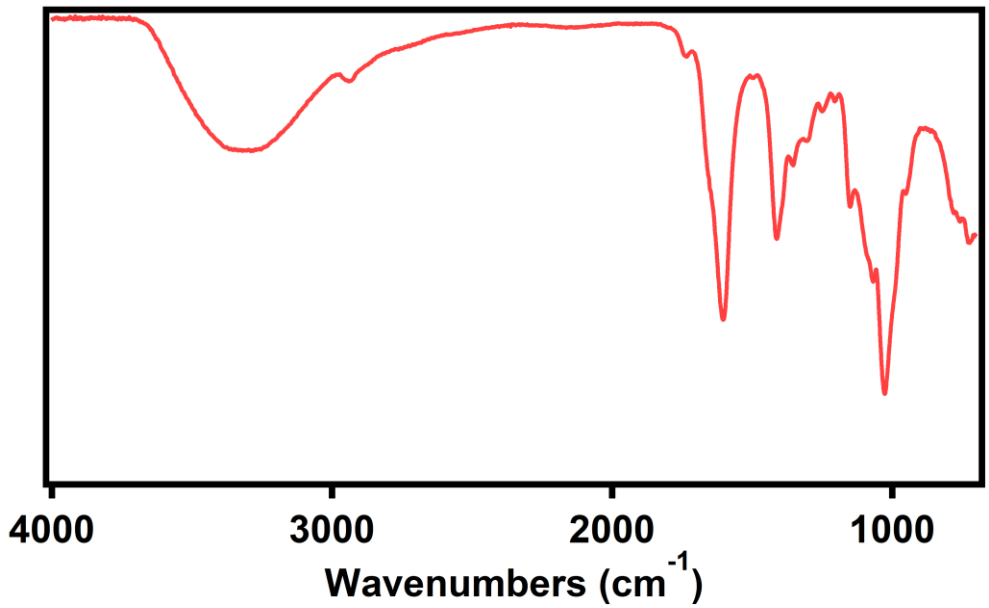

Figure 5.S11 FTIR spectrum of β-CD-CO_2H.

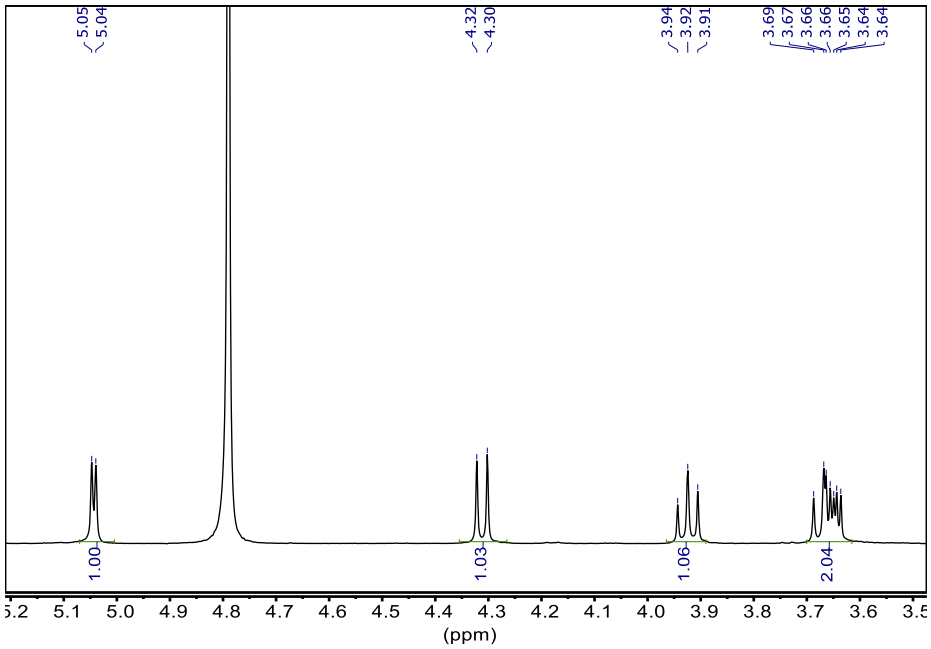

Figure 5.S12 ^{1}H-NMR spectrum of β-CD-CO_2H

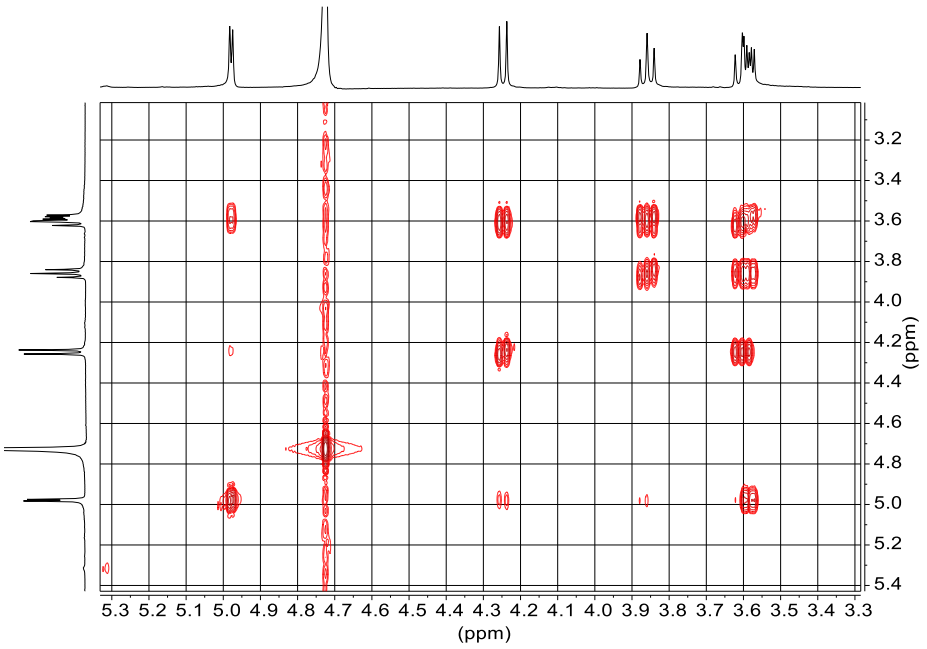

Figure 5.S13 COSY-NMR spectrum of β-CD-CO_2H.

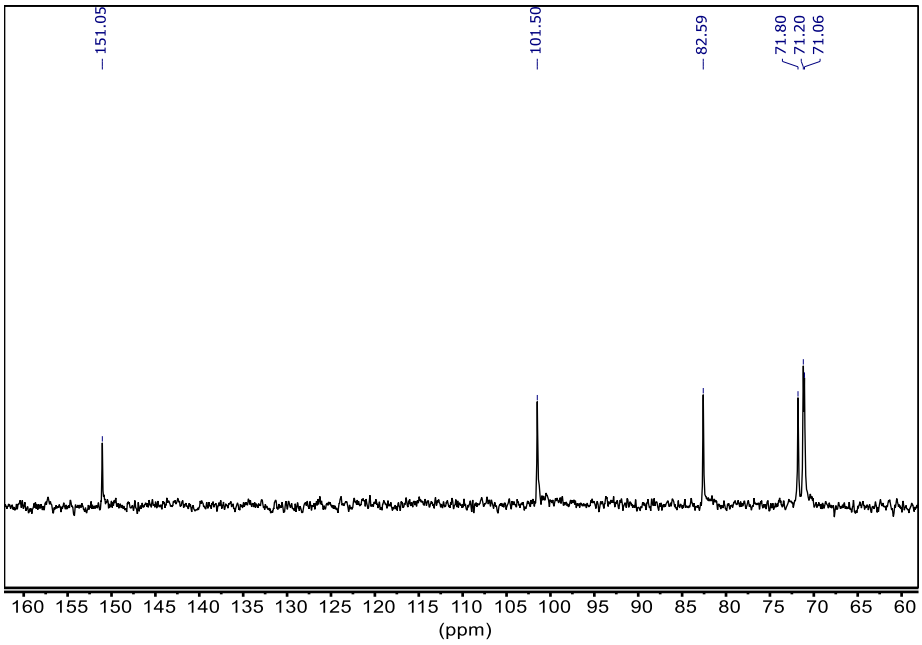

Figure 5.S14 ^{13}C-NMR spectrum of β-CD-CO_2H.

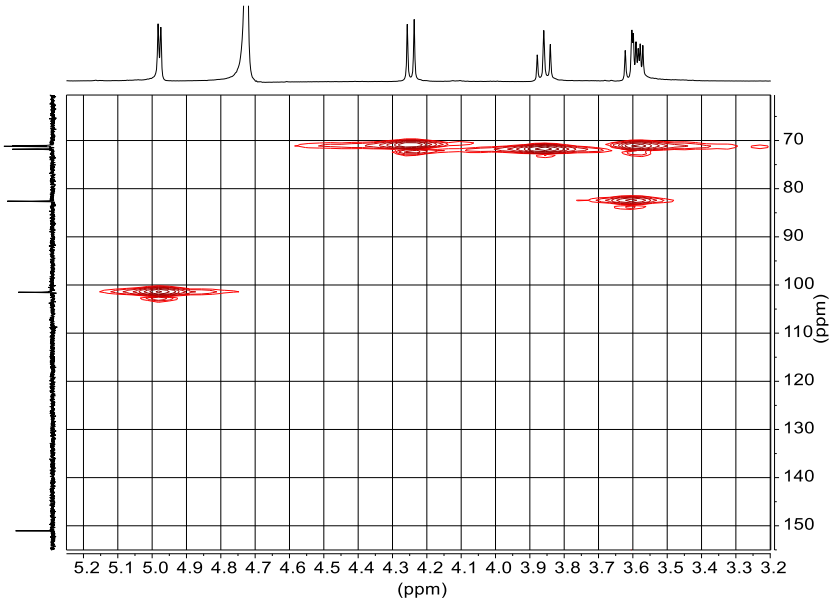

Figure 5.S15 HSQC-NMR spectrum of β-CD-CO_2H.

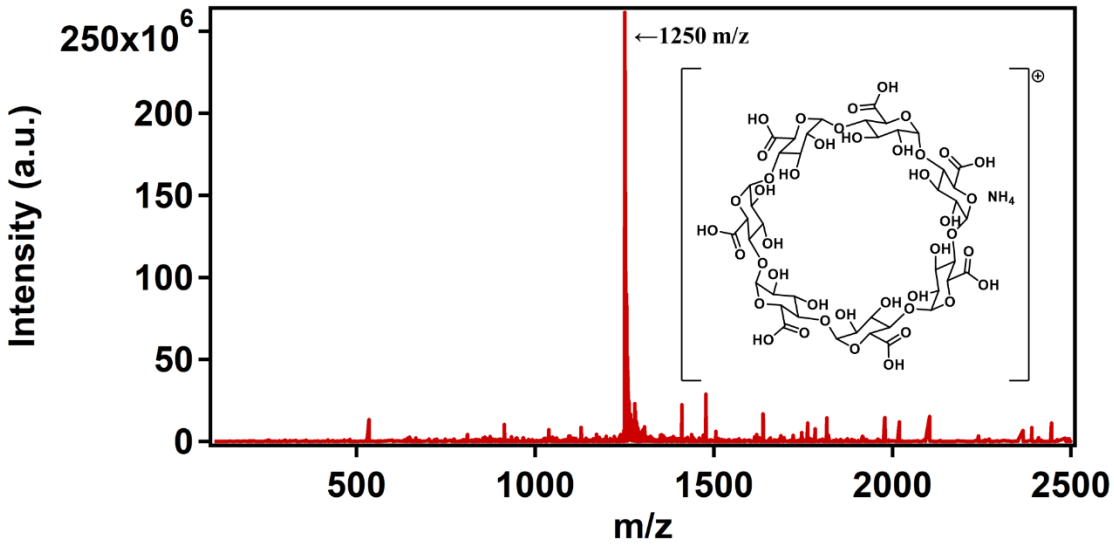

Figure 5.S16 MS spectrum of β-CD-CO_2H.

5.7.4 Additional graphs and images

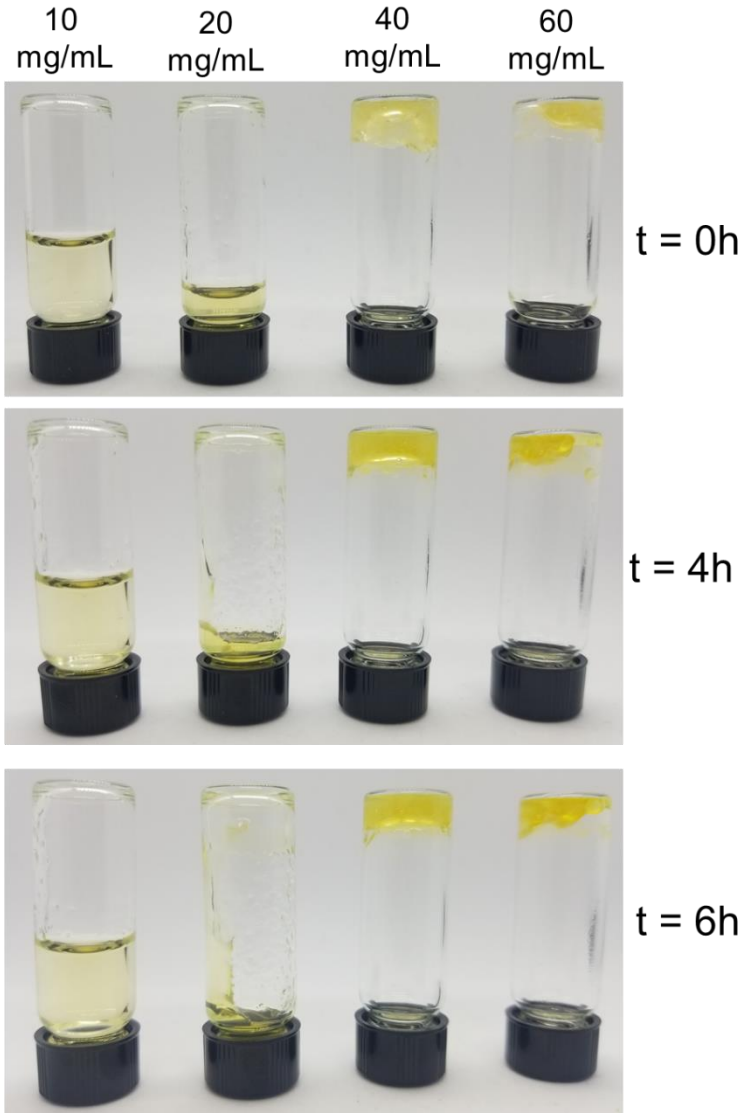

Figure 5.S17 Synthesis of the β-CD-CHO/CS hydrogel at different polymer concentration.

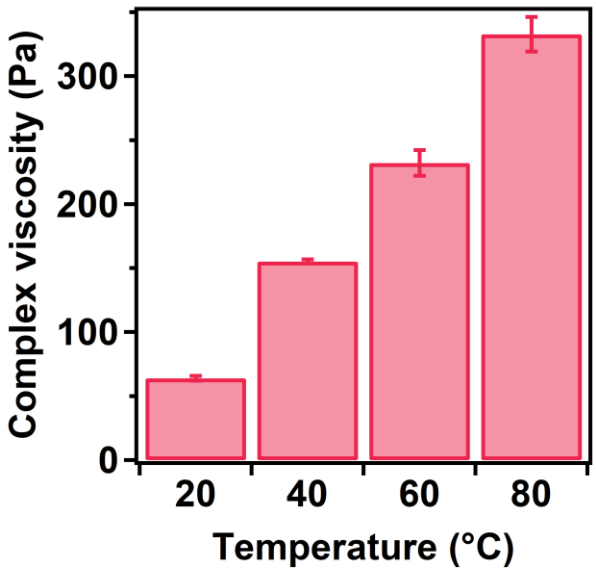

Figure 5.S18 Complex viscosity of β-CD-CHO/CS hydrogels synthesized at different temperatures.

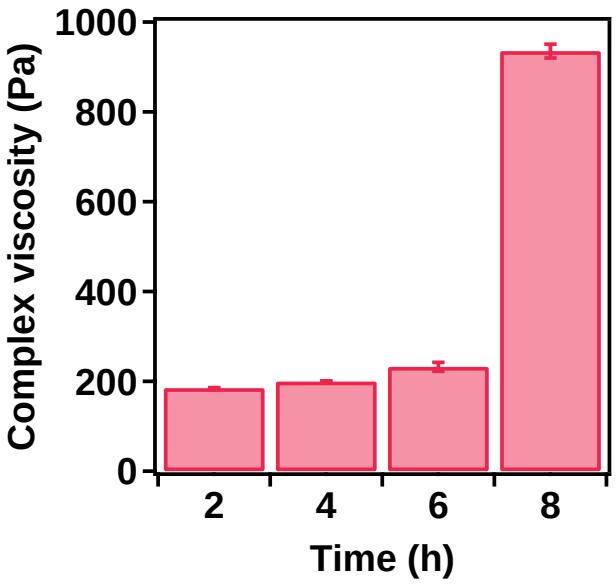

Figure 5.S19 Complex viscosity of β-CD-CHO/CS hydrogels synthesized at different times.

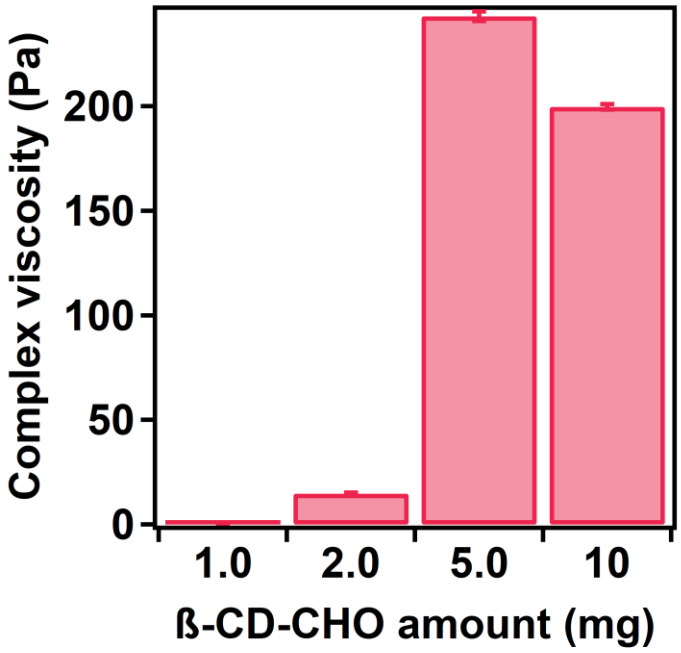

Figure 5.S20 Complex viscosity of β-CD-CHO/CS hydrogels synthesized at different β-CD-CHO amounts.

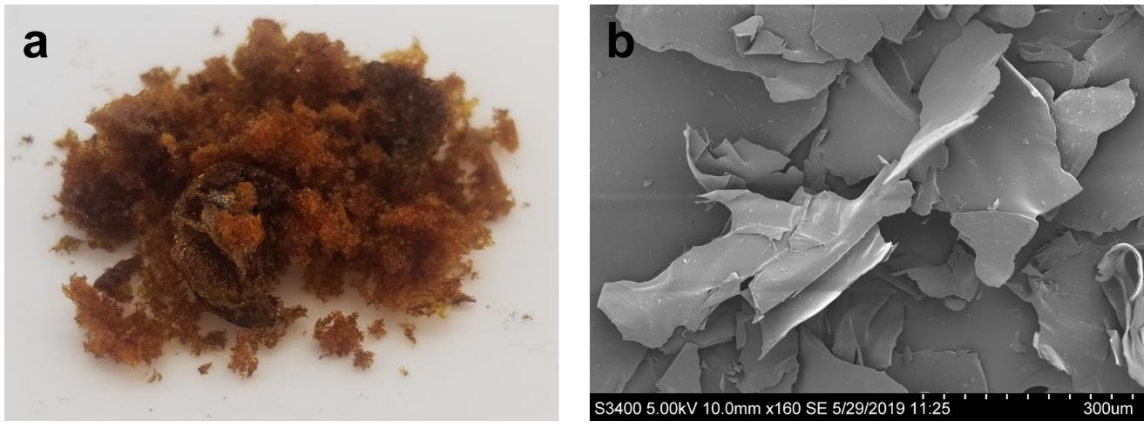

Figure 5.S21 a Photograph, and b. SEM of β-CD-CHO/CS after lyophilization.

6. References

(1) Järup, L. Hazards of Heavy Metal Contamination. *Br. Med. Bull.* **2003**, *68*, 167–182.

(2) Fram, M. S.; Belitz, K. Occurrence and Concentrations of Pharmaceutical Compounds in Groundwater Used for Public Drinking-Water Supply in California. *Sci. Total Environ.* **2011**, *409*, 3409–3417.

(3) Gerecke, A. C.; Schärer, M.; Singer, H. P.; Müller, S. R.; Schwarzenbach, R. P.; Sägesser, M.; Ochsenbein, U.; Popow, G. Sources of Pesticides in Surface Waters in Switzerland: Pesticide Load through Waste Water Treatment Plants—Current Situation and Reduction Potential. *Chemosphere* **2002**, *48*, 307–315.

(4) Montzka, S. A.; Dlugokencky, E. J.; Butler, J. H. Non-CO_2 Greenhouse Gases and Climate Change. *Nature*. Nature Publishing Group August 4, 2011, pp 43–50.

(5) Piccot, S. D.; Watson, J. J.; Jones, J. W. A Global Inventory of Volatile Organic Compound Emissions from Anthropogenic Sources. *J. Geophys. Res. Atmos.* **1992**, *97*, 9897–9912.

(6) Belis, C. A.; Karagulian, F.; Larsen, B. R.; Hopke, P. K. Critical Review and Meta-Analysis of Ambient Particulate Matter Source Apportionment Using Receptor Models in Europe. *Atmos. Environ.* **2013**, *69*, 94–108.

(7) Greenfield, R. A.; Slater, L. N.; Bronze, M. S.; Brown, B. R.; Jackson, R.; Iandolo, J. J.; Hutchins, J. B. Microbiological, Biological, and Chemical Weapons of Warfare and Terrorism. *Am. J. Med. Sci.* **2002**, *323*, 326–340.

(8) Hamilton, P. A.; Helsel, D. R. Effects of Agriculture on Ground-Water Quality in Five

Regions of the United States. *Ground Water* **1995**, *33*, 217–226.

(9) Posthuma, L.; de Zwart, D. Predicted Effects of Toxicant Mixtures Are Confirmed by Changes in Fish Species Assembladges in Ohio, USA, Rivers. *Environ. Toxicol. Chem.* **2006**, *25*, 1094.

(10) Lakatos, G.; Fleit, E.; Mészáros, I. Ecotoxicological Studies and Risk Assessment on the Cyanide Contamination in Tisza River. *Toxicol. Lett.* **2003**, *140–141*, 333–342.

(11) Cordy, P.; Veiga, M. M.; Salih, I.; Al-Saadi, S.; Console, S.; Garcia, O.; Mesa, L. A.; Velásquez-López, P. C.; Roeser, M. Mercury Contamination from Artisanal Gold Mining in Antioquia, Colombia: The World's Highest per Capita Mercury Pollution. *Sci. Total Environ.* **2011**, *410–411*, 154–160.

(12) Malm, O. Gold Mining as a Source of Mercury Exposure in the Brazilian Amazon. *Environ. Res.* **1998**, *77*, 73–78.

(13) Spellman, F. R. *Handbook of Water and Wastewater Treatment Plant Operations*, 2nd ed.; CRC Press: Boca Raton, 2008.

(14) Drinan, J. E.; Spellman, F. *Water and Wastewater Treatment*, 2nd ed.; CRC Press: Boca Raton, 2012.

(15) Schwarzenbach, R. P.; Escher, B. I.; Fenner, K.; Hofstetter, T. B.; Johnson, C. A.; von Gunten, U.; Wehrli, B. The Challenge of Micropollutants in Aquatic Systems. *Science* **2006**, *313*, 1072–1077.

(16) Huber, M. M.; Canonica, S.; Park, G.-Y.; Gunten, U. Von. Oxidation of Pharmaceuticals

during Ozonation and Advanced Oxidation Processes. *Environ. Sci. Technol.* **2003**, *37*, 1016–1024.

(17) Al-Rifai, J. H.; Khabbaz, H.; Schäfer, A. I. Removal of Pharmaceuticals and Endocrine Disrupting Compounds in a Water Recycling Process Using Reverse Osmosis Systems. *Sep. Purif. Technol.* **2011**, *77*, 60–67.

(18) Djilani, C.; Zaghdoudi, R.; Modarressi, A.; Rogalski, M.; Djazi, F.; Lallam, A. Elimination of Organic Micropollutants by Adsorption on Activated Carbon Prepared from Agricultural Waste. *Chem. Eng. J.* **2012**, *189–190*, 203–212.

(19) Le Quéré, C.; Peters, G. P.; Andres, R. J.; Andrew, R. M.; Boden, T. A.; Ciais, P.; Friedlingstein, P.; Houghton, R. A.; Marland, G.; Moriarty, R.; et al. Global Carbon Budget 2013. *Earth Syst. Sci. Data* **2014**, *6*, 235–263.

(20) Dignon, J. NOx and SOx Emissions from Fossil Fuels: A Global Distribution. *Atmos. Environ. Part A. Gen. Top.* **1992**, *26*, 1157–1163.

(21) Bernard, S. M.; Samet, J. M.; Grambsch, A.; Ebi, K. L.; Romieu, I. The Potential Impacts of Climate Variability and Change on Air Pollution-Related Health Effects in the United States. *Environ. Health Perspect.* **2001**, *109*, 199–209.

(22) Friedrich, R.; Obermeier, A. Anthropogenic Emissions of Volatile Organic Compounds. In *Reactive Hydrocarbons in the Atmosphere*; Hewitt, N., 1st ed.; Academic Press: Amsterdam, 1999; pp 1–39.

(23) Dursun, D.; Sengul, F. Waste Minimization Study in a Solvent-Based Paint Manufacturing

Plant. *Resour. Conserv. Recycl.* **2006**, *47*, 316–331.

(24) Dahlgren, J.; Warshaw, R.; Horsak, R. D.; Parker III, F. M.; Takhar, H. Exposure Assessment of Residents Living near a Wood Treatment Plant. *Environ. Res.* **2003**, *92*, 99–109.

(25) Khan, F. I.; Kr. Ghoshal, A. Removal of Volatile Organic Compounds from Polluted Air. *J. Loss Prev. Process Ind.* **2000**, *13*, 527–545.

(26) Sly, L.; Haidamous, S.; Ajroudi, A. Syria Chemical Weapons Attack: Witnesses Say Strong Nerve Agent May Have Killed Victims. *The Washington Post*. April 11, 2018.

(27) Stone, R. U.K. Attack Puts Nerve Agent in the Spotlight. *Science* **2018**, *359*, 1314–1315.

(28) Costanzi, S.; Machado, J.-H.; Mitchell, M. Nerve Agents: What They Are, How They Work, How to Counter Them. *ACS Chem. Neurosci.* **2018**, *9*, 873–885.

(29) Shih, T.-M.; McDonough, J. H. Efficacy of Biperiden and Atropine as Anticonvulsant Treatment for Organophosphorus Nerve Agent Intoxication. *Arch. Toxicol.* **2000**, *74*, 165–172.

(30) Yang, Y.-C. Chemical Detoxification of Nerve Agent VX. *Acc. Chem. Res.* **1998**, *32*, 109–115.

(31) Mondal, S. S.; Holdt, H.-J. Breaking Down Chemical Weapons by Metal-Organic Frameworks. *Angew. Chem., Int. Ed.* **2016**, *55*, 42–44.

(32) Katz, M. J.; Moon, S.-Y.; Mondloch, J. E.; Beyzavi, M. H.; Stephenson, C. J.; Hupp, J. T.; Farha, O. K. Exploiting Parameter Space in MOFs: A 20-Fold Enhancement of Phosphate-

Ester Hydrolysis with UiO-66-NH2. *Chem. Sci.* **2015**, *6*, 2286–2291.

(33) Sánchez-Avila, J.; Tauler, R.; Lacorte, S. Organic Micropollutants in Coastal Waters from NW Mediterranean Sea: Sources Distribution and Potential Risk. *Environ. Int.* **2012**, *46*, 50–62.

(34) Stangroom, S. J.; Collins, C. D.; Lester, J. N. Sources of Organic Micropollutants to Lowland Rivers. *Environ. Technol.* **1998**, *19*, 643–666.

(35) Pera-Titus, M.; García-Molina, V.; Baños, M. A.; Giménez, J.; Esplugas, S. Degradation of Chlorophenols by Means of Advanced Oxidation Processes: A General Review. *Appl. Catal. B Environ.* **2004**, *47*, 219–256.

(36) Ikehata, K.; Jodeiri Naghashkar, N.; Gamal El-Din, M. Degradation of Aqueous Pharmaceuticals by Ozonation and Advanced Oxidation Processes: A Review. *Ozone Sci. Eng.* **2006**, *28*, 353–414.

(37) Oturan, N.; van Hullebusch, E. D.; Zhang, H.; Mazeas, L.; Budzinski, H.; Le Menach, K.; Oturan, M. A. Occurrence and Removal of Organic Micropollutants in Landfill Leachates Treated by Electrochemical Advanced Oxidation Processes. *Environ. Sci. Technol.* **2015**, *49*, 12187–12196.

(38) Pendergast, M. M.; Hoek, E. M. V. A Review of Water Treatment Membrane Nanotechnologies. *Energy Environ. Sci.* **2011**, *4*.

(39) Crittenden, J. C.; Trusell, R.; Hand, D. W.; Howe, K. J.; Tchobanoglous, G. *MWH's Water Treatment : Principles and Design.*, 3rd ed.; John Wiley & Sons: Hoboken, 2012.

(40) Werber, J. R.; Osuji, C. O.; Elimelech, M. Materials for Next-Generation Desalination and Water Purification Membranes. *Nat. Rev. Mater.* **2016**, *1*, 16018.

(41) Peinemann, K.-V.; Abetz, V.; Simon, P. F. W. Asymmetric Superstructure Formed in a Block Copolymer via Phase Separation. *Nat. Mater.* **2007**, *6*, 992–996.

(42) Banerjee, I.; Pangule, R. C.; Kane, R. S. Antifouling Coatings: Recent Developments in the Design of Surfaces That Prevent Fouling by Proteins, Bacteria, and Marine Organisms. *Adv. Mater.* **2011**, *23*, 690–718.

(43) Feng, X.; Kawabata, K.; Kaufman, G.; Elimelech, M.; Osuji, C. O. Highly Selective Vertically Aligned Nanopores in Sustainably Derived Polymer Membranes by Molecular Templating. *ACS Nano* **2017**, *11*, 3911–3921.

(44) Adsorption. In *IUPAC Compendium of Chemical Terminology*; IUPAC: Research Triagle Park, NC.

(45) Kristian Stevik, T.; Kari Aa; Ausland, G.; Fredrik Hanssen, J. Retention and Removal of Pathogenic Bacteria in Wastewater Percolating through Porous Media: A Review. *Water Res.* **2004**, *38*, 1355–1367.

(46) Fu, F.; Wang, Q. Removal of Heavy Metal Ions from Wastewaters: A Review. *J. Environ. Manage.* **2011**, *92*, 407–418.

(47) McKay, G. *Use of Adsorbents for the Removal of Pollutants from Wastewaters*, 1st ed.; CRC Press: Boca Raton, 1996.

(48) Chand, R. C.; Goyal, M. *Activated Carbon Adsorption*, 1st ed.; CRC Press: Boca Raton,

2005.

(49) Pelekani, C.; Snoeyink, V. . Competitive Adsorption in Natural Water: Role of Activated Carbon Pore Size. *Water Res.* **1999**, *33*, 1209–1219.

(50) Quinlivan, P. A.; Li, L.; Knappe, D. R. U. Effects of Activated Carbon Characteristics on the Simultaneous Adsorption of Aqueous Organic Micropollutants and Natural Organic Matter. *Water Res.* **2005**, *39*, 1663–1673.

(51) Newcombe, G.; Drikas, M.; Hayes, R. Influence of Characterised Natural Organic Material on Activated Carbon Adsorption: II. Effect on Pore Volume Distribution and Adsorption of 2-Methylisoborneol. *Water Res.* **1997**, *31*, 1065–1073.

(52) Sabio, E.; González, E.; González, J. .; González-García, C. .; Ramiro, A.; Gañan, J. Thermal Regeneration of Activated Carbon Saturated with P-Nitrophenol. *Carbon N. Y.* **2004**, *42*, 2285–2293.

(53) QU, J. Research Progress of Novel Adsorption Processes in Water Purification: A Review. *J. Environ. Sci.* **2008**, *20*, 1–13.

(54) Morin-Crini, N.; Crini, G. Environmental Applications of Water-Insoluble β-Cyclodextrin–Epichlorohydrin Polymers. *Prog. Polym. Sci.* **2013**, *38*, 344–368.

(55) Del Valle, E. M. M. Cyclodextrins and Their Uses: A Review. *Process Biochem.* **2004**, *39*, 1033–1046.

(56) Ma, M.; Li, D. New Organic Nanoporous Polymers and Their Inclusion Complexes. *Chem. Mater.* **1999**, *11*, 872–874.

(57) Mocanu, G.; Vizitiu, D.; Carpov, A. Cyclodextrin Polymers. *J. Bioact. Compat. Polym.* **2001**, *16*, 315–342.

(58) Alsbaiee, A.; Smith, B. J.; Xiao, L.; Ling, Y.; Helbling, D. E.; Dichtel, W. R. Rapid Removal of Organic Micropollutants from Water by a Porous β-Cyclodextrin Polymer. *Nature* **2016**, *529*, 190–194.

(59) Xiao, L.; Ling, Y.; Alsbaiee, A.; Li, C.; Helbling, D. E.; Dichtel, W. R. β-Cyclodextrin Polymer Network Sequesters Perfluorooctanoic Acid at Environmentally Relevant Concentrations. *J. Am. Chem. Soc.* **2017**, *139*, 7689–7692.

(60) Mohammed, N.; Grishkewich, N.; Tam, K. C. Cellulose Nanomaterials: Promising Sustainable Nanomaterials for Application in Water/Wastewater Treatment Processes. *Environ. Sci. Nano* **2018**, *5*, 623–658.

(61) He, X.; Male, K. B.; Nesterenko, P. N.; Brabazon, D.; Paull, B.; Luong, J. H. T. Adsorption and Desorption of Methylene Blue on Porous Carbon Monoliths and Nanocrystalline Cellulose. *ACS Appl. Mater. Interfaces* **2013**, *5*, 8796–8804.

(62) Kesselmeier, J.; Staudt, M. Biogenic Volatile Organic Compounds (VOC): An Overview on Emission, Physiology and Ecology. *J. Atmos. Chem.* **1999**, *33*, 23–88.

(63) Dewulf, J.; Van Langenhove, H. Anthropogenic Volatile Organic Compounds in Ambient Air and Natural Waters: A Review on Recent Developments of Analytical Methodology, Performance and Interpretation of Field Measurements. *J. Chromatogr. A* **1999**, *843*, 163–177.

(64) Borbon, A.; Gilman, J. B.; Kuster, W. C.; Grand, N.; Chevaillier, S.; Colomb, A.; Dolgorouky, C.; Gros, V.; Lopez, M.; Sarda-Esteve, R. Emission Ratios of Anthropogenic Volatile Organic Compounds in Northern Mid-Latitude Megacities: Observations versus Emission Inventories in Los Angeles and Paris. *J. Geophys. Res. Atmos.* **2013**, *118*, 2041–2057.

(65) Sarigiannis, D. A.; Karakitsios, S. P.; Gotti, A.; Liakos, I. L.; Katsoyiannis, A. Exposure to Major Volatile Organic Compounds and Carbonyls in European Indoor Environments and Associated Health Risk. *Environ. Int.* **2011**, *37*, 743–765.

(66) Wei, W.; Wang, S.; Chatani, S.; Klimont, Z.; Cofala, J.; Hao, J. Emission and Speciation of Non-Methane Volatile Organic Compounds from Anthropogenic Sources in China. *Atmos. Environ.* **2008**, *42*, 4976–4988.

(67) Drysys, H. Thermal Oxidation and Other VOC Abatement Techniques. *Filtr. Sep.* **1997**, *34*, 324–329.

(68) Liotta, L. F. Catalytic Oxidation of Volatile Organic Compounds on Supported Noble Metals. *Appl. Catal. B Environ.* **2010**, *100*, 403–412.

(69) Malhautier, L.; Khammar, N.; Bayle, S.; Fanlo, J.-L. Biofiltration of Volatile Organic Compounds. *Appl. Microbiol. Biotechnol.* **2005**, *68*, 16–22.

(70) Mohseni, M.; Allen, D. G. Biofiltration of Mixtures of Hydrophilic and Hydrophobic Volatile Organic Compounds. *Chem. Eng. Sci.* **2000**, *55*, 1545–1558.

(71) Cheng, Y.; He, H.; Yang, C.; Zeng, G.; Li, X.; Chen, H.; Yu, G. Challenges and Solutions

for Biofiltration of Hydrophobic Volatile Organic Compounds. *Biotechnol. Adv.* **2016**, *34*, 1091–1102.

(72) Spivey, J. J. Complete Catalytic Oxidation of Volatile Organicst. *Ind. Eng. Chem. Res.* **1987**, *26*, 2165–2180.

(73) Dumont, E.; Darracq, G.; Couvert, A.; Couriol, C.; Amrane, A.; Thomas, D.; Andrès, Y.; Le Cloirec, P. VOC Absorption in a Countercurrent Packed-Bed Column Using Water/Silicone Oil Mixtures: Influence of Silicone Oil Volume Fraction. *Chem. Eng. J.* **2011**, *168*, 241–248.

(74) Quijano, G.; Couvert, A.; Amrane, A.; Darracq, G.; Couriol, C.; Le Cloirec, P.; Paquin, L.; Carrié, D. Potential of Ionic Liquids for VOC Absorption and Biodegradation in Multiphase Systems. *Chem. Eng. Sci*. **2011**, *66*, 2707–2712.

(75) Rahbar, M. S.; Kaghazchi, T. Modeling of Packed Absorption Tower for Volatile Organic Compounds Emission Control. *Int. J. Environ. Sci. Technol.* **2005**, *2*, 207–215.

(76) Crittenden, J. C.; Cortright, R. D.; Rick, B.; Tang, S.-R.; Perram, D. Using GAC to Remove VOCs From Air Stripper Off-Gas. *J. Am. Water Works Assoc.* **1988**, *80*, 73–84.

(77) Chiang, Y.-C.; Chiang, P.-C.; Huang, C.-P. Effects of Pore Structure and Temperature on VOC Adsorption on Activated Carbon. *Carbon N. Y.* **2001**, *39*, 523–534.

(78) Lodewyckx, P.; Vansant, E. F. Influence of Humidity on Adsorption Capacity from the Wheeler-Jonas Model for Prediction of Breakthrough Times of Water Immiscible Organic Vapors on Activated Carbon Beds. *Am. Ind. Hyg. Assoc. J.* **1999**, *60*, 612–617.

(79) Chauveau, R.; Grévillot, G.; Marsteau, S.; Vallières, C. Values of the Mass Transfer Coefficient of the Linear Driving Force Model for VOC Adsorption on Activated Carbons. *Chem. Eng. Res. Des.* **2013**, *91*, 955–962.

(80) Singh, K. P.; Mohan, D.; Tandon, G. S.; Gupta, G. S. D. Vapor-Phase Adsorption of Hexane and Benzene on Activated Carbon Fabric Cloth: Equilibria and Rate Studies. *Ind. Eng. Chem. Res.* **2002**, *41*, 2480–2486.

(81) Sidheswaran, M. A.; Destaillats, H.; Sullivan, D. P.; Cohn, S.; Fisk, W. J. Energy Efficient Indoor VOC Air Cleaning with Activated Carbon Fiber (ACF) Filters. *Build. Environ.* **2012**, *47*, 357–367.

(82) Ramos, M. E.; Bonelli, P. R.; Cukierman, A. L.; Ribeiro Carrott, M. M. L.; Carrott, P. J. M. Adsorption of Volatile Organic Compounds onto Activated Carbon Cloths Derived from a Novel Regenerated Cellulosic Precursor. *J. Hazard. Mater.* **2010**, *177*, 175–182.

(83) Tanada, S.; Nakamura, T.; Kawasaki, N.; Kitayama, S.; Takebe, Y. Inclusion of Volatile Organic Compounds into Natural Cyclodextrins and Their Branched Cyclodextrins in the Gaseous Phase. *J. Colloid Interface Sci.* **1997**, *186*, 180–184.

(84) Celebioglu, A.; Sen, H. S.; Durgun, E.; Uyar, T. Molecular Entrapment of Volatile Organic Compounds (VOCs) by Electrospun Cyclodextrin Nanofibers. *Chemosphere* **2016**, *144*, 736–744.

(85) Mallard Favier, I.; Baudelet, D.; Fourmentin, S. VOC Trapping by New Crosslinked Cyclodextrin Polymers. *J. Incl. Phenom. Macrocycl. Chem.* **2011**, *69*, 433–437.

(86) Dehabadi, V. A.; Buschmann, H.-J. J.; Gutmann, J. S. A Novel Approach for Fixation of β-Cyclodextrin on Cotton Fabrics. *J. Incl. Phenom. Macrocycl. Chem.* **2014**, *79*, 459–464.

(87) Everts, S. The Nazi Origins of Deadly Nerve Gases. *Chem. Eng. News* **2016**, *94*, 26–28.

(88) Ellison, D. H. *Handbook of Chemical and Biological Warfare Agents*, 2nd ed.; CRC Press: Boca Raton, 2007.

(89) Wiener, S. W.; Hoffman, R. S. Nerve Agents: A Comprehensive Review. *J. Intensive Care Med.* **2004**, *19*, 22–37.

(90) Lunn, G.; Sansone, E. B. Safe Disposal of Diisopropyl Fluorophosphate (DFP). *Appl. Biochem. Biotechnol.* **1994**, *49*, 165–172.

(91) Stone, R. How to Defeat a Nerve Agent. *Science*. January 4, 2018.

(92) Yang, Y.-C.; Baker, J. A.; Ward, J. R. Decontamination of Chemical Warfare Agents. *Chem. Rev.* **1992**, *92*, 1729–1743.

(93) Wagner, G. W.; Bartram, P. W. Reactions of the Nerve Agent Simulant Diisopropyl Fluorophosphate with Self-Decontaminating Adsorbents. A ^{31}P MAS NMR Study. *J. Mol. Catal. A Chem.* **1999**, *144*, 419–424.

(94) Smith, B. M. Catalytic Methods for the Destruction of Chemical Warfare Agents under Ambient Conditions. *Chem. Soc. Rev.* **2008**, *37*, 470–478.

(95) Morales-Rojas, H.; Moss, R. A. Phosphorolytic Reactivity of O-Iodosylcarboxylates and Related Nucleophiles. *Chem. Rev.* **2002**, *102*, 2497–2522.

(96) Worek, F.; Wille, T. Catalytic Bioscavengers in Nerve Agent Poisoning: A Promising

Approach? *Toxicol. Lett.* **2016**, *244*, 143–148.

(97) Eubanks, L. M.; Dickerson, T. J.; Janda, K. D. Technological Advancements for the Detection of and Protection against Biological and Chemical Warfare Agents. *Chem. Soc. Rev.* **2007**, *36*, 458.

(98) Kinnan, M. K.; Creasy, W. R.; Fullmer, L. B.; Schreuder-Gibson, H. L.; Nyman, M. Nerve Agent Degradation with Polyoxoniobates. *Eur. J. Inorg. Chem.* **2014**, *2014*, 2361–2367.

(99) Harvey, S. P.; Kolakowski, J. E.; Cheng, T.-C.; Rastogi, V. K.; Reiff, L. P.; DeFrank, J. J.; Raushel, F. M.; Hill, C. Stereospecificity in the Enzymatic Hydrolysis of Cyclosarin (GF). *Enzyme Microb. Technol.* **2005**, *37*, 547–555.

(100) Gupta, R. D.; Goldsmith, M.; Ashani, Y.; Simo, Y.; Mullokandov, G.; Bar, H.; Ben-David, M.; Leader, H.; Margalit, R.; Silman, I.; et al. Directed Evolution of Hydrolases for Prevention of G-Type Nerve Agent Intoxication. *Nat. Chem. Biol.* **2011**, *7*, 120–125.

(101) Liu, Y.; Howarth, A. J.; Vermeulen, N. A.; Moon, S.-Y.; Hupp, J. T.; Farha, O. K. Catalytic Degradation of Chemical Warfare Agents and Their Simulants by Metal-Organic Frameworks. *Coord. Chem. Rev.* **2017**, *346*, 101–111.

(102) Russell, V. A.; Evans, J.; Li, N.; Ward, D.; Wachter, J.; O'Keeffe, M.; Yaghi, O. M. Nanoporous Molecular Sandwiches: Pillared Two-Dimensional Hydrogen-Bonded Networks with Adjustable Porosity. *Science* **1997**, *276*, 575–579.

(103) Ma, L.; Abney, C.; Lin, W. Enantioselective Catalysis with Homochiral Metal–Organic Frameworks. *Chem. Soc. Rev.* **2009**, *38*, 1248.

(104) Nijem, N.; Wu, H.; Canepa, P.; Marti, A.; Balkus, K. J.; Thonhauser, T.; Li, J.; Chabal, Y. J. Tuning the Gate Opening Pressure of Metal–Organic Frameworks (MOFs) for the Selective Separation of Hydrocarbons. *J. Am. Chem. Soc.* **2012**, *134*, 15201–15204.

(105) Getman, R. B.; Bae, Y.-S.; Wilmer, C. E.; Snurr, R. Q. Review and Analysis of Molecular Simulations of Methane, Hydrogen, and Acetylene Storage in Metal–Organic Frameworks. *Chem. Rev.* **2012**, *112*, 703–723.

(106) DeCoste, J. B.; Peterson, G. W. Metal–Organic Frameworks for Air Purification of Toxic Chemicals. *Chem. Rev.* **2014**, *114*, 5695–5727.

(107) Katz, M. J.; Mondloch, J. E.; Totten, R. K.; Park, J. K.; Nguyen, S. T.; Farha, O. K.; Hupp, J. T. Simple and Compelling Biomimetic Metal-Organic Framework Catalyst for the Degradation of Nerve Agent Simulants. *Angew. Chem., Int. Ed.* **2014**, *53*, 497–501.

(108) Katz, M. J.; Moon, S.-Y.; Mondloch, J. E.; Beyzavi, M. H.; Stephenson, C. J.; Hupp, J. T.; Farha, O. K. Exploiting Parameter Space in MOFs: A 20-Fold Enhancement of Phosphate-Ester Hydrolysis with UiO-66-NH_2. *Chem. Sci.* **2015**, *6*, 2286–2291.

(109) Peterson, G. W.; Moon, S.-Y.; Wagner, G. W.; Hall, M. G.; DeCoste, J. B.; Hupp, J. T.; Farha, O. K. Tailoring the Pore Size and Functionality of UiO-Type Metal–Organic Frameworks for Optimal Nerve Agent Destruction. *Inorg. Chem.* **2015**, *54*, 9684–9686.

(110) López-Maya, E.; Montoro, C.; Rodríguez-Albelo, L. M.; Aznar Cervantes, S. D.; Lozano-Pérez, A. A.; Cenís, J. L.; Barea, E.; Navarro, J. a. R. Textile/Metal-Organic-Framework Composites as Self-Detoxifying Filters for Chemical-Warfare Agents. *Angew. Chem., Int.*

Ed. **2015**, *54*, 6790–6794.

(111) Zhao, J.; Lee, D. T.; Yaga, R. W.; Hall, M. G.; Barton, H. F.; Woodward, I. R.; Oldham, C. J.; Walls, H. J.; Peterson, G. W.; Parsons, G. N. Ultra-Fast Degradation of Chemical Warfare Agents Using MOF-Nanofiber Kebabs. *Angew. Chem., Int. Ed.* **2016**, *55*, 13224–13228.

(112) Lee, D. T.; Zhao, J.; Peterson, G. W.; Parsons, G. N. Catalytic "MOF-Cloth" Formed via Directed Supramolecular Assembly of UiO-66-NH_2 Crystals on Atomic Layer Deposition-Coated Textiles for Rapid Degradation of Chemical Warfare Agent Simulants. *Chem. Mater.* **2017**, *29*, 4894–4903.

(113) Pye, V. I.; Patrick, R. Ground Water Contamination in the United States. *Science* **1983**, *221*, 713–718.

(114) Schwarzenbach, R. P.; Egli, T.; Hofstetter, T. B.; von Gunten, U.; Wehrli, B. Global Water Pollution and Human Health. *Annu. Rev. Environ. Resour.* **2010**, *35*, 109–136.

(115) Melzer, D.; Rice, N.; Depledge, M. H.; Henley, W. E.; Galloway, T. S. Association between Serum Perfluorooctanoic Acid (PFOA) and Thyroid Disease in the U.S. National Health and Nutrition Examination Survey. *Environ. Health Perspect.* **2010**, *118*, 686–692.

(116) Kim, S.; Aga, D. S. Potential Ecological and Human Health Impacts of Antibiotics and Antibiotic-Resistant Bacteria from Wastewater Treatment Plants. *J. Toxicol. Environ. Heal. Part B* **2007**, *10*, 559–573.

(117) Vandenberg, L. N.; Colborn, T.; Hayes, T. B.; Heindel, J. J.; Jacobs, D. R.; Lee, D.-H.;

Shioda, T.; Soto, A. M.; vom Saal, F. S.; Welshons, W. V.; et al. Hormones and Endocrine-Disrupting Chemicals: Low-Dose Effects and Nonmonotonic Dose Responses. *Endocr. Rev.* **2012**, *33*, 378–455.

(118) Comninellis, C.; Kapalka, A.; Malato, S.; Parsons, S. A.; Poulios, I.; Mantzavinos, D. Advanced Oxidation Processes for Water Treatment: Advances and Trends for R&D. *J. Chem. Technol. Biotechnol.* **2008**, *83*, 769–776.

(119) Worch, E. *Adsorption Technology in Water Treatment, Fundamentals, Processes, and Modeling*, 1st ed.; De Gruyter: Berlin, 2012.

(120) Luo, Y.; Guo, W.; Ngo, H. H.; Nghiem, L. D.; Hai, F. I.; Zhang, J.; Liang, S.; Wang, X. C. A Review on the Occurrence of Micropollutants in the Aquatic Environment and Their Fate and Removal during Wastewater Treatment. *Sci. Total Environ.* **2014**, *473–474*, 619–641.

(121) Ali, I.; Gupta, V. K. Advances in Water Treatment by Adsorption Technology. *Nat. Protoc.* **2007**, *1*, 2661–2667.

(122) Sweetman, M.; May, S.; Mebberson, N.; Pendleton, P.; Vasilev, K.; Plush, S.; Hayball, J. Activated Carbon, Carbon Nanotubes and Graphene: Materials and Composites for Advanced Water Purification. *C* **2017**, *3*, 18–47.

(123) Liu, Z.; Wang, H.; Liu, C.; Jiang, Y.; Yu, G.; Mu, X.; Wang, X. Magnetic Cellulose–Chitosan Hydrogels Prepared from Ionic Liquids as Reusable Adsorbent for Removal of Heavy Metal Ions. *Chem. Commun.* **2012**, *48*, 7350.

(124) Goodman, S. M.; Bura, R.; Dichiara, A. B. Facile Impregnation of Graphene into Porous

Wood Filters for the Dynamic Removal and Recovery of Dyes from Aqueous Solutions. *ACS Appl. Nano Mater.* **2018**, *1*, 5682–5690.

(125) Ali, I. Water Treatment by Adsorption Columns: Evaluation at Ground Level. *Sep. Purif. Rev.* **2014**, *43*, 175–205.

(126) d'Halluin, M.; Rull-Barrull, J.; Bretel, G.; Labrugère, C.; Le Grognec, E.; Felpin, F.-X. Chemically Modified Cellulose Filter Paper for Heavy Metal Remediation in Water. *ACS Sustain. Chem. Eng.* **2017**, *5*, 1965–1973.

(127) Mohammed, N.; Grishkewich, N.; Waeijen, H. A.; Berry, R. M.; Tam, K. C. Continuous Flow Adsorption of Methylene Blue by Cellulose Nanocrystal-Alginate Hydrogel Beads in Fixed Bed Columns. *Carbohydr. Polym.* **2016**, *136*, 1194–1202.

(128) Alhamed, Y. A. Adsorption Kinetics and Performance of Packed Bed Adsorber for Phenol Removal Using Activated Carbon from Dates' Stones. *J. Hazard. Mater.* **2009**, *170*, 763–770.

(129) Yilmaz, E.; Haupt, K.; Mosbach, K. The Use of Immobilized Templates—A New Approach in Molecular Imprinting. *Angew. Chem., Int. Ed.* **2000**, *39*, 2115–2118.

(130) Kong, X.; Gao, R.; He, X.; Chen, L.; Zhang, Y. Synthesis and Characterization of the Core–Shell Magnetic Molecularly Imprinted Polymers (Fe3O4@MIPs) Adsorbents for Effective Extraction and Determination of Sulfonamides in the Poultry Feed. *J. Chromatogr. A* **2012**, *1245*, 8–16.

(131) Roy, D.; Semsarilar, M.; Guthrie, J. T.; Perrier, S. Cellulose Modification by Polymer

Grafting: A Review. *Chem. Soc. Rev.* **2009**, *38*, 1825–2148.

(132) Moon, R. J.; Martini, A.; Nairn, J.; Simonsen, J.; Youngblood, J. Cellulose Nanomaterials Review: Structure, Properties and Nanocomposites. *Chem. Soc. Rev.* **2011**, *40*, 3941–3994.

(133) Eftink, M. R.; Andy, M. L.; Bystrom, K.; Perlmutter, H. D.; Kristolt, D. S. Cyclodextrin Inclusion Complexes: Studies of the Variation in the Size of Alicyclic Guests. *J. Am. Chem. Soc.* **1989**, *111*, 6765–6112.

(134) Sreenivasan, K. Synthesis and Evaluation of a Beta Cyclodextrin-Based Molecularly Imprinted Copolymer. *J. Appl. Polym. Sci.* **1998**, *70*, 15–18.

(135) Wang, D.; Liu, L.; Jiang, X.; Yu, J.; Chen, X. Adsorption and Removal of Malachite Green from Aqueous Solution Using Magnetic β-Cyclodextrin-Graphene Oxide Nanocomposites as Adsorbents. *Colloids Surfaces A Physicochem. Eng. Asp.* **2015**, *466*, 166–173.

(136) Chen, L.; Berry, R. M.; Tam, K. C. Synthesis of β-Cyclodextrin-Modified Cellulose Nanocrystals (CNCs)@Fe_3O_4@SiO_2 Superparamagnetic Nanorods. *ACS Sustain. Chem. Eng.* **2014**, *2*, 951–958.

(137) Ling, Y.; Klemes, M. J.; Xiao, L.; Alsbaiee, A.; Dichtel, W. R.; Helbling, D. E. Benchmarking Micropollutant Removal by Activated Carbon and Porous β-Cyclodextrin Polymers under Environmentally Relevant Scenarios. *Environ. Sci. Technol.* **2017**, *51*, 7590–7598.

(138) Klemes, M. J.; Ling, Y.; Chiapasco, M.; Alsbaiee, A.; Helbling, D. E.; Dichtel, W. R. Phenolation of Cyclodextrin Polymers Controls Their Lead and Organic Micropollutant

Adsorption. *Chem. Sci.* **2018**, *9*, 8883–8889.

(139) Alzate-Sanchez, D. M.; Smith, B. J.; Alsbaiee, A.; Hinestroza, J. P.; Dichtel, W. R. Cotton Fabric Functionalized with a Beta-Cyclodextrin Polymer Captures Organic Pollutants from Contaminated Air and Water. *Chem. Mater.* **2016**, *28*, 8340–8346.

(140) Kačuráková, M.; Wilson, R. H. Developments in Mid-Infrared FT-IR Spectroscopy of Selected Carbohydrates. *Carbohydr. Polym.* **2001**, *44*, 291–303.

(141) Ghosal, P. S.; Gupta, A. K. Determination of Thermodynamic Parameters from Langmuir Isotherm Constant-Revisited. *J. Mol. Liq.* **2017**, *225*, 137–146.

(142) Liu, Y. New Insights into Pseudo-Second-Order Kinetic Equation for Adsorption. *Colloids Surfaces A Physicochem. Eng. Asp.* **2008**, *320*, 275–278.

(143) Guiochon, G. Monolithic Columns in High-Performance Liquid Chromatography. *J. Chromatogr. A* **2007**, *1168*, 101–168.

(144) Angelidaki, I.; Sanders, W. Assessment of the Anaerobic Biodegradability of Macropollutants. *Rev. Environ. Sci. Bio/Technology* **2004**, *3*, 117–129.

(145) Finlayson-Pitts, B. J. Tropospheric Air Pollution: Ozone, Airborne Toxics, Polycyclic Aromatic Hydrocarbons, and Particles. *Science* **1997**, *276*, 1045–1051.

(146) Boeglin, M. L.; Wessels, D.; Henshel, D. An Investigation of the Relationship between Air Emissions of Volatile Organic Compounds and the Incidence of Cancer in Indiana Counties. *Environ. Res.* **2006**, *100*, 242–254.

(147) Mølhave, L.; Grønkjær, J.; Larsen, S. Subjective Reactions to Volatile Organic Compounds

as Air Pollutants. *Atmos. Environ. Part A. Gen. Top.* **1991**, *25*, 1283–1293.

(148) Bale, A. S.; Meacham, C. A.; Benignus, V. A.; Bushnell, P. J.; Shafer, T. J. Volatile Organic Compounds Inhibit Human and Rat Neuronal Nicotinic Acetylcholine Receptors Expressed in Xenopus Oocytes. *Toxicol. Appl. Pharmacol.* **2005**, *205*, 77–88.

(149) Bradley, R. H.; Smith, M. W.; Andreu, A.; Falco, M. Surface Studies of Novel Hydrophobic Active Carbons. *Appl. Surf. Sci.* **2011**, *257*, 2912–2919.

(150) Kayaci, F.; Uyar, T. Electrospun Polyester/Cyclodextrin Nanofibers for Entrapment of Volatile Organic Compounds. *Polym. Eng. Sci.* **2014**, *54*, 2970–2978.

(151) Kim, H. J.; Pant, H. R.; Choi, N. J.; Kim, C. S. Composite Electrospun Fly Ash/Polyurethane Fibers for Absorption of Volatile Organic Compounds from Air. *Chem. Eng. J.* **2013**, *230*, 244–250.

(152) Mallard, I.; Städe, L. W.; Ruellan, S.; Jacobsen, P. A. L.; Larsen, K. L.; Fourmentin, S. Synthesis, Characterization and Sorption Capacities toward Organic Pollutants of New β-Cyclodextrin Modified Zeolite Derivatives. *Colloids Surfaces A Physicochem. Eng. Asp.* **2015**, *482*, 50–57.

(153) Peila, R.; Vineis, C.; Varesano, A.; Ferri, A. Different Methods for β-Cyclodextrin/Triclosan Complexation as Antibacterial Treatment of Cellulose Substrates. *Cellulose* **2013**, *20*, 2115–2123.

(154) Szaniszló, N.; Fenyvesi, É.; Balla, J. Structure-Stability Study of Cyclodextrin Complexes with Selected Volatile Hydrocarbon Contaminants of Soils. *J. Incl. Phenom. Macrocycl.*

Chem. **2005**, *53*, 241–248.

(155) Szejtli, J. Cyclodextrins in Food, Cosmetics and Toiletries. *Starch* **1982**, *34*, 379–385.

(156) Dyes, T. Cyclodextrins in the Textile Industry. *Starch* **2003**, *55*, 191–196.

(157) Grechin, A. G.; Buschmann, H.-J.; Schollmeyer, E. Quantification of Cyclodextrins Fixed onto Cellulose Fibers. *Text. Res. J.* **2007**, *77*, 161–164.

(158) Cabrales, L.; Abidi, N.; Hammond, A.; Hamood, A. Cotton Fabric Functionalization with Cyclodextrins. *J. Mater. Environ. Sci.* **2012**, *3*, 561–574.

(159) Morin-crini, N.; Crini, G. Progress in Polymer Science Environmental Applications of Water-Insoluble -Cyclodextrin – Epichlorohydrin Polymers. *Prog. Polym. Sci.* **2013**, *38*, 344–368.

(160) P. P. Agraval; M. M. C. G. Warmoeskerken. Permanent Fixation of B-Cyclodextrin on Cotton Surface— An Assessment Between Innovative and Established Approaches. *J. Appl. Polym. Sci.* **2011**, *124*, 4090–4097.

(161) Machín, R.; Isasi, J. R.; Vélaz, I. β-Cyclodextrin Hydrogels as Potential Drug Delivery Systems. *Carbohydr. Polym.* **2012**, *87*, 2024–2030.

(162) Rubin, B. S. Bisphenol A: An Endocrine Disruptor with Widespread Exposure and Multiple Effects. *J. Steroid Biochem. Mol. Biol.* **2011**, *127*, 27–34.

(163) García-Zubiri, I. X.; González-Gaitano, G.; Isasi, J. R. Sorption Models in Cyclodextrin Polymers: Langmuir, Freundlich, and a Dual-Mode Approach. *J. Colloid Interface Sci.* **2009**, *337*, 11–18.

(164) Cherry, N.; Gautrin, D. Neurotoxic Effects of Styrene: Further Evidence. *Occup. Environ. Med.* **1990**, *47*, 29–37.

(165) Chemical Sampling Information | Styrene https://www.osha.gov/dts/chemicalsampling/data/CH_268200.html (accessed Feb 12, 2016).

(166) Wellner, T.; Lüersen, L.; Schaller, K. H.; Angerer, J.; Drexler, H.; Korinth, G. Percutaneous Absorption of Aromatic Amines - a Contribution for Human Health Risk Assessment. *Food Chem. Toxicol.* **2008**, *46*, 1960–1968.

(167) Andersen, A. Final Report on the Safety Assessment of Benzaldehyde. *Int. J. Toxicol.* **2006**, *25*, 11–27.

(168) Zhao, F.; Repo, E.; Meng, Y.; Wang, X.; Yin, D.; Sillanpää, M. An EDTA-β-Cyclodextrin Material for the Adsorption of Rare Earth Elements and Its Application in Preconcentration of Rare Earth Elements in Seawater. *J. Colloid Interface Sci.* **2016**, *465*, 215–224.

(169) Crowley, M.; Shang, L.; Dando, M. Preventing Chemical Weapons as Sciences Converge. *Science* **2018**, *362*, 753–755.

(170) Bajgar, J. Organophosphates/Nerve Agents Poisoning: Mechanism of Action, Diagnosis, Prophylaxis and Treatment. In *Advances in Clinical Chemistry, Volume 38*; Makowski, G., Ed.; Academic Press: Cambridge, 2004; pp 151–216.

(171) Kim, K.; Tsay, O. G.; Atwood, D. A.; Churchill, D. G. Destruction and Detection of Chemical Warfare Agents. *Chem. Rev.* **2011**, *111*, 5345–5403.

(172) National Research Council. *Review of Systemization of the Tooele Chemical Agent Disposal Facility*; Washington, D.C., 1996.

(173) Neutralization Followed by Supercritical Water Oxidation | Program Executive Office, Assembled Chemical Weapons Alternatives (PEO ACWA) https://www.peoacwa.army.mil/bgcapp/bgcapp-destruction-technologies/neutralization-followed-by-supercritical-water-oxidation/ (accessed Mar 5, 2019).

(174) Mondloch, J. E.; Katz, M. J.; Isley III, W. C.; Ghosh, P.; Liao, P.; Bury, W.; Wagner, G. W.; Hall, M. G.; DeCoste, J. B.; Peterson, G. W.; et al. Destruction of Chemical Warfare Agents Using Metal–Organic Frameworks. *Nat. Mater.* **2015**, *14*, 512–516.

(175) de Koning, M. C.; van Grol, M.; Breijaert, T. Degradation of Paraoxon and the Chemical Warfare Agents VX, Tabun, and Soman by the Metal–Organic Frameworks UiO-66-NH_2, MOF-808, NU-1000, and PCN-777. *Inorg. Chem.* **2017**, *56*, 11804–11809.

(176) Moon, S.-Y.; Liu, Y.; Hupp, J. T.; Farha, O. K. Instantaneous Hydrolysis of Nerve-Agent Simulants with a Six-Connected Zirconium-Based Metal-Organic Framework. *Angew. Chem., Int. Ed.* **2015**, *54*, 6795–6799.

(177) Katz, M. J.; Klet, R. C.; Moon, S.-Y.; Mondloch, J. E.; Hupp, J. T.; Farha, O. K. One Step Backward Is Two Steps Forward: Enhancing the Hydrolysis Rate of UiO-66 by Decreasing [OH^-]. *ACS Catal.* **2015**, *5*, 4637–4642.

(178) Islamoglu, T.; Ortuño, M. A.; Proussaloglou, E.; Howarth, A. J.; Vermeulen, N. A.; Atilgan, A.; Asiri, A. M.; Cramer, C. J.; Farha, O. K. Presence versus Proximity: The Role of Pendant

Amines in the Catalytic Hydrolysis of a Nerve Agent Simulant. *Angew. Chem., Int. Ed.* **2018**, *57*, 1949–1953.

(179) Schelling, M.; Kim, M.; Otal, E.; Hinestroza, J.; Schelling, M.; Kim, M.; Otal, E.; Hinestroza, J. Decoration of Cotton Fibers with a Water-Stable Metal–Organic Framework (UiO-66) for the Decomposition and Enhanced Adsorption of Micropollutants in Water. *Bioengineering* **2018**, *5*, 14–25.

(180) Abdelhameed, R. M.; Rehan, M.; Emam, H. E. Figuration of Zr-Based MOF@cotton Fabric Composite for Potential Kidney Application. *Carbohydr. Polym.* **2018**, *195*, 460–467.

(181) Dwyer, D. B.; Lee, D. T.; Boyer, S.; Bernier, W. E.; Parsons, G. N.; Jones, W. E. Toxic Organophosphate Hydrolysis Using Nanofiber-Templated UiO-66-NH2 Metal–Organic Framework Polycrystalline Cylinders. *ACS Appl. Mater. Interfaces* **2018**, *10*, 25794–25803.

(182) Lu, A. X.; McEntee, M.; Browe, M. A.; Hall, M. G.; DeCoste, J. B.; Peterson, G. W. MOFabric: Electrospun Nanofiber Mats from PVDF/UiO-66-NH_2 for Chemical Protection and Decontamination. *ACS Appl. Mater. Interfaces* **2017**, *9*, 13632–13636.

(183) Chen, Y.; Li, S.; Pei, X.; Zhou, J.; Feng, X.; Zhang, S.; Cheng, Y.; Li, H.; Han, R.; Wang, B. A Solvent-Free Hot-Pressing Method for Preparing Metal-Organic-Framework Coatings. *Angew. Chem., Int. Ed.* **2016**, *55*, 3419–3423.

(184) Wang, A.; Fan, R.; Zhou, X.; Hao, S.; Zheng, X.; Yang, Y. Hot-Pressing Method To Prepare Imidazole-Based Zn(II) Metal–Organic Complexes Coatings for Highly Efficient Air Filtration. *ACS Appl. Mater. Interfaces* **2018**, *10*, 9744–9755.

(185) Chen, Y.; Zhang, S.; Cao, S.; Li, S.; Chen, F.; Yuan, S.; Xu, C.; Zhou, J.; Feng, X.; Ma, X.; et al. Roll-to-Roll Production of Metal-Organic Framework Coatings for Particulate Matter Removal. *Adv. Mater.* **2017**, *29*, 1606221.

(186) Zhang, K.; Huo, Q.; Zhou, Y.-Y.; Wang, H.-H.; Li, G.-P.; Wang, Y.-W.; Wang, Y.-Y. Textiles/Metal–Organic Frameworks Composites as Flexible Air Filters for Efficient Particulate Matter Removal. *ACS Appl. Mater. Interfaces* **2019**, *11*, 17368–17374.

(187) Garibay, S. J.; Cohen, S. M. Isoreticular Synthesis and Modification of Frameworks with the UiO-66 Topology. *Chem. Commun.* **2010**, *46*, 7700–7702.

(188) DeStefano, M. R.; Islamoglu, T.; Garibay, S. J.; Hupp, J. T.; Farha, O. K. Room-Temperature Synthesis of UiO-66 and Thermal Modulation of Densities of Defect Sites. *Chem. Mater.* **2017**, *29*, 1357–1361.

(189) Katz, M. J.; Brown, Z. J.; Colón, Y. J.; Siu, P. W.; Scheidt, K. A.; Snurr, R. Q.; Hupp, J. T.; Farha, O. K. A Facile Synthesis of UiO-66, UiO-67 and Their Derivatives. *Chem. Commun.* **2013**, *49*, 9449–9451.

(190) Neufeld, M. J.; Harding, J. L.; Reynolds, M. M. Immobilization of Metal–Organic Framework Copper(II) Benzene-1,3,5-Tricarboxylate (CuBTC) onto Cotton Fabric as a Nitric Oxide Release Catalyst. *ACS Appl. Mater. Interfaces* **2015**, *7*, 26742–26750.

(191) Ozer, R. R.; Hinestroza, J. P. One-Step Growth of Isoreticular Luminescent Metal–Organic Frameworks on Cotton Fibers. *RSC Adv.* **2015**, *5*, 15198–15204.

(192) Wang, L.-F.; Pan, S.-Y.; Hu, H.; Miao, W.-H.; Xu, X.-Y. Synthesis and Properties of

Carboxymethyl Kudzu Root Starch. *Carbohydr. Polym.* **2010**, *80*, 174–179.

(193) Pushpamalar, V.; Langford, S. J.; Ahmad, M.; Lim, Y. Y. Optimization of Reaction Conditions for Preparing Carboxymethyl Cellulose from Sago Waste. *Carbohydr. Polym.* **2006**, *64*, 312–318.

(194) Kickelbick, G.; Wiede, P.; Schubert, U. Variations in Capping the Zr6O4(OH)4 Cluster Core: X-Ray Structure Analyses of $[Zr_6(OH)_4O_4(OOC–CH=CH_2)_{10}]_2(\mu\text{-}OOC–CH=CH_2)_4$ and $Zr_6(OH)_4O_4(OOCR)_{12}(PrOH)$ (R = Ph, CMe = CH_2). *Inorganica Chim. Acta* **1999**, *284*, 1–7.

(195) Totten, R. K.; Ryan, P.; Kang, B.; Lee, S. J.; Broadbelt, L. J.; Snurr, R. Q.; Hupp, J. T.; Nguyen, S. T. Enhanced Catalytic Decomposition of a Phosphate Triester by Modularly Accessible Bimetallic Porphyrin Dyads and Dimers. *Chem. Commun.* **2012**, *48*, 41784180.

(196) Casado, J.; Lopez-Quintela, M. A.; Lorenzo-Barral, F. M. The Initial Rate Method in Chemical Kinetics: Evaluation and Experimental Illustration. *J. Chem. Educ.* **1986**, *63*, 450–452.

(197) Ahmed, E. M. Hydrogel: Preparation, Characterization, and Applications: A Review. *J. Adv. Res.* **2015**, *6*, 105–121.

(198) Billiet, T.; Vandenhaute, M.; Schelfhout, J.; Van Vlierberghe, S.; Dubruel, P. A Review of Trends and Limitations in Hydrogel-Rapid Prototyping for Tissue Engineering. *Biomaterials* **2012**, *33*, 6020–6041.

(199) Lee, K. Y.; Mooney, D. J. Hydrogels for Tissue Engineering. *Chem. Rev.* **2001**, *101*, 1869–

1880.

(200) Hoare, T. R.; Kohane, D. S. Hydrogels in Drug Delivery: Progress and Challenges. *Polymer* **2008**, *49*, 1993–2007.

(201) Ionov, L. Hydrogel-Based Actuators: Possibilities and Limitations. *Mater. Today* **2014**, *17*, 494–503.

(202) Lake, G. J.; Thomas, A. G. The Strength of Highly Elastic Materials. *Proc. R. Soc. London. Ser. A. Math. Phys. Sci.* **1967**, *300*, 108–119.

(203) Tse, J. R.; Engler, A. J. Preparation of Hydrogel Substrates with Tunable Mechanical Properties. *Curr. Protoc. Cell Biol.* **2010**, *47*, 10.16.1-10.16.16.

(204) Simha, N. K.; Carlson, C. S.; Lewis, J. L. Evaluation of Fracture Toughness of Cartilage by Micropenetration. *J. Mater. Sci. Mater. Med.* **2004**, *15*, 631–639.

(205) Ke, H.; Yang, L.-P.; Xie, M.; Chen, Z.; Yao, H.; Jiang, W. Shear-Induced Assembly of a Transient yet Highly Stretchable Hydrogel Based on Pseudopolyrotaxanes. *Nat. Chem.* **2019**, *11*, 470–477.

(206) Dai, Q.; Kadla, J. F. Effect of Nanofillers on Carboxymethyl Cellulose/Hydroxyethyl Cellulose Hydrogels. *J. Appl. Polym. Sci.* **2009**, *114*, 1664–1669.

(207) Zhou, C.; Wu, Q.; Yue, Y.; Zhang, Q. Application of Rod-Shaped Cellulose Nanocrystals in Polyacrylamide Hydrogels. *J. Colloid Interface Sci.* **2011**, *353*, 116–123.

(208) Gong, J. P.; Katsuyama, Y.; Kurokawa, T.; Osada, Y. Double-Network Hydrogels with Extremely High Mechanical Strength. *Adv. Mater.* **2003**, *15*, 1155–1158.

(209) Gong, J. P. Why Are Double Network Hydrogels so Tough? *Soft Matter* **2010**, *6*, 2583.

(210) Sun, J.-Y.; Zhao, X.; Illeperuma, W. R. K.; Chaudhuri, O.; Oh, K. H.; Mooney, D. J.; Vlassak, J. J.; Suo, Z. Highly Stretchable and Tough Hydrogels. *Nature* **2012**, *489*, 133–136.

(211) Zhang, H. J.; Sun, T. L.; Zhang, A. K.; Ikura, Y.; Nakajima, T.; Nonoyama, T.; Kurokawa, T.; Ito, O.; Ishitobi, H.; Gong, J. P. Tough Physical Double-Network Hydrogels Based on Amphiphilic Triblock Copolymers. *Adv. Mater.* **2016**, *28*, 4884–4890.

(212) Lu, X.; Chan, C. Y.; Lee, K. I.; Ng, P. F.; Fei, B.; Xin, J. H.; Fu, J. Super-Tough and Thermo-Healable Hydrogel – Promising for Shape-Memory Absorbent Fiber. *J. Mater. Chem. B* **2014**, *2*, 7631–7638.

(213) Li, J.; Suo, Z.; Vlassak, J. J. Stiff, Strong, and Tough Hydrogels with Good Chemical Stability. *J. Mater. Chem. B* **2014**, *2*, 6708–6713.

(214) Wei, Z.; Yang, J. H.; Zhou, J.; Xu, F.; Zrínyi, M.; Dussault, P. H.; Osada, Y.; Chen, Y. M. Self-Healing Gels Based on Constitutional Dynamic Chemistry and Their Potential Applications. *Chem. Soc. Rev.* **2014**, *43*, 8114–8131.

(215) Taylor, D. L.; in het Panhuis, M. Self-Healing Hydrogels. *Adv. Mater.* **2016**, *28*, 9060–9093.

(216) Chen, Q.; Chen, H.; Zhu, L.; Zheng, J. Engineering of Tough Double Network Hydrogels. *Macromol. Chem. Phys.* **2016**, *217*, 1022–1036.

(217) Han, X.; Meng, X.; Wu, Z.; Wu, Z.; Qi, X. Dynamic Imine Bond Cross-Linked Self-Healing

Thermosensitive Hydrogels for Sustained Anticancer Therapy via Intratumoral Injection. *Mater. Sci. Eng. C* **2018**, *93*, 1064–1072.

(218) Chen, Q.; Zhu, L.; Zhao, C.; Wang, Q.; Zheng, J. A Robust, One-Pot Synthesis of Highly Mechanical and Recoverable Double Network Hydrogels Using Thermoreversible Sol-Gel Polysaccharide. *Adv. Mater.* **2013**, *25*, 4171–4176.

(219) Truong, V. X.; Ablett, M. P.; Richardson, S. M.; Hoyland, J. A.; Dove, A. P. Simultaneous Orthogonal Dual-Click Approach to Tough, *in-Situ* -Forming Hydrogels for Cell Encapsulation. *J. Am. Chem. Soc.* **2015**, *137*, 1618–1622.

(220) Crompton, K. E.; Goud, J. D.; Bellamkonda, R. V.; Gengenbach, T. R.; Finkelstein, D. I.; Horne, M. K.; Forsythe, J. S. Polylysine-Functionalised Thermoresponsive Chitosan Hydrogel for Neural Tissue Engineering. *Biomaterials* **2007**, *28*, 441–449.

(221) Wei, Z.; Zhao, J.; Chen, Y. M.; Zhang, P.; Zhang, Q. Self-Healing Polysaccharide-Based Hydrogels as Injectable Carriers for Neural Stem Cells. *Sci. Rep.* **2016**, *6*, 37841.

(222) Angelin, M.; Hermansson, M.; Dong, H.; Ramström, O. Direct, Mild, and Selective Synthesis of Unprotected Dialdo-Glycosides. *European J. Org. Chem.* **2006**, *2006*, 4323–4326.

(223) Guthrie, J. P. Hydration of Carbonyl Compounds, an Analysis in Terms of Multidimensional Marcus Theory. **2000**.

(224) Marin, L.; Ailincai, D.; Mares, M.; Paslaru, E.; Cristea, M.; Nica, V.; Simionescu, B. C. Imino-Chitosan Biopolymeric Films. Obtaining, Self-Assembling, Surface and

Antimicrobial Properties. *Carbohydr. Polym.* **2015**, *117*, 762–770.

(225) Mohtasebi, A.; Chowdhury, T.; Hsu, L. H. H.; Biesinger, M. C.; Kruse, P. Interfacial Charge Transfer between Phenyl-Capped Aniline Tetramer Films and Iron Oxide Surfaces. *J. Phys. Chem. C* **2016**, *120*, 29248–29263.

7. Vita

Diego M. Alzate-Sánchez was born and raised in Bogotá, Colombia on February 24, 1988. His first approach to chemistry was during middle school, where he actively participated in a science club. Afterwards, he was inspired by his high school teacher to pursue a career in chemistry. Upon graduating high school in 2004, Diego applied for a spot in the National University of Colombia, where he got admitted to the chemistry program, after passing a competitive exam. During his time there, he was introduced to research by Professor Cesar Sierra, with whom he worked on the synthesis of phenylene-vinylene systems, published his first scientific paper, and attended his first scientific conference. After graduation, Diego continued working with Professor Sierra as a Masters student, this time developing fluorescent ligands for metal organic frameworks. After completing the Masters program, Diego moved to Manizales, where he worked as a volcanologist, overseeing the physicochemical parameters of 11 active volcanoes in the *cordillera central* of the Colombian Andeans. During this time, Diego decided to apply to the graduate school of Cornell University. He was admitted to the PhD program in the Fiber Science and Apparel Design Department, where he started working under the supervision of Professor Juan Hinestroza in 2014. After a fruitful collaboration with Professor William Dichtel, Diego decided to move with him and his group to Northwestern University in 2016. Diego completed his thesis work developing functional materials from bio-renewable feedstocks. Upon graduation, Diego will begin a postdoctoral position at UIUC in the Moore research group. Besides working in the lab, Diego enjoys dedicating time to his wife, socializing with friends, watching soccer, and visiting his family and friends in Colombia.

8. List of Publications

1. Diego M. Alzate-Sanchez, Yuhan Ling, Chenjun Li, Benjamin P. Frank, Reiner Bleher, Howard Fairbrother, Damian E. Helbling and William R. Dichtel. B-Cyclodextrin Polymers on Microcrystalline Cellulose as a Granular Media for Organic Micropollutant Removal from Water. *ACS Appl. Mater. Interfaces* **2018**, 11 (8), 8089-8096.

2. Cinzia Federico, Salvatore Inguaggiato, Zoraida Chacón, John Makario Londoño, Edwing Gil, Diego Alzate. Vapour discharges on Nevado del Ruiz during the recent activity: Clues on the composition of the deep hydrothermal system and its effects on thermal springs *Journal of Volcanology and Geothermal Research*, **2017**, 346, 40-53.

3. Diego M. Alzate-Sanchez, Brian Smith, Alaaeddin Alsbaiee, Juan P. Hinestroza, William R. Dichtel. Cotton Fabric Functionalized with a β-Cyclodextrin Polymer Captures Organic Pollutants from Contaminated Air and Water. *Chemistry of Materials*, **2016**, 28(22), 8340-8346.

4. Salvatore Inguaggiato, John Makario Londoño, Zoraida Chacón, Marcello Liotta, Edwing Gil, Diego Alzate. The hydrothermal system of Cerro Machín volcano (Colombia): New magmatic signals observed during 2011–2013. *Chemical Geology*, **2016**, 469, 60-68.

5. Claudio Inguaggiato, Paolo Censi, Pierpaolo Zuddas, Jhon M. Londoño, Zoraida Chacon, Diego Alzate, L. Brusca, W D'Alessandro. Geochemistry of REE, Zr and Hf in a wide range of pH and water composition: The Nevado del Ruiz volcano-hydrothermal system (Colombia). *Chemical Geology*, **2015**, 125-133.

6. Sugey M. Martinez-Gomez, Diego M. Alzate-Sanchez, William Rodriguez-Cordoba, Cesar A. Sierra, Cristian Ochoa-Puentes. Competitive One-Pot Reactions: Simultaneous Synthesis of DEcahydroacridine-1,8-diones and 1,8-Dioxi-octahydroxanthenes and Photophysical Characterization. *Synthetic Commun*. **2014**, 44(5), 648-659.

7. Carlos Diaz, Diego Alzate, Ricaurte Rodriguez, Cesar A. Sierra. High yield and stereospecific synthesis of segmented poly (p-phenylene vinylene) by the Heck reaction. *Synthetic Metals*. **2013**, 172, 32-36.

8. Diego M. Alzate, Cesar A. Sierra, Juan P. Hinestroza. High-Yield Synthesis of the novel (E,E)-2,5-dimethoxy-1,4-bis[2-(4-ethylcarboxilatestyril)] benzene by the Heck reaction. *Synth.Commun*. **2013**, 43(17), 2280-2285.

9. Diego M. Alzate., Ricaurte Rodríguez., Cesar A. Sierra. Fluorescence quantum yield in phenylenevinylene systems. *Rev. Colomb. Quím*. **2010**, 39(3): 309-319.